Simulation of isothermal heat flow microcalorimetry measurements of gun propellants stabilized with diphenylamine and akardite II

Daniel G. Itkis

Eingereicht am 02. März 2020
Zur Erlangung des akademischen Grades Bachelor of Science
An der Ludwig-Maximilian-Universität München

Betreuer: Dr. Manfred A. Bohn

Gutachter: Prof. Dr. T.M. Klapötke

Die Arbeit wurde am
Fraunhofer-Institut für Chemische Technologie
(Fraunhofer ICT), 76318 Pfinztal
durchgeführt, dort betreut von Dr. Manfred A. Bohn.
Computer-Resourcen des ICT und der LMU konnten genutzt werden.

Preface

I want to start off by giving my wholehearted thanks to everybody involved in the making of this thesis :

Meinen herzlichen Dank an Dr. Manfred Bohn für die hervorragende Betreuung und kompetente Unterstützung in allen Phasen dieses Projekts.

Ein Danke an Dr. Johannes Lang für die hilfreichen Diskussionen und Erklärungen über die Mysterien der DFT - insbesondere für die wichtige Erkenntnis, dass auch BLYP einen Basissatz braucht.

Ein Danke an Prof. Dr. Thomas Klapötke für die Betreuung dieser Bachelorarbeit von Seiten der LMU und für die Übernahme der Rolle des Erstprüfers. Meinen Dank teilt auch Prof. Dr. Konstantin Karaghiosoff, der für diese Arbeit die Rolle des Zweitprüfers übernahm.

Ein Danke auch an Saverio Nobbe für die aktive Vermittlung, ohne die dieses Projekt nie zustande gekommen wäre.

My final thanks goes to my family. My parents, grandparents and everyone else who has supported me for my entire life.

Abstract

Isothermal heat flow microcalorimetry (I-HFMC) represents a precise and convenient method for following the degradation of nitrocellulose (NC) based gun propellants. The addition of the stabilizer diphenylamine (DPA) creates an initial dip in the heat flow curves (HFC), while the stabilizer akardite II (Ak II) barely has an impact on then. The aims of this thesis were (I) to show the principle way to simulate HFC and the basic prerequisites necessary and (II) to explain the different behavior of the HFC caused by the stabilizers. Using DFT computations with the ωB97X-D functional and an aug-cc-pvtz basis set with an iefPCM solvation model to simulate the propellant matrix, reaction enthalpies and Gibbs free energies were computed for reaction pathways involving NC, DPA and Ak II with the program system Gaussian 2016. Kinetic models consisting of sets of ordinary differential equations (rate laws) were fitted with the *FitODE* application in Origin 2019b™ by the company OriginLab corporation in conjunction with reaction enthalpies from DFT computations to model the HFC's of unstabilized NC, an Ak II-stabilized propellant and a DPA-stabilized propellant. It was found out that current kinetic models using only the concentrations of nitrate ester, the autocatalytically active species and the stabilizer with its consecutive products firmed by its stabilizing action show some major shortcomings. Therefore, the idea was to include a different, previously neglected reaction might be important for the proper description of the HFC's. It is proposed that an organic species capable of reducing autocatalytically active NO_2 and HNO_3 should be included in the kinetic model system. Such a compound can inhibit the autocatalytic degradation of NC to some degree. This process is named "autostabilization", in antithesis to autocatalysis. A simple kinetic model based on this premise is found to reproduce the HFC of the DPA-stabilized sample with an adjusted R^2 of 0.945. The existence of an autostabilization process would have a profound impact on the understanding of propellant shelf lives and propellant-stabilizer interactions.

Index of symbols and abbreviations by occurence

Underlined variables refer to 3- or 4-dimensional vectors.

NC	nitrocellulose (cellulose nitrate)
NO_x	nitrogen oxides, especially NO and NO_2
DPA	diphenylamine, stabilizer for NC
Ak II	akardite II (N,N-diphenyl-N'-methylurea), stabilizer for NC
IR-spectroscopy	infrared-spectroscopy
GC	gas chromatography
ESR	electron spin resonance
NMR	nuclear magnetic resonsance
UV-VIS	ultraviolet-visible
I-HFMC	isothermal heatflow microcalorimetry
dQ/dt	heat flow rate
HFC	heat flow curve
STANAG	Standardization agreement (NATO)
QM	quantum mechanics
$\Psi(\underline{\tau}_1, \underline{\tau}_2, ..., \underline{\tau}_N)$	wavefunction as a function of $\underline{\tau}_i$
N	number of quantum mechanical particles in a system
$\underline{r}_i$	spacial coordinates of particle i
$\underline{\sigma}_i$	spin coordinate of particle i
$\underline{\tau}_i$	combined spacial and spin coordinates of particle i
$\hat{T}_{nuc}$	nuclear kinetic energy operator
$\hat{T}_{el}$	electronic kinetic energy operator
$\hat{V}_{nuc,nuc}$	internuclear potential energy operator
$\hat{V}_{nuc,el}$	potential energy operator for electron-nucleus interactions
$\hat{V}_{el,el}$	interelectronic potential energy operator
E	energy (eigen)value
HF method	Hartree-Fock method
BO approximation	Born-Oppenheimer approximation
MO	molecular orbital
SCF cycle	self consistent field cycle
$\rho(\underline{r}_1)$	electron density as a function of 3-dimensional spatial coordinates
$E[\rho]$	total energy functional
$E_{kin}[\rho]$	kinetic energy contribution functional

$E_{Coulomb}[\rho]$	Coulomb interaction contribution functional
$E_X[\rho]$	exchange energy contribution functional
$E_c[\rho]$	correlation energy contribution functional
$E_{xc}[\rho]$	exchange-correlation contribution functional
LDA	local density approximation
GGA	generalized gradient approximation
$\underline{\bigtriangledown}\rho$	gradient (of electron density)
$\underline{\Delta}\rho = \underline{\bigtriangledown}^2\rho$	Laplacian (of electron density)
φ_i	molecular orbital with number i
BLYP	Becke, Lee, Yang, Parr correlation functional (GGA-type)
B3LYP	Becke, 3 parameter, Lee, Yang, Parr correlation functional (hybrid-GGA functional)
ωB97X-D	long range corrected (ω) Becke 97 (B97) with exchange and correlation within a hybrid scheme (X) and empirical Grimme dispersion correction (D) functional
6-31++G(d,p)	split valence Pople type basis set, double zeta for valence orbitals with polarization and diffuse functions added to H and heavy atoms
aug-cc-pvtz	augmented correlation-consistent triple zeta basis set
ONIOM	our own n-layered integrated molecular orbital and orbital mechanics
iefPCM	integral-equation formalism polarizable continuum model (solvation model)
COSMO	conductor-like screening model (solvation model)
ε_r	relative permittivity of medium
ω	angular velocity of quantum harmonic oscillator
$\hbar$	reduced Planck constant, $\hbar = h/2\pi$
S	absolute entropy
V	volume
p	pressure
T	temperature
U	absolute internal energy
H	absolute enthalpy
F	absolute Helmholtz free energy
G	absolute Gibbs free energy
p°	reference pressure = 1 atm

K_p	equilibrium constant with reference to p°
M°	reference molality = 1 µmol/g
K_M	equilibrium constant with reference to M°
R	ideal gas constant 8.314 J mol^{-1} K^{-1}
Q	reaction quotient (like K, but concentrations not necessarily at equilibrium)
ρ_m	mass density
Δ_rH/ Δ_rG	enthalpy/ Gibbs free energy change for a reaction
$\Delta H^\ddagger$/ $\Delta G^\ddagger$	enthalpy/ Gibbs free energy of a transition state relative to the educts
Δ_fH/ Δ_fG	enthalpy/ Gibbs free energy of formation, i.e. for formation of a given compound directly from the elements in their most stable form at standard pressure
HSM	Harmonic solvation model
ODE	Ordinary differential equation
R^2	Coefficient of determination of a fit
Adj. R^2	Coefficient of determination adjusted for number of free parameters
P	global reagent in NC, autocatalytically active degradation product
S	general stabilizer
R	global reagent in NC, not autocatalycitally active byproduct of NC degradation
$[S-P]$	undefined product of the reaction of S and P
PETN	pentaerythritol tetranitrate, high explosive
RDX	1,3,5-trinitro-1,3,5-triazinane, high explosive
TS	transition state
FTIR	Fourier transform infrared spectroscopy
NG	nitroglycerin, used in double-base propellants
m-%, mass-%	mass fraction in percent
S_{EAr}	electrophilic aromatic substitution
CAR	carbazole
C-390	carbazole-stabilized propellant sample
SEM	scanning electron microscopy
EDX	energy-dispersive X-ray spectroscopy
NC-37	DPA-stabilized single-base propellant

EM2	Ak II-stabilized double-base propellant
HPLC	high-performance liquid chromatography
NBO	natural bond orbital
CP1	unstabilized NC-sample (13 mass-% content nitrogen)
k_{NC}	reaction rate constant for intrinsic NC-degradation, in s^{-1}
k_{auto}	reaction rate constant for autocatalytic NC-degradation, in g µmol^{-1} s^{-1}
d^2Q/dt^2	time derivative of heat flow rate dQ/dt
C/S0200	Ak II-stabilized single-base propellant
C/S0400	Ak II-stabilized single-base propellant
K6210	DPA-stabilized double-base propellant
RS3	reaction system III
k_{NNO}	reaction rate constant for DPA to NNO-DPA, in g µmol^{-1} s^{-1}
k_{DPANNO}	reaction rate constant for NNO-DPA to DPA, in s^{-1}
k_{4N}	reaction rate constant for DPA to $4NO_2$-DPA, in g µmol^{-1} s^{-1}
k_{2N}	reaction rate constant for DPA to $2NO_2$-DPA, in g µmol^{-1} s^{-1}
k_{NNO-}	reaction rate constant for NNO-DPA to undefined product, in g µmol^{-1} s^{-1}
k_{4N-}	reaction rate constant for $4NO_2$-DPA to NNO-$4NO_2$-DPA, in g µmol^{-1} s^{-1}
k_{2N-}	reaction rate constant for $2NO_2$-DPA to NNO-$2NO_2$-DPA, in g µmol^{-1} s^{-1}
k_{NNO4N-}	reaction rate constant for NNO-DPA to NNO-$4NO_2$-DPA, in g µW^{-1} s^{-1}
k_{NNO2N-}	Reaction rate constant for NNO-DPA to NNO-$2NO_2$-DPA, in g µmol^{-1} s^{-1}

Contents

1 Introduction

In 1846 Swiss-German chemist Christian Schönbein made an unanticipated discovery. While handling concentrated nitric acid Schönbein noticed an accidental spill. He proceeded to wipe the spilled acid up with a cotton apron and, not aware of what had just transpired, suspended it for drying. Before long the apron was completely engulfed in flames[1].

Two aspects of this short anecdote need to be called to attention: (I), what Schönbein had come upon, and (II), in what manner.

(I): Schönbein had unwittingly performed an esterification between the cellulose in the cotton textile and the nitric acid he had spilled, yielding cellulose nitrate - more commonly known as nitrocellulose (NC) or "guncotton". Varying degrees of nitration are attainable by adjusting the conditions during the nitration process. Theoretically, fully nitrated NC with three nitrate ester groups per anhydroglucose ring corresponds to the chemical formula of $(C_6H_7O_2(NO_3)_3)_n$ (Figure 1) and a nitrogen content of 14.15%. In practice, samples nitrated up to 2.7 nitrate ester groups/ring (∼13.3% N) are commonly used, although the synthesis of cellulose nitrate with over 14 % N using a mixture of nitric acid and acetic anhydride has been claimed[2].

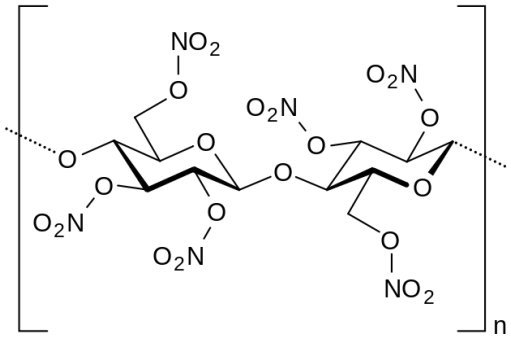

Figure 1: Fully nitrated repeating cellobiose hexanitrate unit in nitrocellulose[3].

In contrast to traditional charcoal-sulfur based gunpowder, the combustion of NC generates a large volume of hot gas without producing solid products as residues. The gas can be used to inflate airbags or for gas generators for seat belts; NC also plays a big role as in gun and rocket propellants. Single-base propellants with only stabilized NC are used as gun propellants.

Double-base propellants additionally contain nitroglycerin and are widely used as gun and rocket propellants. Finally, triple-base propellants consist of a mixture of NC, nitroglycerin and nitroguanidine $(NH_2)_2CNNO_2$[4].

(II): The autoignition of the fabric is indicative of the instability of NC. Like most other organic nitrate esters, NC has a tendency to degrade over time[5]. This degradation of the NC fibers manifests as a gradual deterioration of its physical properties and an increased risk of accidental ignition. The slow breakdown of NC produces NO_x, nitrous and nitric acids as well as aldehydes and other gaseous products. Some of these products, in turn, catalyze the deterioration of more NC. Runaway autocatalytic decomposition tends to occur in samples with higher nitrogen content and can cause dangerous premature combustion or explosion accidents just like what Schönbein had experienced. The NC sample in question was heavily contaminated with leftover acid, causing the autocatalytic decomposition to get out of hand rapidly. This problem becomes more pronounced in highly nitrated propellant grade NC. In more recent history, the explosion of a container of dry NC has set off a chain of detonations with casualties in the hundreds in Tianjin, China in 2015[6]. As a measure to limit decomposition and to extend storage time while also reducing the risk of accidents, commercially available propellant mixtures customarily contain stabilizers that react with and remove contaminants and decomposition products that have the potential to cause autocatalytic degradation of the propellant. These stabilizers usually also act as antioxidants and bind free radicals. Two commonly encountered stabilizers used in propellant formulas include diphenylamine (DPA) and N,N-diphenyl-N'-methylurea, often called akardite II (Ak II). Other aromatic urea derivatives like N,N'-diethyl-N,N'-diphenylurea (ethyl centralite) or 1,1-diphenylurea (akardite I) as well as derivatives of DPA are also employed as stabilizers. They subsequently react with degradation products of NC, interrupting the autocatalytic decay cycle. DPA and Ak II (structures in Figure 2) will be discussed in more detail over the course of this work.

Not least due to the sheer number of different possible substances and interactions in a mixture of NC and a stabilizer the course of NC degradation in the presence of different stabilizers is to this day a field of active research. Many methods, including IR-spectroscopy, GC, mass spectroscopy, electron spin resonance (ESR) and calorimetric measurements have been used to study NC degradation. This work places a spotlight on the latter: The heat generation from propellant samples stabilized with DPA and Ak II has been measured at elevated temperatures using isothermal microcalorimetry

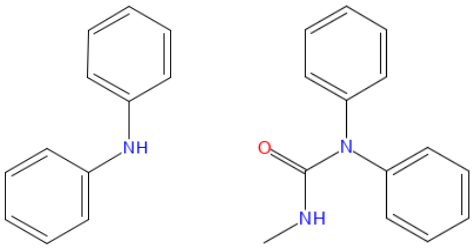

Figure 2: Stabilizers diphenylamine (left) and akardite II (right).

to reveal curiously different heat flow patterns over time. Figure 3 shows typical heat flow curves at 90°C for two propellants, one with DPA and one with Ak II, side by side. Ak II stabilization results in a high initial rate of heat generation which after some equilibration settles to a fairly constant baseline. DPA, on the other hand, shows an initial dip followed by an increase and sometimes a local maximum of heat flow dQ/dt.

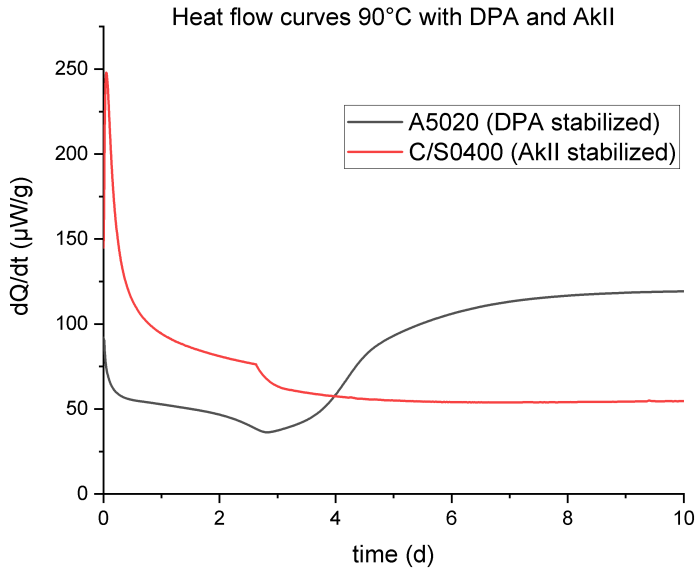

Figure 3: Heat flow curves of two propellants at 90°C, stabilized with DPA and Ak II.

2 Aim

The aim of this thesis is to simulate and construct the heat flow patterns of Ak II- and DPA-stabilized gun propellants using various kinetic models and thermodynamic data from quantum mechanical DFT calculations. A number of reactions and mechanisms are additionally studied to shed light on the feasibility of certain NC decay products, mechanisms and interactions with the stabilizers.

3 Theory and computational considerations

3.1 Isothermal heatflow microcalorimetry (I-HFMC)

One widely used method for analyzing the progress of sample degradation is following the evolution of heat over time. When studying the long term storage properties of NC samples in accelerated aging tests, the decomposition proceeds painstakingly slow. It is spread over many tens or up to hundreds of days and the rates of heat production are accordingly low. For this reason, a special type of calorimetry is required for this application, namely isothermal heatflow microcalorimetry (I-HFMC). The sample is placed in a heat reservoir and kept at a constant temperature together with a second inert sample. The tiny heat generation from the sample is registered as a minuscule heat flow between the samples. Typical heat generation rates at 80°C can be on the order of 40 up to some 100 µW per g propellant. To properly detect the small temperature differences and heat flows caused by the sample, the constancy of temperature and accuracy of the sensor must be very high in the range of 10^{-4} K to 10^{-6} K. The heat generation curves of multiple propellant mixtures have been recorded and discussed by Bohn[7]. More recent measurements on unstabilized NC have been performed by Heil[8]. Datas Measurements from these sources will be used in section 7 as references for propellant heat flow curves. The I-HFMC experiments are performed in airtight ampules made of either glass or stainless steel. It has been shown repeatedly that experimental conditions such as exposure to air, moisture, pressure equilibration and even outwardly inert material like glass beads can have a substantial but poorly predictable effect on the heat flow curves[9]. The conditions for the experiments are hence highly standardized as laid out in NATO STANAG 4582 Ed.1[10].

3.2 Computational methods

When working within the framework of non-relativistic quantum mechanics the search for the spectrum of expected values for any given observable is reduced to finding the eigenstates of the wavefunction Ψ and their associated eigenvalues under the corresponding operator. Ψ is a function of all $3N$ spacial and N (artificially added in non-relativistic QM) spin coordinates of all N involved particles. In the following, $\underline{r}_i$ is used to denote three dimensional spatial coordinates, $\underline{\sigma}_i$ to express spin coordinates and $\underline{\tau}_i$ to signify

the combined four-dimensional vector of a given particle. The approach to finding the energy of a system is no different from the one recited above: In this case the operator acting on the wavefunction is called the *Hamiltonian* of the system, in analogy to the *Hamiltonian function* in classical mechanics. It can be split up into multiple operators, each one accounting for a different contribution to the total energy. For a molecule, these contributions are the kinetic energies of nuclei and electrons, the repulsive interaction between like or equally signed charges and the attraction between electrons and protons. The eigenvalue equation as a whole is universally known as the *time-independent Schrödinger equation* and can be written in the form given in equation 1:

$$[\hat{T}_{nuc}+\hat{T}_{el}+\hat{V}_{nuc,nuc}+\hat{V}_{nuc,el}+\hat{V}_{el,el}]\Psi(\underline{\tau}_1,\underline{\tau}_2,...,\underline{\tau}_N)=E\Psi(\underline{\tau}_1,\underline{\tau}_2,...,\underline{\tau}_N) \quad (1)$$

While simple single-electron quantum systems oftentimes can be solved analytically, there exists no such solution for the *Schrödinger equation* for atoms and molecules with multiple electrons. Accordingly, many numerical computational methods have been introduced over the years; these may vary significantly in accuracy, precision, computational complexity. It is therefore essential to identify a suitable *level of theory* which meets the required standards to adequately describe any property of interest in a molecule.

3.2.1 Hartree-Fock method

Some methods use approximations to model a wavefunction that is gradually optimized to ideally converge towards the elusive exact solution. The most ubiquitously employed groundwork for many types of computations is the *Hartree-Fock method*. The foundation for this method was laid by English mathematician Douglas R. Hartree and built upon by Soviet physicist Vladimir A. Fock in the 1930's and 1940's[11][12]. There are six essential features and steps in this method:

- *Born-Oppenheimer (BO) approximation:* Motions of nuclei and electrons are decoupled since they occur on vastly different timescales. The positions of the nuclei are fixed and the electronic wavefunction is computed with only parametric influence of the nuclear coordinates. The nuclear wave function can later be computed in the potential field of the electronic wavefunction.

- *Slater determinant:* Ψ is approximated as a determinant that consists of products of single-particle functions (molecular orbitals MO) combined in all permutations of particle and MO. This ansatz has the benefit of replicating the antisymmetry of fermionic wavefunctions as required by the Pauli exclusion principle.

- *Mean-field approximation:* The electrons are assumed to only experience the mean-field of the other electrons (average interaction). The interaction is assumed to be limited to the Coulomb and exchange interaction of pairs of electrons. Correlation between the movements of the individual electrons is ignored, hence the difference between the HF energy and exact energy of a system is termed the *correlation energy*.

- *Algebraization:* The MO's are further written as a linear combination of simple basis functions, commonly known as the *basis set*. These are usually Gaussian functions (bell curves) Slater-functions (exponential decay in radial part) or linear combinations thereof, centered on the atomic nuclei. It is often argued that Slater-type functions are superior to Gaussians, as they mimic the radial part of hydrogenic wave functions. In practice, the Gaussian functions have a number of computational advantages. For instance, the integral over the product of two Gaussians is also a Gaussian function according to the Gaussian product theorem. This simplifies many computations to the point that using a linear combination of multiple (usually up to 6) Gaussians fitted to a Slater-type function is faster than using a single Slater-type function and thus preferred. Auxiliary factors can be affixed to capture angular variations and polarization. The choice of the basis set has a profound impact on the accuracy of a computation.

- *Variational principle:* For a system with a ground state (with minimum energy) and a complete basis of complementary excited states any approximated wavefunction (not energy eigenstate) can be written as a linear combination in this complete basis. As the energy of the excited states is higher than the ground state's, the approximated wavefunction must have an energy expectation value higher than the ground state. Conversely, the lower the energy of any given approximated wavefunction, the closer it resembles the ground state. Thus the variation of the coefficients of the basis functions comprising the MO's under the constraint of wavefunction normalization represents a practical method

for wavefunction optimization. The constrained optimization problem can be solved with the help of *Lagrange multipliers* and leads to the so-called *Fock equations*, eigenvalue equations that dictate the character of the optimal MO's to yield minimum total energy. The complicated operator in these equations is called the *Fock operator*.

- *Self consistent field (SCF):* As the Fock equations are effectively single-particle eigenvalue problems they are easily solvable. This allows for the use of an iterative approach: A set of initially guessed MO is used to compute the *Fock operator*. The *Fock operator* is used to solve the *Fock equations* and give improved MO's. The improved MO's are in turn used to compute more accurate *Fock operators*, which in turn give rise to more and more accurate MO's. Upon satisfactory convergence of the MO's the total wavefunction can be constructed and the total electronic energy calculated.

Other properties, including infrared and Raman spectra, NMR-shifts, atomic charges, and potential surfaces can then be determined from the wavefunction. Many more sophisticated methods like Møller-Plesset perturbation theory, configuration interaction and coupled-cluster methods use the results of a HF-computation and introduce corrections to account for the correlation energy[13].

3.2.2 Density functional theory

An analogous description of a system can be achieved by using the electron density ρ instead of the wavefunction. This is done by taking the inner product of the wavefunction with itself in all but 3 spacial coordinates, thus greatly reducing the number of free coordinates from a complex function of $4N$ dimensions to a non-negative real function in three dimensions:

$$\rho(\underline{r}_1) = N \cdot \int |\Psi(\underline{\tau}_1, \underline{\tau}_2, ..., \underline{\tau}_N)|^2 d\underline{\sigma}_1 d\underline{\tau}_2 ... d\underline{\tau}_N \tag{2}$$

Instead of using the Schrödinger equation to find the energy for a given wavefunction one can also directly derive the energy from ρ. The mathematical procedure of mapping a function onto a number is called a *functional*. A functional is a function that uses a function as input and assigns it a numerical value. It can thus be looked at as a function of a function. An appropriate

functional acts on a density function and outputs the energy value associated with that electron density distribution; the theory underlying this approach is known as *density functional theory* (*DFT*). The *Hohenberg-Kohn theorems* guarantee the existence of a functional which assigns exactly one energy value to every charge distribution and possibly more importantly prove that under such a functional there exists a charge distribution yielding the minimal energy, corresponding to the ground state. Using steps similar to those outlined for HF, the electron density can be expressed through a basis set and optimized in a SCF-type cycle. This approach to DFT is commonly known as *Kohn-Sham-DFT*[14]. The biggest conumdrum with DFT nevertheless concerns the functional: No exact functional relating the electron density function to the energy is known. Inevitably, approximations must be introduced once more. The DFT functional is often arranged into different contributions as given in equation 3:

$$E[\rho] = E_{kin}[\rho] + E_{Coulomb}[\rho] + E_x[\rho] + E_c[\rho] \tag{3}$$

The Coulomb potential energy term $E_{Coulomb}[\rho]$ for a stationary charge distribution can be written out explicitly and exactly. The other terms, namely the kinetic energy of the charge distribution $E_{kin}[\rho]$ and in particular the exchange energy $E_x[\rho]$ terms are more complicated. The kinetic energy term can be accounted for by including the second derivatives of the charge distribution $\Delta\rho$. The exchange interaction is not automatically included in DFT and must be constructed. Differently from HF, the self-interaction of an electron does not necessarily vanish here. The $E_c[\rho]$ term accounts for the correlation in the electron motions. The exchange and correlation terms are sometimes combined into exchange-correlation E_{xc}.

A plethora of DFT functionals exists for various applications. Their advantage is that they oftentimes can greatly outperform similarly accurate wavefunction based methods in terms of computation time. As such, DFT methods find widespread use for larger systems, which can not be computed using wavefunction methods in a reasonable amount of time. DFT functionals are benchmarked to give results with a certain level of accuracy for a set of molecules, making their performance drastically varying depending on whether or not a functional was designed with a given substance class in mind. This makes it intrinsically troublesome to try ranking functionals by their performance. In 2001 Perdew proposed a Jacob's ladder (Figure 4) of accuracy, ranging from the exact functional (heaven) to HF (earth).

Climbing the rungs of this ladder is supposed to progressively give better results[15].

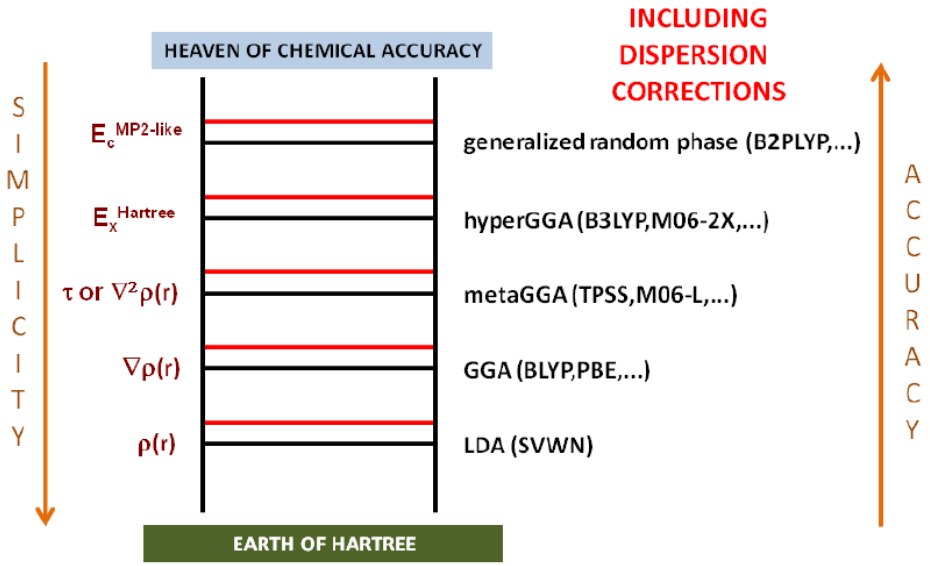

Figure 4: Jacob's ladder of DFT methods[16].

The first rung of the ladder only uses a rudimentary *local density approximation* (LDA), so $E = E[\rho]$. The second rung includes the first derivative of the charge density in the *generalized gradient approximation* (GGA), $E = E[\rho, \bigtriangledown\rho]$. The BLYP (**B**ecke, **L**ee, **Y**ang, **P**arr correlation) functional used in some parts of this work is of this type. The third rung, *meta-GGA*, also accounts for the electronic kinetic energy by using the Lapacian of the density as mentioned above, $E = E[\rho, \bigtriangledown\rho, \Delta\rho]$. The next step up are *hybrid-GGA/ hybrid-meta-GGA* functionals. These functionals additionally perform a HF-calculation and include some amount of HF exchange energy from the occupied MO's. Here $E = E[\rho, \bigtriangledown\rho, \Delta\rho, \varphi_i]$ with the HF-orbitals φ_i. B3LYP and ωB97X-D, as used for most computations in this work, are of this type[17]. ωB97X-D additionally introduces the Grimme D2 dispersion correction. This term helps to better capture non-local interaction that are poorly represented otherwise by introducing an attractive r^{-6}-potential akin to London dispersion and similar intermolecular forces[18]. On the last step of the ladder, the *double-hybrid methods* are found, which additionally use the virtual, i.e. unoccupied, HF-orbitals. The more involved methods

towards the top of the ladder become more and more computationally demanding as a payoff for the alleged high accuracy. Note here that - no matter how sophisticated they may be - methods exceeding pure DFT provide no guarantee of being variational, i.e. the computed energy may fall below the exact result. In fact, the Hohenberg-Kohn-theorem itself loses its vailidity as soon as current-density terms are included in the functional[19].

To be able to estimate the capacity and accuracy of the functional in use benchmarks and other references are needed. The ωB97X-D functional has, not least due to the included dispersion term, been found to perform significantly better than many other common functionals. In a benchmark study of reaction enthalpies, it was ranked second with a mean unsigned error (MUE) of 2.0 kcal/mol behind M06 with 1.9 kcal/mol. B3LYP has shown a poor result with 8.6 kcal/mol in the same ranking[20]. Besides for reaction enthalpies, ωB97X-D has more distinctly strong points: A study with its focus on noncovalent interactions has placed ωB97X-D second only behind B2PLYP-D3, a more demanding double hybrid functional, in fact, concluding that "if stranded on a desert island, the computational method of choice to salvage from one's luggage must be ωB97X-D/aug-cc-pvtz if accuracy is what is needed". The mean absolute deviation was found to be 1.12 kJ mol^{-1} for the systems studied[21]. Another benchmark study of eight different functionals (including B3LYP, PBE) has established that ωB97X-D produces the most accurate optimized geometries when compared to X-ray crystal structures, with a mean unsigned error of 0.012 Å for the molecules in question. The functional has also been applied in kinetic studies of catalysts to gauge the activation energy barriers[22]. It should also be noted however that unexpectedly large error margins can be encountered in DFT calculations. One study (which does not include ωB97X-D) focusing on radical reactions warns that the computed reaction enthalpies were found to sometimes have unpredictable deviations of up to 40 kJ mol^{-1} for all functionals tested due to strong nonlocal interactions with the unpaired electron[23].

3.2.3 ONIOM and iefPCM

Oftentimes only a small part of a molecule undergoes a noticeable transformation during a reaction. For such cases, the ONIOM (our own n-layered integrated molecular orbital and molecular mechanics) model allows one to drastically cut computation time without sacrificing much of the accuracy. In an ONIOM calculation different molecular regions (often layerwise, like

those of an onion) are designated to be processed using different levels of theory and basis sets. In a typical ONIOM computation only the part of a molecule which is directly involved in the reaction is computed with high accuracy while the rest can be inculded with a cheaper QM method, a smaller basis set or even a molecular mechanics force field[24].

Since only single molecules or small clusters are usually considered, both the geometries and the thermodynamical data pertain to the gas phase and are inaccurate for condensed phase reactions. For this reason the *integral equation formalism polarizable continuum model* (IefPCM) model is used in condensed phase processes. In IefPCM a molecule is considered to take up a certain volume in a polarizable continuum ($\varepsilon_r > 1$). Due to the presence of the molecule with its charge distribution, the continuum is polarized, which stabilizes charge separation, dipole moments and other multipole terms relative to a vacuum and hence mimics the effects of a solvent on a reaction[25]. There is a whole host of closely related solvation models besides iefPCM. The conductor-like screening model (COSMO) for is implemented in a number of computational chemistry software packages. While PCM uses an exact dielectric boundary condition for the electric fields at the cavity surface, COSMO introduces a scaling function in an attempt to reduce deviations from experimental data. One study comparing the two models ultimately found no significant differences in the performances of iefPCM and COSMO[26].

3.3 Thermodynamics

One of the main uses of QM computations lies in the prediction of thermodynamic data as stable reactants, fleeting intermediates, and transition states are attainable conveniently. A geometry optimization is always performed to find the molecular geometry with the lowest energy. The positions of the atomic nuclei are gradually adjusted to yield either an energetic minimum or a saddle point in the case of a transition state optimization. The next step is the quantum mechanical treatment of the nuclei. For a parametrical dependence of the nuclear wavefunction in accordance with the BO approximation, the potential wells surrounding the nuclei can be approximated as parabolic potentials of a coupled quantum harmonic oscillator. The second derivative of the energy with respect to the nuclear coordinates is calculated and used to determine the eigenfrequencies and normal modes. The ground state of a quantum harmonic oscillator with angular velocity ω is $\frac{1}{2}\hbar\omega$. This energy difference is added to the electronic energy for every vibrational mode. This

difference is called the *zero point energy*. The sum of the electronic and zero point energy is the energy of a (noninteracting) molecule in gas phase in its ground state[27].

For higher temperatures, an ensemble of molecules with different allowed energy levels follows the *Boltzmann distribution* for a given temperature. Statistical thermodynamics is utilized to relate the distribution of available energy states to the overall energy of a system. The so-called *partition function* reflects how many states of the availabe are effectively occupied. It is in that sense similar and closely related to the entropy of a system. The energy of a system is proportional to the derivative of the partition function with respect to T^{-1}. Different models are used to evaluate the number of available states and partition function of different degrees of freedom. For vibrations the quantum harmonic oscillator model with its equidistant energy spectrum is assumed. Rotations are treated with the quantum rigid rotor model. Finally, the translational degrees of freedom are described using a quantum ideal gas model, i.e. a number of noninteracting particles (treated as matter waves with a thermal wavelength) in a 3D-box; the entropy for this system is given by the Sackur-Tetrode equation. The electronic wavefunction is assumed to be fully in the ground state. With these models in place, the energy can be computed at any desired temperature and pressure. The output of such a computation is the internal energy U of the gaseous molecule. The other thermodynamic potentials (H enthalpy, F Helmholtz free energy, G Gibbs free energy) are derived from U(S,V) through a *Legendre transform*. The four potentials with their associated transform as well as the conditions under which they are minimized are summarized in table 1[28].

Table 1: Thermodynamic potentials and their minimizing conditions.

Potential	Transform	Conditions
U(S,V)	-	V constant, isolated
H(S,p)	H = U + pV	p constant, isolated
F(T,V)	F = U - TS	T, V constant
G(T,p)	G = U + pV - TS	T, p constant

Given the isochoric nature of the microcalorimetry experiment, it is evident from table 1 that the pertinent potentials are U and F. As no mechanical work is performed against the atmosphere, this is one of the infrequent cases where it is sufficient to consider the energy differences rather than enthalpies. In

the same way, it is not G that is minimized over the course of the reaction but F. The changes in energy are observed in the form of the heat flow in the experiment, while F suggests which reactions are favorable thermodynamically and low enough their activation Helmholtz free energy to proceed. Pressures of multiple atmospheres can build up in I-HFMC ampules. This is evident from the sudden endothermal dips in heat flow curves found towards the later stages of NC decomposition, when the ampules become unable to withstand the burgeoning pressure and start leaking. Experiments are also performed at different temperatures, typically in the range of 60-90°C. Consequently, the question arises to what extent these factors - temperature and pressure - each affect the thermodynamic potentials. The thermodynamic potentials of a reaction particularly change with the pressures and concentrations of substances. For the sake of consistency it is crucial to estabilsh a fixed notation. Δ_rU, Δ_rH, Δ_rF and Δ_rG are the molar changes in thermodynamic potentials for the proceeding reaction specifically at a given temperature and given partial pressures of reactands. Δ_rU°, Δ_rH°, Δ_rF° and Δ_rG°, on the other hand, are used to denote the molar standard thermodynamic potentials, i.e. with all pressures set to a specific reference. Since Gaussian 16 uses $p^\circ = 1$ atm as the default pressure for thermodynamic computations this value will be used as the reference from here on. The partial pressures will also be assumed to be equal to the gases' fugacities.

To get an estimate of how sensitive the potentials are with respect to changes in temperature and pressure, the gas phase disproportionation of nitrous acid will be considered as a sample case. The chemical equation is as follows:

$$2\,\mathrm{HNO_2(g)} \rightleftharpoons \mathrm{H_2O(g)} + \mathrm{NO(g)} + \mathrm{NO_2(g)}$$

This reaction generates one more moiety of gas than it consumes and is accordingly affected by both an increase in pressure and temperature. From Le Chatelier's principle one would predict that an increase in temperature should favor the forward reaction due to the products' higher entropy, while a rise in pressure should favor the reverse reaction. The four potential differences are computed in ωB97X-D/aug-cc-pvtz in four different environments: 5 atm (2 atm HNO_2, others 1 atm) at 25°C, the same 5 atm at 90°C, 1 atm (all pressures divided by 5) at 25°C and 1 atm at 90°C. These explicit values were chosen to adequately demonstrate the trends which the potentials follow and have no further significance. The results are depicted in Figure 5.

The internal energy and enthalpy values for this reaction are indepen-

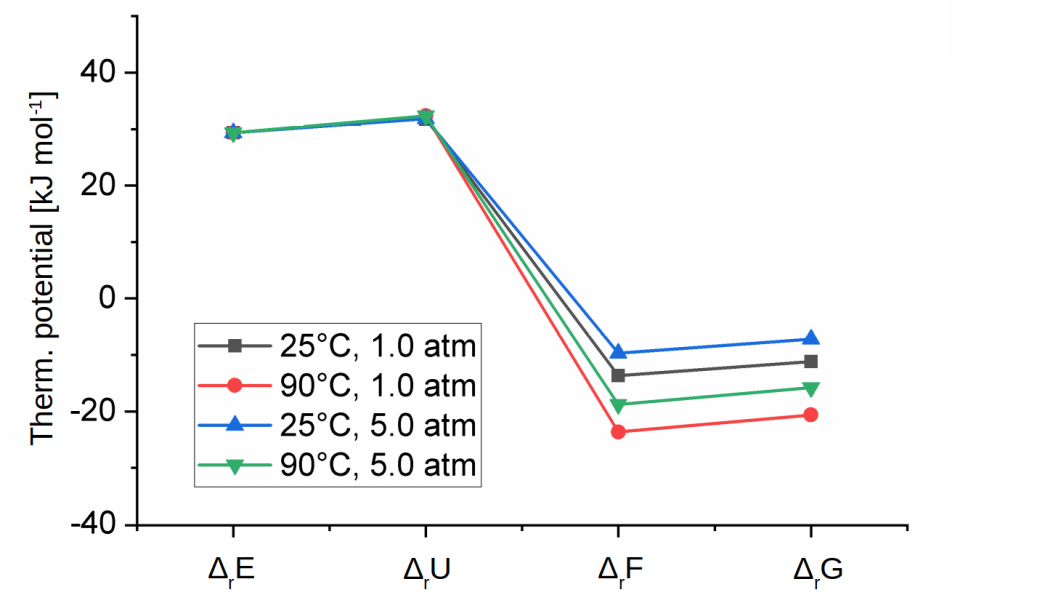

Figure 5: Computed data for the gas phase disproportionation of HNO_2.

dent of the partial pressures and change with temperature by 0.5 kJ mol^{-1} in the case of Δ_rH and only 0.05 kJ mol^{-1} for Δ_rU. This means that the variation of reaction enthalpies within the scope of relevant temperatures is negligible compared to the inaccuracy of the computation itself. The difference between the pairs Δ_rU/Δ_rH or ΔF/ΔG is on the order of 2.5 kJ mol^{-1}. This is again within the range of expected inaccuracy of the functional; ergo, as the distinction is inconsequential, so the habitually used potentials ΔH and ΔG will be consulted when discussing subsequent thermodynamic data. The one important divergence appears for ΔG or ΔF. These two potentials vary significantly with both temperature and partial pressures, amounting to about ca. 10 kJ mol^{-1} and 5 kJ mol^{-1} respectively. With partial pressures deviating from reference conditions, the relation between Δ_rG° and Δ_rG can be written with the reaction quotient Q:

$$\Delta_r G = \Delta_r G^\circ + RT\ ln(Q)$$

From this equation one can, however, not only compute the $\Delta_r G$ for any given pressures but also derive equilibrium constants for various reactions. With the fact that difference of chemical potentials of educts and products vanishes and therefore Δ_rG = 0 at equilibrium, one can derive the following

expression. At equilibrium the value of the reaction quotient is the equilibrium constant K_p:

$$\Delta_r G^\circ = -RT\ ln(K_p) \Longleftrightarrow K_p = e^{\frac{-\Delta_r G^\circ}{RT}}$$

Both K_p and Q are dimensionless as pressures always appear divided by the reference standard. To refer to these dimensionless pressures the notation $[\mathrm{X}] = \frac{p_X}{p^\circ}$ is used. K_p has an exponential dependence on $\Delta_r G^\circ$; this leads to the unfortunate consequence that even small errors in the computed energies can massively skew the computed K_p.

Computing $\Delta G^\ddagger$, the difference in Gibbs free energy between educts and a transition state, all at standard pressures, moreover offers some information about the rate at which a reaction may proceed. In this case, the reaction rate is proportional to $e^{\frac{-\Delta G^\ddagger}{RT}}$ according to the Arrhenius equation. A similar result is deduced from the Eyring-equation. This means that usually, reactions should proceed exponentially faster the lower their $\Delta G^\ddagger$-barriers. This fact is particularly important when comparing different pathways a reaction could take that all lead to the same products. Here normally the pathway with the lowest barrier will be exponentially faster and thus more relevant.

The situation gets considerably more complicated when dealing with condensed state reactions. As the first difference to gas phase computations, optimizations are carried out with the iefPCM model, leading to somewhat different potentials. Δ_rU can be directly calculated from these values. Pressure–volume work is usually imperceptible in condensed state reactions, so Δ_rH $\approx$ Δ_rU rather than Δ_rH = Δ_rU + $p{\cdot}\Delta$V. If the number of reactand molecules before and after the reactions stays the same Δ_rH, Δ_rU and the other two potentials can in fact be calculated accurately in this manner. A problem arises if Δn=0 is not the case. In the calculation of the zero point energy, the employed model of translational motion assumes the molecules are spread over a large volume so there is no interaction between their wavefunctions, i.e. they behave like a quantum ideal gas. This leads to a contribution of $\frac{3}{2}RT$ to the zero point energy for every molecule. These translational degrees of freedom are not available to a molecule in condensed phase. Accordingly, if the number of molecules changes during the reaction, these contributions do not cancel out. At 90°C this introduces an error of 4.5 kJ mol^{-1} per molecule difference. As the rotational freedom of molecules in condensed phase is also very restricted the de facto error is higher. Since Δ_rG = Δ_rH - T$\cdot\Delta_r$S the Gibbs free energy is even more affected by this model incon-

sistency in the calculation of Δ_rS. As an example, in the calculation of the enthalpy and Gibbs free energy of formation of water it was found that while the Δ_fH deviates only by 4.8 kJ mol^{-1} from the experimental value, Δ_fG was calculated 30.6 kJ mol^{-1} too low, mainly due to the overestimation of the entropy of liquid water. To get a more accurate value, a better model for the translational and rotational movements of condensed phase molecules is necessary. Such a model has been introduced recently: The molecular geometry is first optimized in a solvent environment which is simulated by PCM. As the main difference the invalid quantum ideal gas model is replaced with a harmonic oscillator potential inside the the PCM cavity. This change significantly enhances the accuracy of the calculation through an improved treatment translational and rotational degrees of freedom in the partition function. With the same level of theory, this so-called harmonic solvation model (HSM) predicts the Δ_fG of water to within 0.2 kJ mol^{-1} accuracy. It has also been used in an endeavour to computationally predict the boiling points of different solvents[29].

However, it still remains unclear how well such a model could perform for NC based propellants. While the NC itself is a solid, stabilizers and other additives may melt or dissolve into the NC matrix. For this reason it is a matter of debate whether the system should be treated as liquid, solid or maybe even gaseous for some reactions. As Gaussian 16 does not have HCM implemented to reliably and consistently make corrections to thermodynamic data, the unmodified data of the default model is used. This means that while enthalpies should be accurate, Gibbs free energies e.g. for fragmentations, are likely overestimated as a consequence of a systematic computational error. Finally, equilibrium constants for gas-phase reactions are different from equilibrium constants that use concentrations or molalities of substances in the condensed phase. The use of molalities (measured in µmol/g) gives rise to an equilibrium constant K_M where the reference molality is M°=1 µmol/g. The one measure of the particle density that can be directly controlled in a Gaussian 16 computation input is the pressure p. For a condensed phase reaction one can simply convert the effective particle density (i.e. particles per volume) given by the pressure into a more useful measure of the particle density, such as a concentration, molality, or mass percentage. To calculate a molality, the mass density ρ_m of the sample is also necessary. The resulting relationship is written as:

$$p = M\rho_m RT$$

$$K_M = K_p(\rho_m RT)^{-\Delta n}$$

Δn refers to the change of the number of separate molecules in the reaction. R is the ideal gas constant and T the absolute temperature. These to relationships create a bridge between pressures used in Gaussian 16 and molalities used for kinetic modeling. If the number of molecules is not altered then $K_M = K_P$. Assuming a density of about $2\mathrm{g/cm^3}$ for a propellant mixture leads to a factor of approximately 0.0604 $\frac{\text{atm g}}{\mu\text{mol}}$ per extra moiety of gas. As the Δ_rG used to calulate K_p is systematically unreliable and deviations are exaggerated exponentially, it is however unadvisable to confide in K_M calculated in this manner.

3.4 Kinetic modelling

Numerous kinetic models have been put forward and fitted to suit experimental data describing NC degradation; the approach for this is generally as follows: First, a model must be decided upon. A kinetic model consists of a set of coupled rate equations, i.e. ordinary differential equations (ODE) that express the reaction rates of an assortment of compounds assumed to be involved in the reactions of interest. In the case of an NC/stabilizer system, these reactions of interest are broadly speaking the intrinsic and autocatalytic decompositions of NC as well as the mutual consumption of stabilizer and the autocatalytically acting species. The (numerically) integrated forms of these coupled ODE's express the concentrations of the various compounds over time.

The models at this point still contain a number of unknowns. These free parameters, namely undetermined rate constants k and the initial concentrations of the reactants need to be ascertained by fitting the predicted concentration curves to their experimental counterparts. In propellants, the changing concentrations of stabilizers and their derivatives over time are particularly well researched. They can directly be obtained for instance through spectroscopic methods (IR-absorbances, UV-VIS absorption intensities) or chromatography. The resulting measurements are pointwise sampled concentrations at certain intervals. The optimal set of parameters for a reaction scheme then affords the least possible deviation of the predicted curves from the measured points. This deviation may be expressed through the adjusted correlation coefficient R^2 value of a fit. Compared to the R^2 value commonly

referenced in simple fits, the adjusted R^2 incorporates the number of free parameters of the model. This helps to paint a more realistic picture of the credibility of a fit: As the addition of more free parameters will always improve a fit's plasticity and variability, thus reducing deviations from experimental data, this metric penalizes high numbers of free parameters in . As such the if two fits with different numbers of free parameters give equally good, the adj. R^2 value of one with fewer parameters will be higher. The closer the adjusted R^2 value of a fit is to 1 the better the fit represents the experimental data. The problem of finding the best possible fit is recast as a problem of finding the set of parameters with the highest possible adj. R^2 value. The *FitODE* extension in Origin 2019b is used for this application.

In this work, in addition to the concentration curves, heat flow curves from I-HFMC experiments were also fitted using the outlined method. This data is a pivotal extension of the kinetic fits, as it offers an independent and unique way to validate a kinetic model. In particular, the heat flow curves of a sample represent the net heat generation rate of all reactions that are simultaneously taking place in a sample. With the expected range of reaction enthalpies known from QM computations, a lack of agreement between experimental and fitted curves would suggest the inadequacy of a model. It can point to the existence of additional reactions that the model does not account for.

3.5 Software packages

The computational software package Gaussian 16 was utilized for the QM computations[30]. Systems of differential equations relating the kinetics of the NC-stabilizer systems to the heat flow curves have been fitted using the Runge-Kutta 45 method in the "*FitODE*" and "*SimpleFit*" tools in Origin(pro)™ 2019b[31].

4 Nitrocellulose degradation

This chapter focuses on NC degradation itself. Figure 6 shows the model a NC fiber undergoing the early stages of this process. The nitrate ester groups break down, generating NO_2. NO_2 is reduced to NO by aldehydic species in NC; the oxidation of these aldehydes releases CO and CO_2. NO can be reoxidized by oxygen gas from the surroundings. Other gases like N_2O, N_2, CH_2O and even HCN are also known to form in varying amounts depending on the conditions the NC is subjected to[32]. These gases can become trapped in the NC matrix or be released into the gas surrounding the solid propellant over time. There are indications that the diffusion of these trapped gases in NC might be a critical factor in understanding the interactions of NC with stabilizer. A whole kinetic model based on random walk diffusion of trapped NO_x has proposed[33].

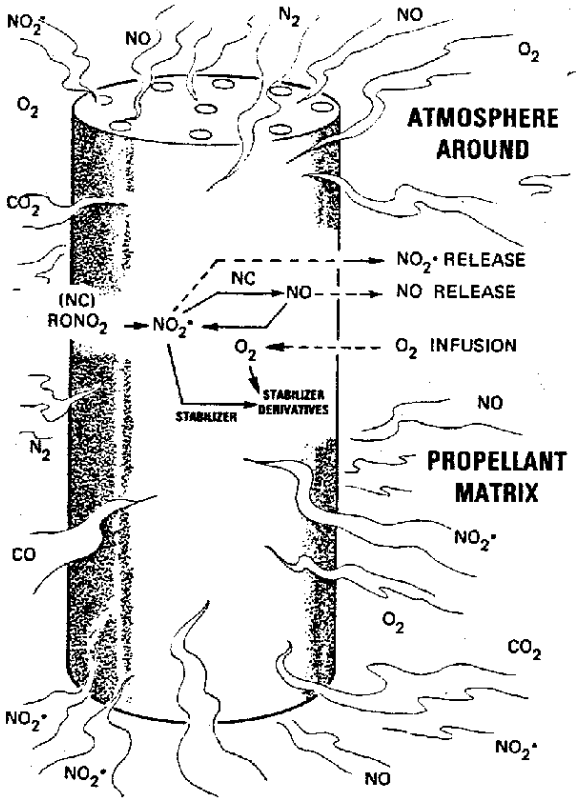

Figure 6: Gas production and reactions during the degradation of NC[34].

There are two processes at play in the degradation of the nitrate esters: NC shows an intrinsic decomposition rate in an approximately first-order reaction, which is inevitable even with the use of stabilizers. Products of this intrinsic decomposition as well as residual water and acids, collectively called P, catalyze the further degradation of NC, which in turn produces even more of these autocatalytically active species. The other products of the NC degradation are referred to as R. It is at this point where stabilizers S come into the picture. A good stabilizer binds P, effectively keeping the rate of NC decomposition as close to the uncatalyzed rate as possible. These three reactions can be summarized as:

$$\begin{aligned} \mathrm{NC} &\longrightarrow P + R && \text{intrinsic decomposition} \\ \mathrm{NC} + P &\longrightarrow 2P + R && \text{autocatalysis} \\ S + P &\longrightarrow [S - P] && \text{stabilization} \end{aligned}$$

4.1 What is *P*?

P refers to products of NC degradation that autocatalytically accelerate the degradation process. They are treated as one global reactand in kinetic modeling. There is, however, an abundance of different nitrogen containing species that coexist in an equilibrium, many of which could fit this description. DFT calculations can help to narrow down the range of possible candidates. Table 2 lists a number of N species and water with the corresponding Δ_fH and Δ_fG computed at 90°C both in the gas phase and in simulated NC. An iefPCM-computation with an $\varepsilon_r = 7.0$ was applied to simulate the influence of polarizable NC-strands surrounding the reagents. The experimental dielectric constant for NC is $\varepsilon_r = 6.0 - 7.5$ dependending on the measuring frequency[35]. Gas-phase computations are relevant in this case as every single compound involved, with the exception of water, has a boiling point below 90°C. This means that many of these reactions can take place either in the NC matrix or in the gas phase. The reference state for the elemental gases is 1 atm at 90°. Out of the listed species only HNO_2, HNO_3 and H_2O form exergonically.

All of the values are found to be lower in the simulated NC due to the better stabilization of the polar products compared to the completely non-polar elements, i.e. H_2, N_2 and O_2. Figure 7 shows a flow diagram containing

Table 2: Computed molar enthalpies and Gibbs free energies of formation at 90°C in kJ mol^{-1}.

	in gas phase		in NC simulate	
Compound	$\Delta_f H^\circ$	$\Delta_f G^\circ$	$\Delta_f H^\circ$	$\Delta_f G^\circ$
NO	91.1	88.6	91.1	88.6
NO_2	30.8	51.3	28.4	48.9
N_2O	75.0	102.4	71.4	98.8
N_2O_3	95.2	168.9	83.8	157.0
N_2O_4	14.6	123.2	5.8	114.4
N_2O_5	22.3	154.4	16.6	148.6
HNO_3	-130.4	-55.4	-144.1	-69.0
HNO_2	-70.7	-26.8	-81.1	-37.1
HNO	110.7	127.0	103.4	119.7
H_2O	-230.9	-214.1	-244.4	-227.7

possible reactions between the compounds from Table 2. These are the reactions assumed to take place involving only species of P for reactions 1 to 6, between P and oxygen gas for 7 - 8 and for a reduction by aldehydes formed in the decomposition of NC for equations 9 - 12. 13 is a secondary step following 12 and 14 is the combination of 12 and 13. Balanced chemical equations for reactions 1-14 are also given below.

$$2\,HNO_3 \rightleftharpoons N_2O_5 + H_2O \tag{1}$$

$$2\,NO_2 \rightleftharpoons N_2O_4 \tag{2}$$

$$NO_2 + NO \rightleftharpoons N_2O_3 \tag{3}$$

$$2\,HNO_2 \rightleftharpoons NO_2 + NO + H_2O \tag{4}$$

$$HNO_2 + HNO_3 \rightleftharpoons 2\,NO_2 + H_2O \tag{5}$$

$$3\,HNO_2 \rightleftharpoons HNO_3 + 2\,NO + H_2O \tag{6}$$

$$2\,NO + O_2 \rightleftharpoons 2\,NO_2 \tag{7}$$

$$2\,HNO_2 + O_2 \rightleftharpoons 2\,HNO_3 \tag{8}$$

$$2\,HNO_3 + CH_2O \longrightarrow 2\,NO_2 + CO + 2\,H_2O \tag{9}$$

$$2\,NO_2 + CH_2O \longrightarrow 2\,HNO_2 + CO \tag{10}$$

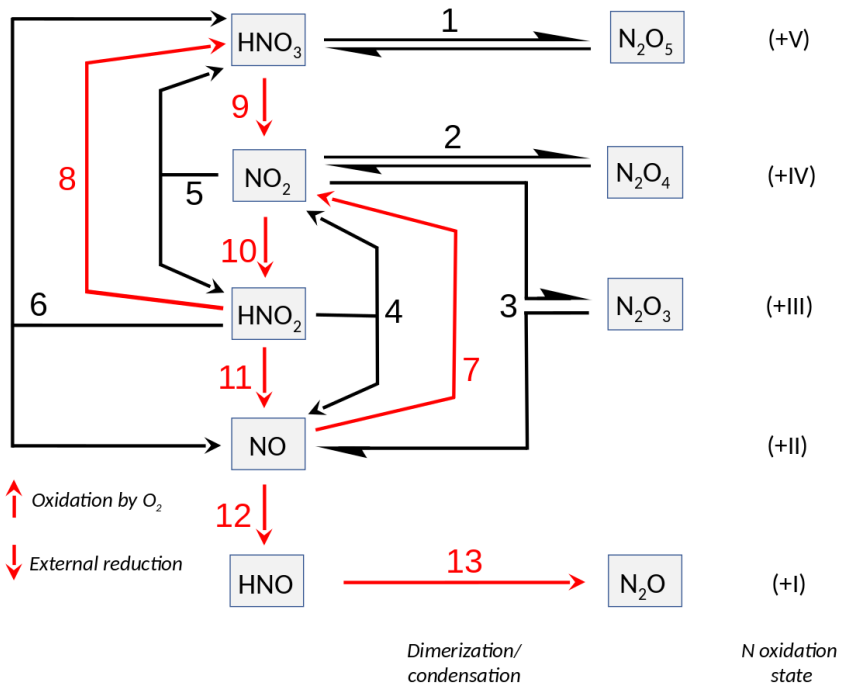

Figure 7: Flow diagram of the reactions of nitrogen oxides and oxoacids.

$$2\,HNO_2 + CH_2O \longrightarrow 2\,NO + CO + 2\,H_2O \tag{11}$$

$$2\,NO + CH_2O \longrightarrow 2\,HNO + CO \tag{12}$$

$$2\,HNO \longrightarrow N_2O + H_2O \tag{13}$$

$$2\,NO + CH_2O \longrightarrow N_2O + CO + H_2O \tag{14}$$

Working within the framework of this system it would be helpful to know where the equilibrium between these species lies. Table 3 lists the $\Delta_f H^\circ$ and $\Delta_f G^\circ$ for reactions 1 - 14. The reaction rates of the interconversion of the various nitrogen oxides and acids are assumed to be much faster than the reactions with stabilizers or other products of NC decomposition. In this case the pressures of these compounds can establish steady state pressures, which only slowly drift over the course of days. Knowledge of the state of this equilibrium would give a reference to what species (and to what extent) constitute the global P, for which little conclusive information can be found in the literature. In Figure 7 this corresponds to just the reactions in black.

Table 3: Computed molar enthalpies and Gibbs free energies of reaction at 90°C in gas phase and simulated NC in kJ mol^{-1}.

	in gas phase		in NC simulate	
reaction	$\Delta_r H°$	$\Delta_r G°$	$\Delta_r H°$	$\Delta_r G°$
1	52.3	51.1	60.3	58.8
2	-46.9	20.7	-50.9	16.6
3	-26.6	29.0	-35.7	19.6
4	32.3	-20.6	37.2	-16.1
5	31.7	-29.3	37.5	-23.8
6	-31.1	38.1	-37.8	31.6
7	-120.6	-74.6	-125.4	-79.4
8	-119.4	-57.1	-126.0	-63.8
9	-122.5	-237.2	-117.8	-232.6
10	-186.0	-178.5	-192.7	-184.9
11	-121.3	-219.7	-119.7	-218.3
12	56.2	54.6	52.2	50.5
13	-379.8	-368.2	-377.3	-365.6
14	-325.2	-315.1	-323.7	-313.6

Oxygen gas from the atmosphere is also included in a second equilibrium calculation. Using equations 1 to 6 and the computed $\Delta_r G°$ values one can solve for the equilibrium partial pressures of every species involved. At initial conditions all pressures are 0 except for water $[H_2O]_0$ and nitrogen dioxide $[NO_2]_0$. This leads to the following equations for the equilibrium concentrations:

$$K_1 = \frac{[N_2O_5][H_2O]}{[HNO_3]^2} = 4.467 \cdot 10^{-8}$$

$$K_2 = \frac{[N_2O_4]}{[NO_2]^2} = 1.066 \cdot 10^{-3}$$

$$K_3 = \frac{[N_2O_3]}{[NO_2][NO]} = 6.643 \cdot 10^{-5}$$

$$K_4 = \frac{[H_2O][NO_2][NO]}{[HNO_2]^2} = 9.258 \cdot 10^{2}$$

$$K_5 = \frac{[H_2O][NO_2]^2}{[HNO_2][HNO_3]} = 1.665 \cdot 10^{4}$$

More equations are necessary to uniquely find a solution. As 8 compounds are in equilibrium, a total of 8 equations is required:

$$\begin{aligned}[\mathrm{NO_2}] &= [\mathrm{NO_2}]_0 - [\mathrm{HNO_2}] - [\mathrm{HNO_3}] - [\mathrm{NO}] - 2\cdot[\mathrm{N_2O_3}] - 2\cdot[\mathrm{N_2O_4}] - 2\cdot[\mathrm{N_2O_5}] \\ &\approx [\mathrm{NO_2}]_0 - [\mathrm{HNO_2}] - [\mathrm{HNO_3}] - [\mathrm{NO}]\end{aligned}$$

This equation represents the overall conservation of nitrogen atoms with the approximation that the dimeric oxides don't contribute to the overall number of N atoms. It is applied because the concentrations of any of the dimeric oxides are much lower than the concentrations of the principal P-compounds. They have been found to make up about 0.25% of P at the most.

$$[\mathrm{H_2O}] = [\mathrm{H_2O}]_0 - \frac{1}{2}[\mathrm{HNO_2}] - \frac{1}{2}[\mathrm{HNO_2}]$$

This equation comes from the conservation the number of hydrogen atoms.

$$[\mathrm{HNO_2}] + 2[\mathrm{NO}] = [\mathrm{HNO_3}]$$

This equation comes from the conservation of electrons accounted for by following changes in oxidation number relative to the initial NO_2. In the presence of oxygen NO and HNO_2 can be oxidized according to chemical equations 7 and 8. Assuming a large gas reservoir of oxygen that can constantly replenish the lost $[O_2]$ inside the propellant, the initial concentration of oxygen $[O_2]_0$=0.21 does not change over the course of the equilibration. While this is not true in a closed microcalorimetry ampules, this assumption serves as the opposite extreme to a complete abesnce of oxygen. The two extremes delineate the range of possible conditions. The introduction of oxygen renders the last equation invalid so that the following is used instead:

$$K_8 = \frac{[\mathrm{NO_2}]^2}{[\mathrm{NO}]^2[\mathrm{O_2}]_0} = 5.334 \cdot 10^{10}$$

This system of 8 equations is numerically solved for different initial conditions, with $[H_2O]_0$ and $[NO_2]_0$ corresponding to pressures ranging from 0.01 atm to 1 atm. The equilibrium pressures of the involved species are summarized in Table 4. Figure 8 shows the same information in the form of the molar distribution (i.e. dimeric oxides count double here) of nitrogen in different forms.
It was found that in all cases the major components were NO_2 and HNO_3. In the absence of oxygen, more than 97% of NO_2 remains unchanged and

Table 4: Calculated chemical equilibrium of nitrogen oxides, oxoacids, water and oxygen at 90°C. Initial pressures of NO_2, H_2O and O_2 vs final equilibrium pressures, pressures in atm.

$[H_2O]_0$	$[NO_2]_0$	$[NO_2]$	$[NO]$	$[HNO_2]$	$[HNO_3]$	$[N_2O_5]$	$[N_2O_4]$	$[N_2O_3]$	$[H_2O]$
		No O_2 present:							
1	1	0.970	$8.16 \cdot 10^{-3}$	$2.91 \cdot 10^{-3}$	0.0192	$1.67 \cdot 10^{-11}$	$1.00 \cdot 10^{-3}$	$5.26 \cdot 10^{-7}$	$9.89 \cdot 10^{-1}$
0.1	1	0.987	$4.04 \cdot 10^{-3}$	$6.40 \cdot 10^{-4}$	0.00871	$3.56 \cdot 10^{-11}$	$1.04 \cdot 10^{-3}$	$2.64 \cdot 10^{-7}$	0.0953
0.01	1	0.994	$1.83 \cdot 10^{-3}$	$1.26 \cdot 10^{-4}$	0.00379	$7.99 \cdot 10^{-11}$	$1.05 \cdot 10^{-3}$	$1.21 \cdot 10^{-7}$	$8.04 \cdot 10^{-3}$
1	0.1	0.0970	$8.18 \cdot 10^{-4}$	$2.93 \cdot 10^{-4}$	0.00193	$1.66 \cdot 10^{-13}$	$1.00 \cdot 10^{-5}$	$5.27 \cdot 10^{-9}$	0.999
1	0.01	0.00970	$8.17 \cdot 10^{-5}$	$2.93 \cdot 10^{-5}$	0.000193	$1.66 \cdot 10^{-15}$	$1.00 \cdot 10^{-7}$	$5.26 \cdot 10^{-11}$	1.00
		0.21 atm O_2 present:							
0.01	1	0.980	$8.75 \cdot 10^{-11}$	$3.20 \cdot 10^{-7}$	0.0200	$1.61 \cdot 10^{-3}$	$1.02 \cdot 10^{-3}$	$5.70 \cdot 10^{-15}$	$1.11 \cdot 10^{-8}$
0.1	1	0.800	$7.14 \cdot 10^{-11}$	$3.20 \cdot 10^{-7}$	0.200	$1.07 \cdot 10^{-3}$	$6.82 \cdot 10^{-4}$	$3.80 \cdot 10^{-15}$	$1.66 \cdot 10^{-6}$
1	1	0.00724	$6.47 \cdot 10^{-13}$	$1.60 \cdot 10^{-5}$	0.993	$8.74 \cdot 10^{-8}$	$5.59 \cdot 10^{-8}$	$3.11 \cdot 10^{-19}$	0.504

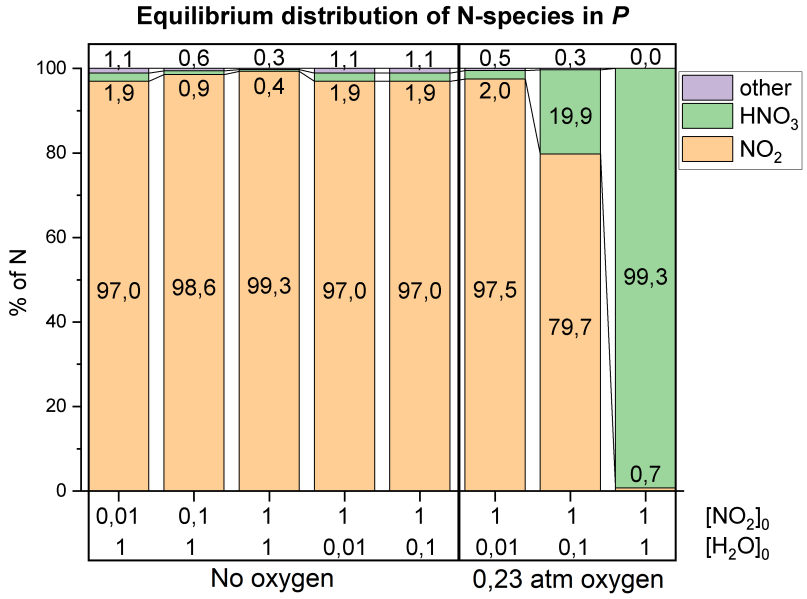

Figure 8: Chemical equilibrium between nitrogen oxides, oxoacids, water and oxygen gas. Percentages of total nitrogen present as NO_2, HNO_3 or other species in gas-phase at 90°C. Initial conditions on the bottom. 3 columns on right with constant 0.23 atm of O_2.

about 2% are found as nitric acid. A great majority of reactions in the practically air-free bulk of propellant mixtures and especially under inert gas is therefore expected to involve NO_2 and to a lesser degree also HNO_3. It is a remarkable observation that the presence of even impossibly high 1 atm of water vapor at 90°C does not affect this equilibrium noticeably under O_2-free conditions. While water can of course still e.g. hydrolyze nitrate esters on its own, varying moisture contents do not change the mode of interaction of *P* with NC and stabilizers directly. Changing the pressure of NO_2 does not significantly alter these general trends. An increase in NO_2 pressure leads to an increase in N_2O_4. In the presence of oxygen, the system is much more variable. HNO_3 is formed preferentially in this case. When water is a limiting reagent, i.e. under dry conditions, N_2O_5 is also found to contribute to about 0.3% of the total nitrogen. The concentrations of HNO_2 and HNO_3 on the other hand was found to remain low if water is the limiting reagent. In these cases (0.01 atm and 0.1 atm H_2O) it was found that water is almost exhaustively used up to form HNO_3. If enough water is available, practically

the entirety of NO_2 is converted to HNO_3 in the presence of air. Exposure to air and moisture is manifestly able to completely change the character of P and prompt more reaction with HNO_3. HNO_2, on the other hand, is not significantly represented in the equilibrium mixture, peaking at 0.3% in the absence of oxygen.
Furthermore, different aldehydes have been shown to form as sideproducts of NC degradation. In one study, the decomposition of sheets of NC at pressures below 15 mbar was found to yield volatile compounds which, upon condensation in a cold trap, form a red residue. This residue was found to consist largely of formaldehyde, formic acid, glyoxal and solvents used in the preparation of the samples[36]. In a different study with methyl nitrate and pentaerythritol tetranitrate (PETN), another organic nitrate ester, it was found that the NO_2 which is initially formed in the degradation is consumed in a secondary reaction. NO, CO and CO_2 were reported as the primary products of the reaction. Additionally, a deposit of formaldehyde polymer has been found in the reaction chamber[36]. Furthermore, another study investigating reactions between formaldehyde and NO_2 found that a mixture of 2 parts NO_2 and 1 part CH_2O subjected to elevated temperatures yields NO, CO and CO_2[36]. Based on these facts one should expect that even in the absence of stabilizer, the aldehydic degradation products reduce the generated P to some extent. If oxygen is also available, P might actually facilitate the redox reaction between O_2 and the aldehydes. An oxidation cycle as shown in Fig. 9 is conceivable. In it, NO_2 oxidizes the aldehydes to CO and CO_2 and is itself reduced to NO. NO is then reoxidized by O_2 to begin the cycle anew.

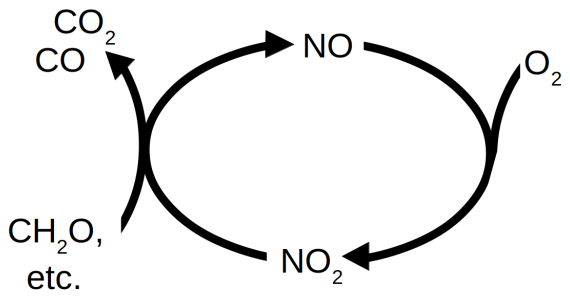

Figure 9: Suggested reaction cycle of the oxidation of aldehydic materials by O_2 with NO/NO_2 catalysis.

The net chemical equations for the oxidation of formaldehyde in such a manner, along with their gas phase standard reaction enthalpies, are:

$$CH_2O + \frac{1}{2}O_2 \longrightarrow CO + H_2O \text{ with } \Delta_r H^\circ = -214.0 \text{ kJ mol}^{-1}$$

$$CH_2O + O_2 \longrightarrow CO_2 + H_2O \text{ with } \Delta_r H^\circ = -503.2 \text{ kJ mol}^{-1}$$

The existence of such a cycle would be difficult to ascertain from kinetic measurements of stabilizer concentrations and would only show up in microcalorimetry experiments as an overly high heat output which is unexplicable through the reactions of P and the stabilizer alone.

In Figure 7 the reactions of CH_2O with nitrogen species in different oxidation stages are included as reactions 9 - 13. Each consecutive reaction reduces the oxidation number of the nitrogen atom by one. For these reactions $\Delta_f H^\circ$ and $\Delta_f G^\circ$ are both significantly negative, i.e. the reactions are all highly favorable, with the exception of reaction 12, the reduction of NO to HNO. This means that, provided low enough energetic barriers, all these reactions are very likely to occur and the reduction by CH_2O can swiftly reduce P down to NO. Further reduction leads to the intermediate nitroxyl HNO. This molecule is known to dimerize to hyponitrous acid $H_2N_2O_2$, which in turn decomposes into water and N_2O. This reaction is suggested to be the source of nitrous oxide formed during the degradation of NC. This overall reaction, reaction 14, is remarkably exergonic. Due to a very weak H-N bond in HNO its formation is thermodynamically unfavorable even with a reducing agent like CH_2O. For the first step of the reaction, a hydrogen transfer from CH_2O to NO leading to HNO and a CHO radical, the transition state is shown in Figure 10.
It was computed to have a fairly high Gibbs free activation energy with $\Delta G^\ddagger$ = 200.3 kJ mol^{-1} in NC simulate and 200.0 kJ mol^{-1} in the gas phase. The initial formation of HNO thus represents a considerable barrier for this reaction, acting as a bottleneck for the reduction of P. This means that if this reaction really does take place it is slow and limited to elevated temperatures. The existence of HNO as an intermediate also partially explains the formation of hydrogen cyanide which is formed in considerable amounts when NC is burned in a confined space. HNO is known to react e.g. with methane at elevated temperatures to yield HCN via the formation of methyl radicals[37]. While the typical conditions for this reaction are different from those in

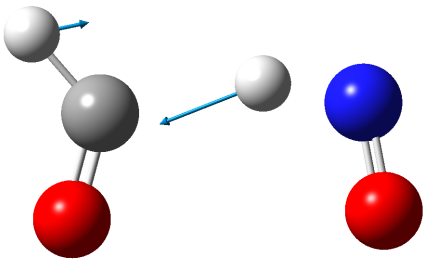

Figure 10: Transition state of the H-transfer between formaldehyde and nitrogen monoxide in NC simulate. The blue arrow represents the displacement vectors of the imaginary vibration.

accelerated aging tests, a likely appearance of HNO at high temperatures still helps to corroborate the case for this being a potential pathway for N_2O formation. The final products of the reduction N_2O and NO are much less aggressive than HNO_3 and NO_2 towards NC and likely do not significantly contribute to further autocatalytic degradation processes.

4.2 Initial degradation

The initial step of the intrinsic decomposition revolves around the formation of a species P from a nitrate ester group. This initial step is the topic of this section. It is a matter of debate where on a NC chain this degradation process tends to occur. While some studies suggest the ends of a chain might be more susceptible and thus claim decomposition is essentially limited to these loose termini, a typical NC chain has on the order of thousand monomers bound along as non-terminal units and only 2 ends, i.e. only 2 terminal units[38]. This points to a statistical preference for reactions along the body of the chain rather than at the ends. This is supported by the fact that the distribution of chain lengths in NC over time can be effectively modeled as a random splitting along the chain rather than a gradual length reduction originating at the ends[39][40]. It could be worth investigating what effect crosslinkers might have on NC degradation. Hydroxy-group crosslinkers like dimethylol ethylene urea are used to interconnect the chains of normal cellulose to make the material resistant to wrinkling[41]. Using a similar reagent to reconnect the open chain termini of NC might help understand what role the open

chain termini play in its degradation.

4.2.1 Homolytic splitting of $CO-NO_2$

The model system used for the NC filaments consists of three fully nitrated glucose rings with methoxy ether groups instead of the subsequently connected glucose rings, as shown in Figure 11. Any reactions are assumed to take place on the middle ring. The outer rings are used to include the steric influence of neighboring nitrate groups while not taking part in the decomposition. As the reactions are localized, an ONIOM model can be used to significantly reduce the computation time without sacrificing accuracy; the central ring (ball-and-stick atoms in Fig. 11) is computed using ωB97X-D/aug-cc-pvtz and the outer two rings (tube atoms in Fig. 11) are calculated in BLYP/6-31++G(d,p). This model system will be referred to as the Trimer.

It is widely assumed that the first step of the decomposition is a direct homolytic splitting of the weak $O-NO_2$ bond. The products are NO_2 and an alkoxyl radical. The bond dissociation energies for the three nitrate groups were calculated for the Trimer (table 5). Both relaxed and unrelaxed structures were computed for the radicals. The values for the unrelaxed structures approximately correspond to the activation energies for the splitting as the

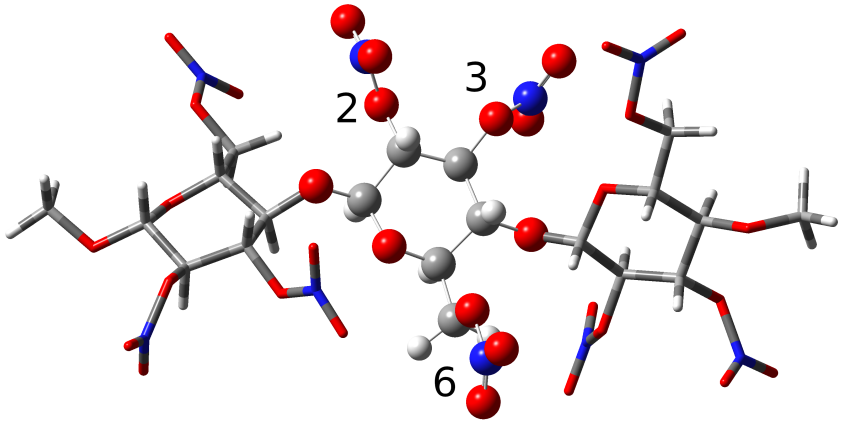

Figure 11: Optimized geometry of the NC Trimer model. Colors: O red, N blue, C gray and H white.

homolytic splitting is assumed to follow a Morse potential curve with no additional barriers. The values for the relaxed radical structures give the reaction energies. It should be noted, that as the structure of the radicals is allowed to freely relax, probable restrictions on the mobility of the real NC strands are ignored. In contrast to the trimer being studied, all glucose rings in real NC are anchored in place by the long chain bodies to both sides of a given ring. The glucose rings in real NC are therefore more limited in both their distance and angle to each other, keeping the radical structures from relaxing fully and thereby increasing the reaction enthalpies somewhat. This interpretation is in agreement with the literature values 161.1 kJ mol^{-1} for 2, 154.0 kJ mol^{-1} for 3 and 161.1 kJ mol^{-1} for the 6 position[42]. These bond dissociation enthalpies are also very good agreement with the empirical value of 157.77 kJ mol^{-1} for NC decomposition measured trough Arrhenius plots[43].

Table 5: Computed $O-NO_2$ bond dissociation enthalpies and Gibbs free energies for relaxed (optimized) and unrelaxed products in kJ mol^{-1} at 90°C.

	unrelaxed		relaxed	
Position	$\Delta_r H^\circ$	$\Delta_r G^\circ]$	$\Delta_r H^\circ$	$\Delta_r G^\circ$
2	161.5	119.9	150.2	83.8
3	160.8	111.7	157.8	92.5
6	160.5	103.5	153.9	83.2

4.2.2 NC degradation by HONO elimination

In the following paragraphs, a different initial step is proposed and computed for the first time: Instead of the liberation of NO_2 it is conjectured that HNO_2 can be produced directly. This reaction is a type of monomolecular elimination, and would involve a five membered transition state and leave an aldehyde/ketone group behind. It has been found to be the energetically most favorable decomposition pathway for some nitramines like methylenenitramine and gas phase RDX; in both cases, the activation energy for this elimination has been found to be lower than the $N-NO_2$ bond dissociation energy[44][45]. Furthermore, the formation of these carbonyl compounds by HNO_2 elimination is well documented in NC in a different setting: The basic hydrolysis of NC yields nitrite salts and carbonyl compounds as the

main products[46]. Thus this pathway is proposed as an alternative to the homolytic O−NO_2 bond cleavage.

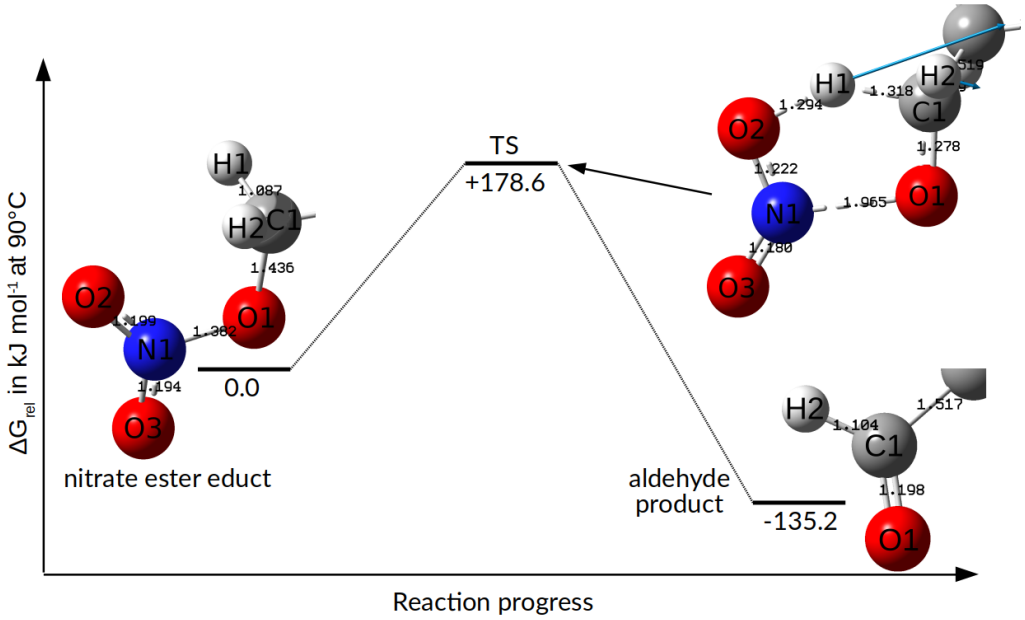

Figure 12: Gibbs free energy along reaction coordinate for the HNO_2-elimination at the 6-position of nitrocellulose and optimized structures of relevant part of the educt. The blue shows the displacement vector of the imaginary vibration. Bond lengths are given in Å.

The transition states and products were computed for the Trimer from section 4.2.1. The activation energies and reaction enthalpies are given in in Table 6. The structures of the transition states are analogous for the three O−NO_2 positions. As an example, the transition state for the 6th position is shown in Figure 12. The O−NO_2 bond has a length of 1.97 Å and is already significantly elongated relative to its minimum energy bond length of 1.38 Å. The C1-O1 bond is shortened with notable double bond character. The five involved atoms lie in a plane to within 4°. H1 migrates between C1 and O2 along the single imaginary vibration mode of the molecule.

The $\Delta G^{\ddagger}$ for the transition states is higher than the corresponding values for homolytic NO_2 formation but are low enough (170-180 kJ mol^{-1}) to realistically proceed. The reactions as a whole are exothermic and exergonic. The reverse reaction has a much higher activation energy (313.8 kJ mol^{-1}

Table 6: Computed TS activation and reaction enthalpies and free energies for HONO elimimination at 90°C.

	TS		Products	
pos.	$\Delta H^{\ddagger}$[kJ mol^{-1}]	$\Delta G^{\ddagger}$[kJ mol^{-1}]	$\Delta_r H$[kJ mol^{-1}]	$\Delta_r G$[kJ mol^{-1}]
2	177.9	173.7	-77.5	-147.2
3	181.9	187.2	-93.7	-160.5
6	183.7	178.6	-69.4	-135.2

for pos. 6), hence this reaction can be assumed to be completely irreversible. Finally, as explained in section 3.3, the $\Delta G^{\ddagger}$ is underestimated for the homolytic splitting of the O$-$NO$_2$ bond, further shrinking the gap between the two degradation pathways.

This leads to an interesting consequence: While the homolytic NO$_2$ formation is lower in activation energy, it is thermodynamically unfavorable. The reverse reaction, i.e. rebonding, is thermodynamically favorable and readily takes place. There is also reason to suspect that the generated NO$_2$ in the rigid framework of the NC strands remains in the proximity of the cleavage site for a period of time while repeatedly rebonding and breaking the O$-$NO$_2$ bond[47]. Since the elimination of HONO is irreversible, it may contribute to the initial stages of NC degradation more than the reversible, thermodynamically unfavorable homolytic cleavage. Thus a compelling case can be made for an alternative first step of NC decomposition.

4.2.3 C$-$ONO$_2$ bond cleavage

One more potential decomposition route needs to be mentioned. Aside from the oxides discussed thus far, the radical NO$_3$ has been proposed to be involved in the degradation of nitrate esters. This species might exist as a short lived intermediate in reactions in which it would act as a potent oxidizing agent. One study observed a very high activation energy of 377 kJ mol^{-1} for the rate determining step of the degradation of a double-base propellant at temparatures close to 200°C. The authors attributed this high value to the formation of NO$_3$ through the breaking of C$-$ONO$_2$ bonds in NC. Processes like these are conceivable at such high temperatures, but would are unlikely to occur lower temperatures such as at room temperature or even at 90°C. In fact, the same study observed a much lower activation energy at temper-

atures in the range of 90-160°C, suggesting distinctly different mechanisms for the degradation in the two temperature regions[48].

4.3 Subsequent degradation

Following the initial release of P, NC degrades further in a cascade of reactions propagating from the initial release site. These reactions may be separate from the autocatalytic reactions of NC with P, instead being directly connected to the decay of the reactive alkoxyl radical. In the case of an elimination of HONO the remaining carbonyl compounds are more stable; the decay is hence assumed to come to a halt right after the elimination. To estimate the expected $\Delta_r H$ of the overall reaction upon NO_2 liberation, it is not enough to consider only one pathway as the degradation process is highly complex and variable. Instead, multiple potential degradation routes are explored to give an assortment of possible enthalpies. The computed reaction enthalpies vary between +60.1 kJ mol^{-1} and -246.5 kJ mol^{-1}, depending on the reaction and products.

4.3.1 Chemiluminescence

In a series of studies the emission of visible light (chemiluminescence) by decomposing samples of NC and PETN was measured at elevated temperatures. In both substances a steady luminescence with multiple emission peaks between 420 nm and 600 nm was observed. Based on the wavelengths of these transitions it was concluded that the glow could be attributed to the decay excited trplet carbonyl groups $^3(R'C{=}O)^*$ and excited singlet oxygen $^1O_2{}^*$ into their ground state[49]. The following reaction scheme was proposed based on this information:

$$RONO_2 \longrightarrow RO\cdot + NO_2 \qquad \text{Homolytic O}{-}NO_2\text{-splitting}$$

$$RO\cdot + NO_2 \longrightarrow ROO\cdot + NO \qquad \text{Oxidation of alkoxy radical}$$

$$2ROO\cdot \longrightarrow {}^3(R'C{=}O)^* + {}^1O_2{}^* + ROH \qquad \text{Peroxy radical disproportionation}$$

After the homolytic splitting of the weak $O{-}NO_2$-bond the resulting alkoxy radical is oxidized by NO_2, froming NO and a peroxy radical. The peroxy radicals react in a second order recombination reaction, yielding the excited carbonyl and singlet oxygen. It was found that the chemiluminescent glow also increases in the presence of atmospheric oxygen, since autocatalytically

active NO_2 can then be regenerated from NO. In this model the decomposition stops at a carbonyl compound (the same products as in section 4.2.2), a free alcohol, NO and O_2. As the quantum yield of the chemiluminescence was reported to be very low, it is assumed that the entire energy is liberated in the form of heat. The overall reaction is:

$$2\ RONO_2 \longrightarrow R'C{=}O + ROH + \ 2\ NO + O_2$$

Table 7: Computed reaction enthalpies and Gibbs free energies for degradation of NC to carbonyl, alcohol, NO and O_2 at 90°C. Values are given per nitrate group.

posistion	$\Delta_r H$[kJ mol^{-1}]	$\Delta_r G^{\ddagger}$[kJ mol^{-1}]
2	53.0	-35.5
3	58.9	-31.1
6	60.1	-25.5

The computed enthalpies and Gibbs free energies for this reaction are summarized in Table 7. The reaction is slightly endothermic, but is overall exergonic and thus favored. Subsequent degradation steps would further reduce the enthalpy and make the reaction more exothermic.

4.3.2 Gas-phase FTIR

Based on measurements of the gas-phase degradation products of NC using Fourier transform IR (FTIR) spectroscopy, a different mechanism for the further degradation of NC has been proposed[50]. This mechanism is depicted in Figure 13.
First, the nitrate groups in the 2- and 3-positions decompose and leave behind alkoxy radicals. The C-C bond between the 2- and 3-position of this intermediate immediately ruptures, yielding a product with two aldehyde groups. The rupturing of this bond has also been confirmed in DFT-calculations. This product further decomposes, releasing more gaseous and volatile products. The final products of the degradation of one mole anhydroglucose rings are one mole CO, CO_2,CH_2O,NO, formic acid, two moles of NO_2. In the condensed phase, IR-absorption bands corresponding to carbonyl C=O double bonds have be detected troughout and even after the complete degradation of the NC sample, indicating the presence a significant amount of carbonyl

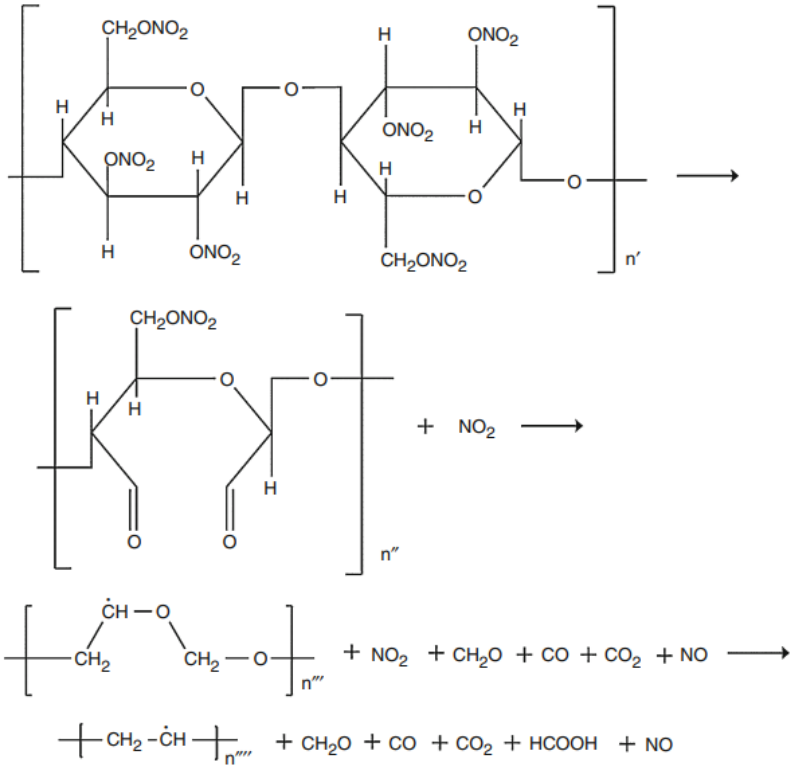

Figure 13: Proposed degradation mechanism based on FTIR data[50].

compounds like aldehydes. The release of formic acid is observed only after the degradation of the majority of the nitrate groups. In this mechanism the chain does not rupture; instead, a $-\mathrm{CH}\cdot-\mathrm{CH_2}-$ group carrying an unpaired electron remains in place of the sugar ring. The products of the reaction are selected to mirror the amounts and order of appearance of the observed gaseous products. The overall chemical reaction for this process is:

$$\mathrm{C_6H_7O_2(ONO_2)_3} \longrightarrow 2\,\mathrm{NO_2} + \mathrm{NO} + \mathrm{CO} + \mathrm{CO_2} + \mathrm{CH_2O} + \mathrm{HCOOH} + \text{remaining chain } (-\mathrm{CH}\cdot - \mathrm{CH_2}-)$$

The net enthalpy and Gibbs free energy for this reaction are $\Delta_r\mathrm{H} = -110.3$ kJ mol^{-1} and $\Delta_r\mathrm{G} = -559.5$ kJ mol^{-1} per anhydroglucose ring in NC simulate using the Trimer model. This corresponds to $\Delta_r\mathrm{H} = -36.8$ kJ mol^{-1} and $\Delta_r\mathrm{G} = -186.5$ kJ mol^{-1} per nitrate group.

There are some improvements to be made with this reaction. As is stated in the original publication, very little NO_2 has been detected. It was suggested that most the NO_2 that is generated is quickly reduced to experimentally observed NO and N_2O. This process has been discussed in section 4.1. Furthermore the remainder of the sugar ring is highly unstable and would abstract a hydrogen atom for instance from a nearby aldehyde. For these reasons the above is a rather low (not very exothermic) estimate. The following changes are made:

$$(-\mathrm{CH}\cdot - \mathrm{CH_2}-) + \frac{1}{2}\,\mathrm{CH_2O} \longrightarrow (-\mathrm{CH_2} - \mathrm{CH_2}-) + \frac{1}{2}\,\mathrm{CO}$$

$$\mathrm{NO_2} + \mathrm{CO} \longrightarrow \mathrm{NO} + \mathrm{CO_2}$$

With these changes to the reaction, the new values for the enthalpy and Gibbs free energy are $\Delta_r\mathrm{H} = -739.4$ kJ mol^{-1} and $\Delta_r\mathrm{G} = -1153.9$ kJ mol^{-1} per anhydroglucose ring or $\Delta_r\mathrm{H} = -246.5$kJ mol^{-1} and $\Delta_r\mathrm{G} = -384.6$ kJ mol^{-1} per nitrate group. A large portion of the heat generated in this reaction can be attributed to subsequent reactions between NO_2 and CO or the organic products of NC degradation like CH_2O.

4.3.3 Radical propagation mechanism

An alternative potential degradation mechanism is proposed in Figure 14. The intermediate alkoxy radical (b) produced by the cleavage of the $\mathrm{O}-\mathrm{NO_2}$ bond of the 2-position nitate group of the Trimer (a) further degrades via an additional loss of NO_2 from the 3-position in analogy with the first step of the mechanism in Figure 13. Instead of breaking the 2C-3C bond however, in this mechanism glyoxal $C_2H_2O_2$ is eliminated. This process ruptures the NC chain, leading to two products: A formate ester (d) and intermediate (c). The former anhydroglucose unit is gradually destroyed as it progresses through an allylradical stage (e) and further loses CH_2O to from a vinylradical intermediate. This vinylradical is unstable and can react with one of the NO_2 that were released prior to form a alkyne type product (f). The formate ester can futher degrade, yielding an hemiacetal (loose chain end ROH) and CO. The chemical reactions for these steps with the reaction enthalpies at 90°C in iefPCM NC simulate are:

$$\text{(a)} \longrightarrow \text{(b)} + \mathrm{NO_2} \text{ with } \Delta_r H^\circ = +150.2\text{kJ mol}^{-1}$$

$$\text{(b)} \longrightarrow \text{(c)} + \text{(d)} + NO_2 + C_2H_2O_2 \text{ with } \Delta_r H^\circ = -105.2\text{kJ mol}^{-1}$$

$$\text{(c)} \longrightarrow \text{(e)} + NO_2 \text{ with } \Delta_r H^\circ = +173.0\text{kJ mol}^{-1}$$

$$\text{(e)} + NO_2 \longrightarrow \text{(f)} + HNO_2 + CH_2O \text{ with } \Delta_r H^\circ = -37.8\text{kJ mol}^{-1}$$

$$\text{(d)} \longrightarrow \text{ROH} + \text{CO} \text{ with } \Delta_r H^\circ = +31.5\text{kJ mol}^{-1}$$

The overall chemical reaction is written as:

$$C_6H_7O_2(ONO_2)_3 \longrightarrow \text{RO}{-}\text{CCH} + 2\,NO_2 + HNO_2 + \text{CO} + CH_2O + C_2H_2O_2 + \text{ROH}$$

The net enthalpy and Gibbs free energy for this reaction are Δ_rH = 211.8 kJ mol^{-1} and Δ_rG =-256.3 kJ mol^{-1} per anhydroglucose ring. As in the previous section, the NO_2 can react with the aldehydes that are formed in this reaction. The net reaction then becomes:

$$C_6H_7O_2(ONO_2)_3 \longrightarrow \text{RO}{-}\text{CCH} + 2\,\text{NO} + HNO_2 + \text{CO} + CO_2 + H_2O + C_2H_2O_2 + \text{ROH}$$

For this new reaction the new values for the enthalpy and Gibbs free energy are Δ_rH = $-$175.6 kJ mol^{-1} and Δ_rG =-682.4 kJ mol^{-1} per anhydroglucose ring or Δ_rH = $-$58.5kJ mol^{-1} and Δ_rG = $-$227.5 kJ mol^{-1} per nitrate group.

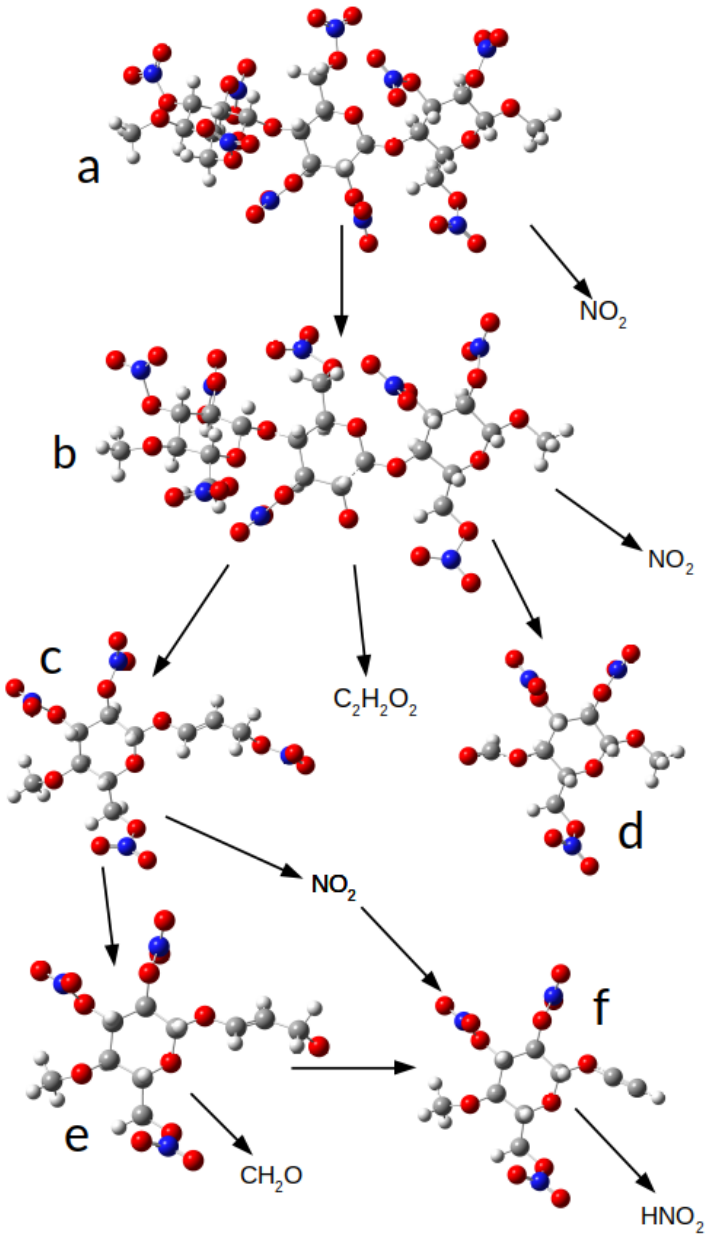

Figure 14: Proposed degradation mechanism of NC with optimized intermediates and product structures. Note that the ONIOM method was used to compute the outer rings with BLYP/6-31++G(d,p).

4.4 Nitroglycerin in double-base propellants

As previously stated, one energetic material often in found conjunction with NC in propellants is nitroglycerin (NG). Just like NC, NG can be synthesized through the complete esterification of glycerol (1,2,3-propanetriol) with nitric acid[51]. While it finds uses in the medical field in the treatment of heart conditions and elsewhere, its most widespred and infamous use is an an explosive[52]. NG owes much of its infamy to its low threshold for detonation through physical shock, making it a dangerous contact explosive in its pure liquid form. It is well known as the energetic material in Dynamite, where it is desensitized and bound by an adsorbent[53]. The decomposition process of NG is similar to NC, although it more easily followed. The first step again is the cleavage of an O-NO_2-bond. There are two distictly different such bonds in the molecule (Figure 15). The O-NO_2-bond from the central carbon is found to be the weaker of the two by 5 kJ mol^{-1}. The dissociacion enthalpy is also found to be very similar to NC, with the two values falling into the range of 150.2-161.5 kJ mol^{-1} established for the nitrate groups in NC. Since NG is a liquid, however, liberated NO_2 can quickly diffuse away, making this process completely irreversible in contrast to NC.

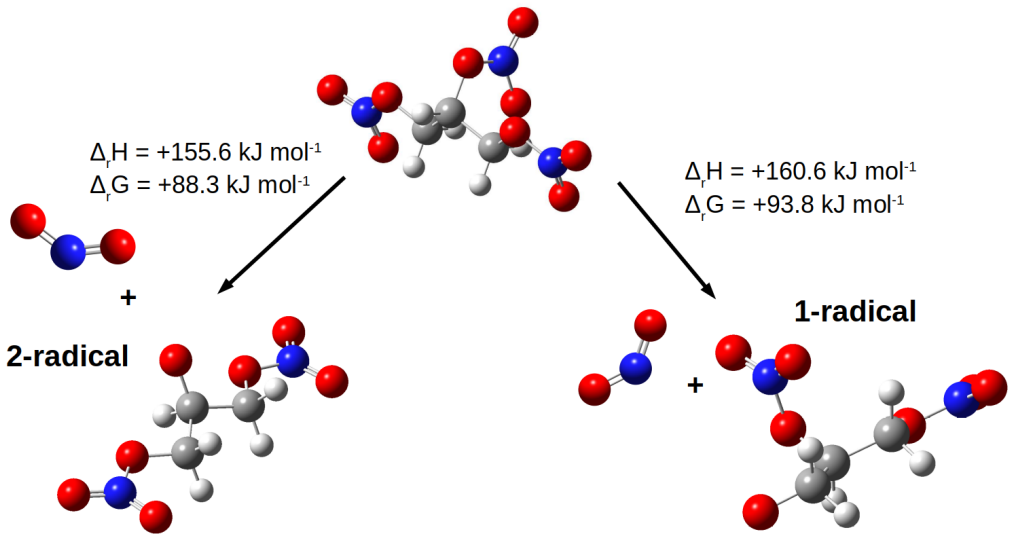

Figure 15: Initial step in the decomposition of nitroglycerin (top) leading to different radicals and NO_2 with computed enthalpies at 90°C.

For a complete decomposition of NG the balanced chemical equation is:

$$\mathrm{C_3H_5N_3O_9} \longrightarrow 3\,\mathrm{CO_2} + \frac{3}{2}\,\mathrm{N_2} + \frac{1}{4}\,\mathrm{O_2} + \frac{5}{2}\,\mathrm{H_2O}$$

Due to the slightly positive oxygen balance of NG some oxygen is formed as one of the products of decomposition. The enthalpy for this reaction in NC simulate is computed as $\Delta_r\mathrm{H} = -1449.6$ kJ mol^{-1} per mol NG or $\Delta_r\mathrm{H} = -483.3$ kJ mol^{-1} per mol nitrate ester.

5 Diphenylamine

5.1 Characterization

One of the first stabilizers which have been added to NC is DPA, with its application dating all the way back to its use by Alfred Nobel starting in 1889[54]. A number of closely related derivatives of DPA, including Ak II and some nitroso/nitro-derivatives like N-Nitroso-DPA and 2-Nitro-DPA also find use as stabilizers. The high electron density on the aromatic rings owing to electron donating amine group leads to a high reactivity of DPA with electrophiles and oxidizing agents. As DPA can form deep-colored blue products upon oxidation it also is used as redox indicator and a testing reagent for different kinds of oxidizing ions such as ClO_3^- and NO_3^- in acidic solution[55]. Noteworthy examples are the historical qualitative assay of nitrate contamination in different crops or its application in testing for gunshot residues[56]. This use also extends to organic nitrate esters[57]. DPA has been recommended as a nondestructive testing reagent for NC in exhibition pieces for museums[58]. Another common use of DPA is in the so called Dische test for DNA. In this reaction DPA reacts with carbonyl compounds that are generated from desoxyribose in acidic solution (purpordedly ω-hydroxylevulinyl aldehyde), thus forming a blue quinonoid product in the presence of DNA[59]. DPA naturally occurs in some plants like onions ($\sim$1% of extract) or green tea (up to 2% of extract) and has been found to act as a potent hypoglycemic drug, meaning that it can effectively lower blood glucose levels[60]. In higher doses DPA poses a risk to human health, with exposure potentially causing eczema formation, hypertension and bladder diseases[61].
Typically, about 1 mass-% DPA is added to NC as stabilizer, corresponding to approximately one stabilizer molecule per 50 NC-units[62]. It is not unusual to find uneven distributions of stabilizer throughout propellant mixtures. In practice the migration of P and stabilizer molecules through diffusion has been found to counteract this inhomogeneity and prevent serious adverse effects on the stability of propellants. Due to its relatively low melting point of 53-54°C DPA is present as a liquid in most I-HFMC experiments[63]. As a matter of fact, it has been shown that even at lower temperatures most of the stabilizing reactions take place in eutectic mixtures that consist of a wide range of stabilizer and non-stabilizer species[64].

5.2 Stabilizer reactions

The major role of DPA in stabilizing NC lies in its ability to bind NO_x and acids that form in the first stages of the decomposition of NC. The products associated with this process include 4-Nitro-DPA ($4NO_2$-DPA), 2-Nitro-DPA ($2NO_2$-DPA), Nitroso-DPA (NNO-DPA) and a slew of multisubstituted derivatives. Figure 16 shows the structures of the up to doubly substituted derivatives.

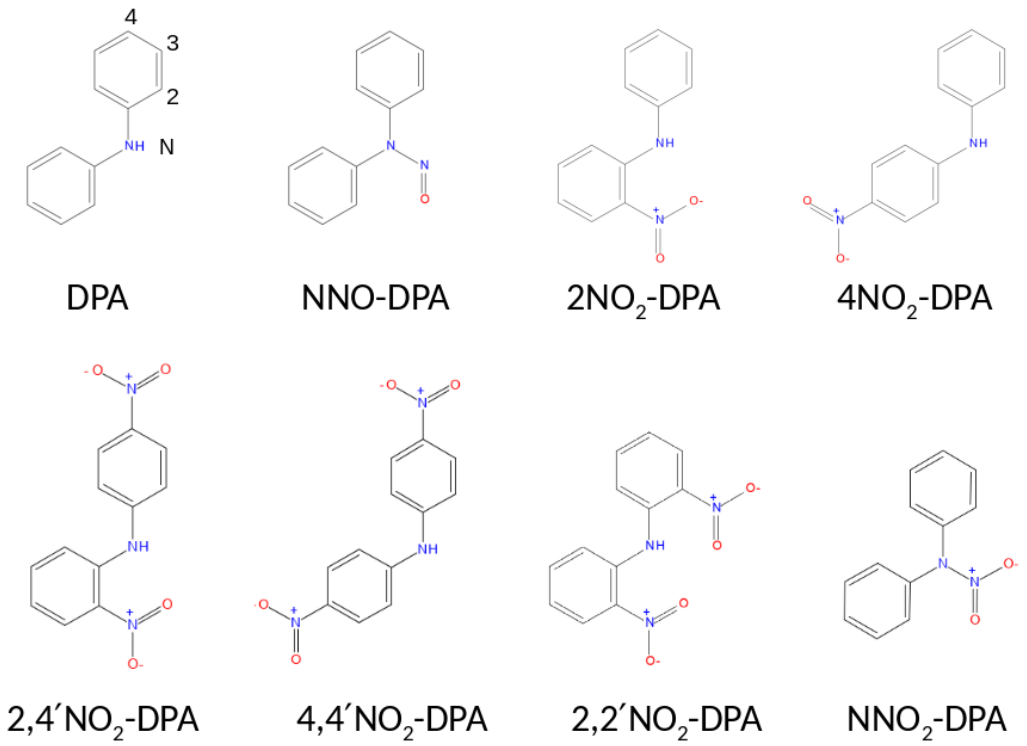

Figure 16: Products of stabilizer reactions of DPA with NC.

Up to sixfold nitration of the two phenyl rings, i.e. in the form of 2,2',4,4',6,6'NO_2-DPA (hexanitro-DPA) has been reported; this compound has been found to further decompose e.g. yielding picric acid. Figure 17 shows the mass-percentages of DPA, NNO-DPA and the sums of all species up to mono-, di- or even tri-substituted DPA's in DPA-stabilized NC at 90°C. The sum up to dinitro-DPA for example includes the amounts of all of the compounds shown in Figure 16. As the concentration of DPA quickly drops off, most of

this DPA is initially transformed to NNO-DPA. Over time more mono-nitro-DPA's, than di-nitro-DPA's and finally tri-nitro-DPA's (not shown in Figure 16 but treated in section 5.5) are encountered. Note however, that although the substituted DPA's have a higher molar mass, the overall mass-percentage of stabilizer accounted for by any of these curves gradually decreases over time. In fact, only about 50% of the DPA present in the beginning can be accounted for by combining the concentrations of nitro- and nitroso-DPA products. A stabilizer loss of ca. 25% associated with the first reactions involving DPA alone[65]. The ca. 50% of DPA that are unaccounted for must partake in other reactions, which have not been ascertained conclusively. In this section a number of potential reaction pathways leading to the known derivatives of DPA are evaluated.

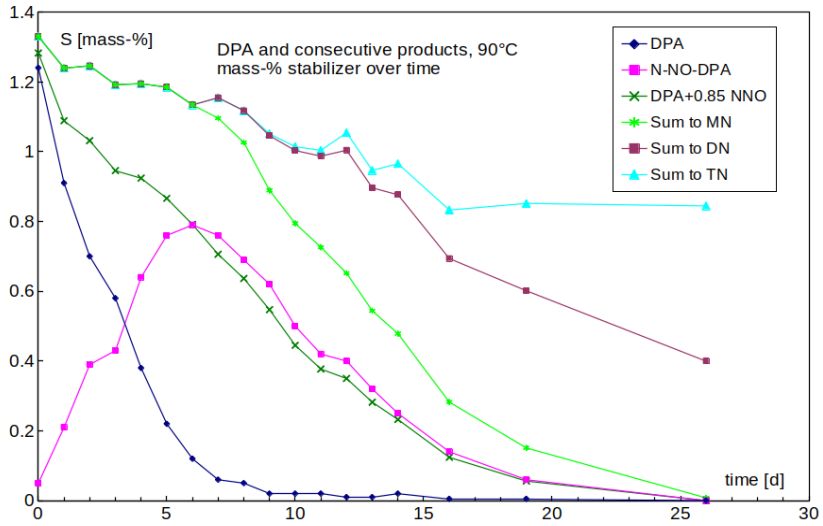

Figure 17: Experimental stabilizer derivative concentrations in mass-% in DPA-stabilized propellant at 90°C[7].

5.2.1 Reactivity and overall favorability

DPA has essencially four chemically different positions bearing hydrogen atoms which could be involved in substitution reactions: N, 2, 3 and 4 as shown in Figure 16. One way to assess the reactivity of each of these is to compute and compare the homolytic bond dissociation enthalpies as shown in Table 8.

Table 8: Computed DPA N-H and C-H bond dissociation enthalpies at 90°C in NC simulate.

Position	N	2	3	4
Δ_{bond}H [kJ mol^{-1}]	357.6	471.3	466.0	471.2

The N-H bond is evidently the weakest, while the three C-H bonds are about 110 kJ mol^{-1} stronger and within 1% of one another. The computed value of 357.6 kJ mol^{-1} is also in good agreement with the experimental value of 364.8 kJ mol^{-1}[42]. This implies that the N-position in DPA should be the most reactive by a wide margin and attacked preferentially over the other positions in most reactions.

For a single substitution by *P*, in principle eight products are possible: NNO-DPA, DPA nitramide NNO_2-DPA, 2/3/4NO_2-DPA and nitroso-DPA derivatives 2/3/4NO-DPA. The nitroso compounds can form according to reactions (IIa) and (IIb). The equations are written in a general form with x = 2,3,4 or N. While no nitroso besides NNO-DPA compounds have been detected in NC stabilized with DPA, the possibility of such compounds acting as intermediates cound not be denied conclusively. It is possible that following their formation they are quickly oxidized by oxygen or other oxidizing agents. For the nitro/nitramide compounds two net formation reactions (Ia) and (Ib) are assumed. The reactions of types (IIa) and (IIb) include HNO_2 as an educt. As has been shown in section 4.1 HNO_2 is present in only small quantities in *P*. Reactions (Ia) and (IIa) are accordingly much more probable and meaningful. The nitrosation of amines usually involves the electrophilic attack of a nitrosonium ion, which is generated in situ from HNO_2 in acidic solution or in a concerted reaction with N_2O_3[66]. The thermodynamic data for the overall reactions is summarized in Table 9.

$$\mathrm{DPA} + 2\,\mathrm{NO_2} \longrightarrow \mathrm{HNO_2} + \mathrm{xNO_2{-}DPA} \qquad \text{(Ia)}$$

$$\mathrm{DPA} + \mathrm{NO_2} + \mathrm{NO} \longrightarrow \mathrm{HNO_2} + \mathrm{xNO{-}DPA} \qquad \text{(Ib)}$$

$$\mathrm{DPA} + \mathrm{HNO_2} + \mathrm{NO_2} \longrightarrow \mathrm{H_2O} + \mathrm{NO} + \mathrm{xNO_2{-}DPA} \qquad \text{(IIa)}$$

$$\mathrm{DPA} + \mathrm{HNO_2} \longrightarrow \mathrm{H_2O} + \mathrm{xNO{-}DPA} \qquad \text{(IIb)}$$

Each of these reactions is exergonic and therefore would be thermodynamically favorable. Among the four positions substitutions on the 2- and 4-positions are the most favorable and their products are the most stable; for

Table 9: Computed enthalpies and Gibbs free energies for reactions of DPA with P at 90°C.

Product	reaction	Δ_rH [kJ mol^{-1}]	Δ_rG [kJ mol^{-1}]
NNO_2	(Ia)	-86.7	-20.7
$2NO_2$		-162.4	-91.5
$3NO_2$		-160.3	-94.3
$4NO_2$		-172.2	-104.0
NNO_2	(IIa)	-50.2	-37.4
$2NO_2$		-125.9	-108.2
$3NO_2$		-123.8	-111.0
$4NO_2$		-135.7	-120.7
NNO	(Ib)	-87.3	-26.1
2NO		-102.7	-38.4
3NO		-84.1	-28.8
4NO		-100.4	-38.8
NNO	(IIb)	-50.7	-42.9
2NO		-66.2	-55.2
3NO		-47.6	-45.5
4NO		-63.9	-55.5

the nitroso compounds the difference in stability relative to the less stable NNO-DPA and 3NO-DPA is only on the order of 10-15 kJ mol^{-1}, while among the nitro/nitramine compounds the aromatic nitro derivatives are on about equal footing with the nitramine being less favorable by more than 70 kJ mol^{-1}. The overall tendency from the combination of bond dissociation enthalpies and free reaction energies point towards a high reactivity and lower energy barriers for the amine group while the aromatic nitro compounds are overall the more stable and desirable configurations. This overall trend dictates the reactivity of DPA towards P and serves as a guideline for the considered reaction pathways.

5.2.2 Radical substitution

First a radical mechanism is considered. A direct abstraction of a hydrogen atom from DPA by a molecule of NO_2 or HNO_2 is followed by the recombination with an equivalent of NO_2 or NO leading to the nitro or nitroso compounds. The first step involves the cleavage of fairly stable N-H or C-H

bonds and is endergonic. This step is hence the rate determining one. It has been found that for these radical reactions no transition state accompanying a activation barrier could be found. The overall activation energy is therefore assumed to be just the Δ_rG for the following reactions:

$$\mathrm{DPA} + \mathrm{NO_2} \longrightarrow \mathrm{HNO_2} + \text{rad-DPA} \quad \text{(Ic)}$$

$$\mathrm{DPA} + \mathrm{HNO_2} \longrightarrow \mathrm{H_2O} + \mathrm{NO} + \text{rad-DPA} \quad \text{(IIc)}$$

Table 10: Computed enthalpies and Gibbs free energies for reactions of DPA with P at 90°C.

Product	reaction	Δ_rH [kJ mol^{-1}]	Δ_rG [kJ mol^{-1}]
N-rad	(Ic)	34.4	35.5
2-rad		148.1	144.4
3-rad		142.8	139.9
4-rad		148.1	143.9
N-rad	(IIc)	70.9	18.8
2-rad		184.6	127.7
3-rad		179.4	123.2
4-rad		184.6	127.2

The data in Table 10 shows that N-rad-DPA is by far the most stable of the four radicals. This is to be expected as it is the only mesomerically stabilized radical with good delocalization of the unpaired electron. The exceedingly low free activation energies for the formation of this radical makes this reaction very fast compared to other processes in the decomposing NC. The activation energies for the other positions are, albeit higher than for N-H, still low enough to allow for the rections to occur to some extent. There are, however, two cogent arguments to be made why radical reactions must only occur with N-H. Both are based on the presence or otherwise of certain products. For one, a radical substitution does not favor the 2 and 4 positions of the aromatic ring due to the lack of mesomeric stabilization. In fact the free activation energy for the H-abstractions from the 3 position of the ring is lower than of the other two aromatic positions. One would then expect that in at least as much 3NO_2-DPA should be formed as 2NO_2-DPA or 4NO_2-DPA. 3NO_2-DPA has not been claimed to have been found as one of the products of DPA nitration in NC, thus making this mechanism unlikely. The prevalence of ortho/para products points towards an electrophilic

aromatic type substitution. Additionally, 2-rad-DPA should undergo an intramolecular ring formation yielding carbazole. The ring formation has a low barrier and is unimolecular so that 2-rad-DPA would be expected to turn into carbazole long before it could encounter a second molecule of *P*. The fact that a significant amount of $2NO_2$-DPA is found further repudiates a radical mechanism for the aromatic ring nitrations. The carbazole-forming reaction is further discussed in section 5.3.

There is one more option for the a radical substitution mechanism which is more in line with DFT data and substitution patterns of the observed products. As was previously established, the first and most likely product of the interaction of DPA with NO_2 is the DPA-N radical, i.e. DPA missing the aminic H. This radical is particularly stable due to the delocalization of the unpaired electron. However, this delocalization has one more consequence: The inclination to pair up and form a new bond with a second molecule of NO_2 or other radicals is proportionate to the local spin density. A delocalized electronic spin means that even DPA-Nrad can be attacked in positions other than the N atom. The excess spin density can be interpreted as the difference between the local electron density of spin up (alpha) and spin down (beta) electrons. The three-dimensional spin density can be projected onto a two-dimensional contour plot. Figure 18 shows the isosurface where the excess spin density of the DPA-N radical at a value of 0.005.

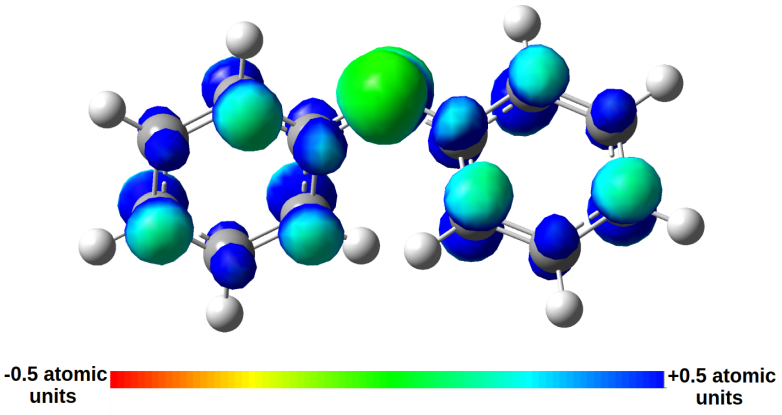

Figure 18: Spin dencity isosurface (density=0.005) in DPA-N racidal with colored electrostatic potential between -0.5 and +0.5 atomic units.

The isosurface is additionaly colored to show the local electrostatic potential at on the isosurface. A high potential is indicative of a low local total electronic density and the other way around. While the atom bearing the highest spin denisty is the aminic nitrogen, it is evident that the spin density is significantly delocalized onto C-atoms of the phenyl rings. The spin density is, however, not spread out evenly over the rings. The 2- and 4-positions of the aromatic rings have more of the spin density than the 1-position (ipso) and the 3-positions. Additionally, their electrostatic potential is lower, showing that the 2- and 4-positions in the radical are more susceptible to a attack by an electrophilic radical. This means that after the abstraction of a hydrogen atom from the weak N-H bond, a radical like NO_2 can also attack the 2- and 4-positions of the aromatic rings. The products of such an attack are shown in as (a) and (b) in Figure 19. These structures are tautomers of $2NO_2$-DPA and $4NO_2$-DPA which can rearrange into these via a proton-shift. A structure analogous to these two also exists as a $3NO_2$-DPA tautomer. However, it was found that that structure only represents a local energetic minimum. Structure (c) in Figure 19 instead shows the true energetic minimum. The addition of a NO_2 to the 3-position of one of the aromatic rings leads to the formation of a new bond between two of the ring's carbon atoms. This leads to a substituted bicyclo[3.1.0]hex-2-ene and the irreversible loss of aromaticity. Such a structure is unfavorable and unlikely to form compared to the structure (a) for instance, structure (c) is energetically disadvantageous by $\Delta_r H^\circ = 93.0$ kJ mol^{-1} and $\Delta_r G^\circ = 96.3$ kJ mol^{-1}. The chemical equations for the formation of these intermediates are:

DPA-N·rad.+NO_2 $\longrightarrow$ $2NO_2$-DPA-tautomer (a) with $\Delta_r H^\circ = -61.4$ kJ mol^{-1}

DPA-N·rad.+NO_2 $\longrightarrow$ $3NO_2$-DPA-tautomer (c) with $\Delta_r H^\circ = +31.7$ kJ mol^{-1}

DPA-N·rad.+NO_2 $\longrightarrow$ $4NO_2$-DPA-tautomer (b) with $\Delta_r H^\circ = -73.5$ kJ mol^{-1}

These reactions have a $\Delta_r G^\circ = 0.7$kJ mol^{-1} in the case of the $2NO_2$-DPA-tautomer, $\Delta_r G^\circ = 97.0$ kJ mol^{-1} for the $3NO_2$-DPA-tautomer and $\Delta_r G^\circ =$ -9.9 kJ mol^{-1} for the $4NO_2$-DPA-tautomer at 90°C in NC simulate. Relative to $2NO_2$-DPA, the tautomer (a) has a $\Delta_r H^\circ = 135.4$ kJ mol^{-1} and $\Delta_r G^\circ =$ 127.7 kJ mol^{-1}. For (b), the $4NO_2$-DPA tautomer, $\Delta_r H^\circ = 133.0$ kJ mol^{-1} and $\Delta_r G^\circ = 129.6$ kJ mol^{-1} relative to $4NO_2$-DPA. For the hypothetical $3NO_2$-DPA intermediate, $\Delta_r H^\circ = 226.4$ kJ mol^{-1} and $\Delta_r G^\circ = 226.8$ kJ mol^{-1} relative to $3NO_2$-DPA. This would explain why only $2NO_2$-DPA and $4NO_2$-DPA are experimentally detected rather than $3NO_2$-DPA.

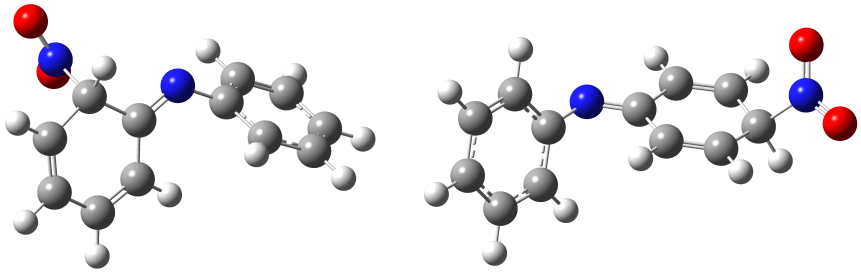

(a) $2NO_2$-DPA precursor

(b) $4NO_2$-DPA precursor

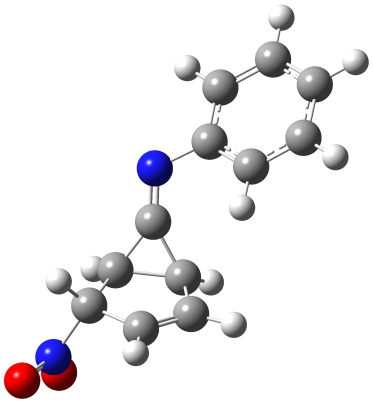

(c) Hyoothetical $3NO_2$-DPA precursor

Figure 19: Optimized structures of tautomers of nitro-DPA's which are proposed to exist as intermediates during a radical substitution by NO_2.

To summarize, a radical substitution mechanism makes sense for the N position of DPA and can account for a fast build-up of NNO-DPA. A direct radical substitution of the hydrogen atoms on the aromatic rings is highly unlikely. Rather, mechanism involving an intermediate DPA-N radical and tautomers of $2NO_2$-DPA and $4NO_2$-DPA can account for reasonably low activation energies and the observed substititution pattern. It thus stands to argue that it is this latter mechanism of nitro-DPA formation can be presumed to be the prevailing reaction pathway under conditions where water is a limiting factor and little HNO_3 can be found.

5.2.3 Electrophilic aromatic substitution

Aromatic nitrations are typically performed with a mixture of concentrated HNO_3 and H_2SO_4 (nitrating acid mixture) or the stronger N_2O_5 as the nitrating agent. The mechanism for this reaction is an archetypal electrophilic aromatic substitution (S_{EAr}). In both reagents the active species is the nitronium cation NO_2^+ which attacks electron rich (activated) aromatic systems as an electrophile. This reactiong is known to go through an intermediate carbocation/arenium form, often called σ- or *Wheland-complex*. The ring's aromacity is temporarily lost in the σ-complex form before being restored by deprotonation. As demonstrated in section 4.1, HNO_3 is a major component of *P*. The Δ_rG for reaction 1 in Figure 7, the formation of N_2O_5 from HNO_3, was found to be 58.8 kJ mol^{-1}. Depending on outside conditions N_2O_5 can make up anywhere up to 0.16% of free nitrogen species. N_2O_5 can act as a source of NO_2^+: In this context it can be seen as an loosely bound aggregate of nitronium and nitrate. Two minimum energy structures have been found for N_2O_5, shown in Figure 20.

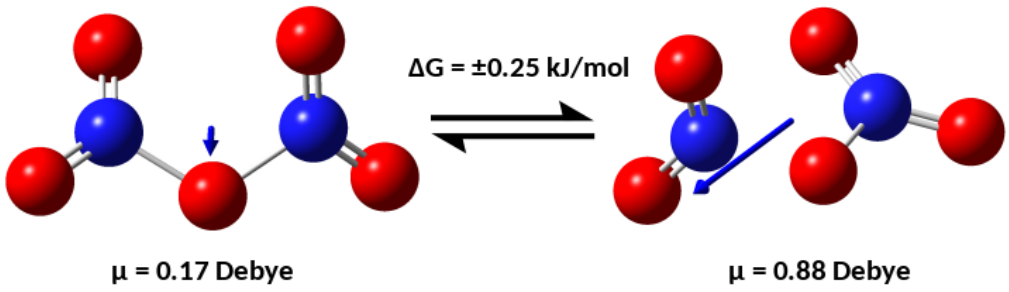

Figure 20: N_2O_5 minimum geometries and blue dipole vectors.

These two structures are within 0.25 kJ mol^{-1} of each other in the ief-PCM NC simulate, i.e. equal in energy within the expected precision of the computation. One is a molecular form with C_2 symmetry and a low dipole moment. The other is a strongly polarized form with C_s symmetry and a much higher dipole moment of 0.88 D, indicating a significant charge separation between the preformed nitronium and nitrate ions. The stabilization of charge imbalances compared to the gas phase is indeed one of the most noticable effects of the used PCM model. The stability of predissociated

form is suggestive of the generally low energy of dissociacion of N_2O_5 in NC: $N_2O_5 \rightleftharpoons NO_2^+ + NO_3^-$ has a $\Delta_r G^\circ = 115.4$ kJ mol^{-1}, thus being a viable source of nitronium.

It thus stands to argue that an S_{EAr} mechanism could likely be responsible for the nitration of the aromatic rings of DPA. Different from the radical mechanism, which does not particularly favor any of the aromatic ring's hydrogens, S_{EAr} has a clear preference for positions 2 and 4 due to the ortho/para directing influence of the amine group. Hence the observed substitution pattern in DPA is consistent with this reaction type. The search for tranistion states for the nitration with NO_2^+ determined the absence of energetic barriers; instead the NO_2^+ is consistently attracted to DPA down to an energetic minimum, a σ-complex. No transition states involving nitration with N_2O_5 itself were found either. The σ-complexes that lead to $2NO_2$-DPA and $4NO_2$-DPA are shown in fig. 21. The formation reaction of these complexes starting from DPA and N_2O_5 can be written as:

$$\text{DPA} + N_2O_5 \longrightarrow NO_3^- + \sigma\text{-complex}^+$$

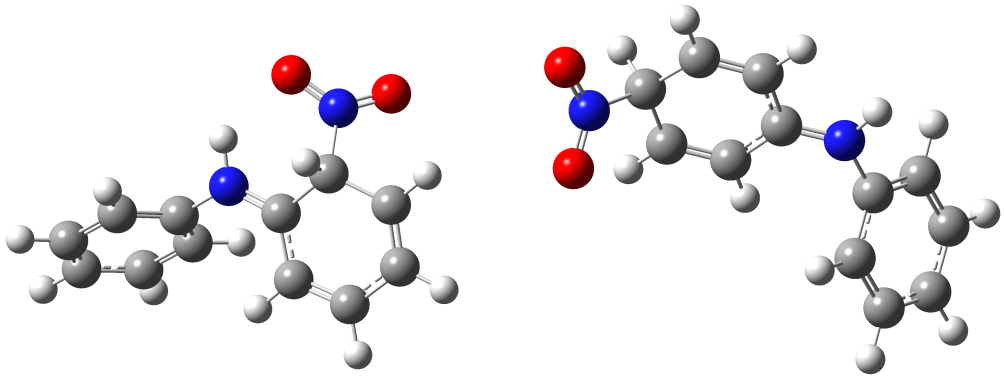

Figure 21: Optimized structures of arenium ion intermediates for nitration of $2NO_2$-DPA (left) and $4NO_2$-DPA (right).

The reaction Gibbs free energies for this reaction in NC simulate are $\Delta_r G^\circ_{4N}$ = -20.7 kJ mol^{-1} and $\Delta_r G^\circ_{2N} = 4.3$ kJ mol^{-1}. A relaxed scan using ωB97X-D/6-31G* was performed starting from the σ-complex leading to $4NO_2$-DPA. This means that, aside from the scan coordinate, a geometry optimization was performed at every step of the scan. As the scan coordinate the C-N bond between the nitro group and phenyl ring was chosen. The resulting

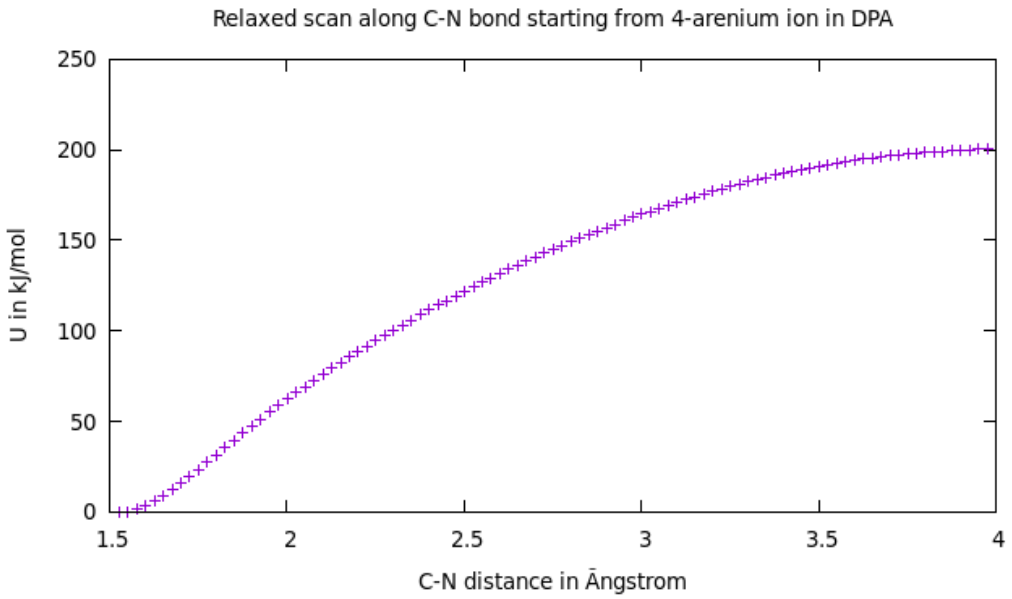

Figure 22: Electronic energy curve, relative to 4-arenium/ Wheland-complex, for relaxed scan along 4C-NitroN bond.

internal energy (not including zero point energy) curve relative to the energy minimum is depicted in Figure 22. The curve shows no maxima along the scan coordinate indicating no energy barriers for this reaction. The potential is reminiscent of a Morse-potential. The σ-complex for $2NO_2$-DPA gives an analogous result. The overall activation energy then amounts to approximately the energy cost of generating the NO_2^+ ion in situ, so that $\Delta_r G^\ddagger = 115.4$ kJ mol^{-1} starting from N_2O_5 or $\Delta_r G^\ddagger = 174.2$ kJ mol^{-1} starting from HNO_3. The net chemical equations for nitration reactions with HNO_3 and N_2O_5 along with their reaction enthalpies in NC simulate are given as:

$$\text{DPA} + \text{HNO}_3 \longrightarrow 2\text{NO}_2\text{-DPA} + \text{H}_2\text{O} \text{ with } \Delta_r H^\circ = -124.9 \text{ kJ mol}^{-1}$$

$$\text{DPA} + \text{HNO}_3 \longrightarrow 4\text{NO}_2\text{-DPA} + \text{H}_2\text{O} \text{ with } \Delta_r H^\circ = -134.7 \text{ kJ mol}^{-1}$$

$$\text{DPA} + \text{N}_2\text{O}_5 \longrightarrow 2\text{NO}_2\text{-DPA} + \text{HNO}_3 \text{ with } \Delta_r H^\circ = -185.2 \text{ kJ mol}^{-1}$$

$$\text{DPA} + \text{N}_2\text{O}_5 \longrightarrow 4\text{NO}_2\text{-DPA} + \text{HNO}_3 \text{ with } \Delta_r H^\circ = -195.0 \text{ kJ mol}^{-1}$$

As DPA is a base, can also be protonated in the presence of HNO_3, yielding diphenylammonium nitrate. One study has found this diphenylammonium nitrate salt to melt at 52°C and decompose to carbon and unidentified

gaseous products at higher temperatures[67]. It is not clear if and how much of an effect this reaction has on the stabilization process. As the protonation decreases the electron density of the phenyl rings, a protonation could significantly decrease the reactivity of DPA towards *P*.

5.2.4 Intramolecular rearrangements

In addition to the aromatic rings themselves, the amine group can also react with nitronium. This reaction was also found to have no discernable energy barrier. A direct reaction with HNO_3 akin to an esterification would also be possible, in each case leading to NNO_2−DPA. NNO_2−DPA can also be formed in the reaction of NNO-DPA with N_2O_5, and has been suggested to be an intermediate during the formation of $2NO_2$-DPA[68]. This nitroamine intermediate is not very stable compared to $2NO_2$−DPA and $4NO_2$−DPA as has been pointed out in section 5.2.1. At temperatures as low as 46°C it was found to decompose to $2NO_2$−DPA and $4NO_2$−DPA in a matter of days[69]. NNO_2−DPA has not been detected in significant amounts in DPA-stabilized NC samples, but in may act as a short lived intermediate. There are many known intramolecular rearrangements of aromatic nitro- and nitroso compounds such as the Fischer-Hepp reaction or the acid-catalyzed nitramine rearrangement[70]. Numerous variations of such a process are conceivable: Different migrating species (NO_2, NO_2^+, NO, NO^+, etc.), optional intermediate steps (e.g. protonation) and even intermolecular migrations are just some of the alterations. No transition state for a direct transfer of the NO_2 group from the N-atom to the 2- or 4-positions of one of the aromatic rings has been found. One example of a NO_2-rearrangement mechanism which involves different intermediates is shown in Figure 23. In this reaction NNO_2-DPA is protonated on the aminic N. The weakened N−NO_2 bond breaks and a N-nitrite intermediate is generated. In a second rearrangement step the N-nitrite binds to the 2-position of one of the aromatic rings, yielding the carbenium complex from Figure 21. A deprotonation leads to $2NO_2$-DPA. The protonated NONO-DPA was computed to be less stable than the protonated NNO_2-DPA by $\Delta_r H^\circ = 74.4$ kJ mol^{-1} and $\Delta_r G^\circ = 73.6$ kJ mol^{-1}. No transition state between the two forms has been found; it would be expected to involve the coordination of the aminic nitrogen atom by a total of five atoms. Such geometries are generally non-rigid and subject to pseudorotations, which may be one of the reasons for the difficult search. Interestingly, the protonation destabilizes the N-nitrite form more than the NNO_2-isomer.

In unprotonated NNO_2-DPA, the N-nitrite form has a $\Delta_r H^\circ$ of only 53.5 kJ mol^{-1} and $\Delta_r G^\circ = 48.9$ kJ mol^{-1} relative to the NNO_2-form. The role of the protonation therefore is not to make the N-nitrite form more favorable. Instead, the protonation loosens the N-N bond and presumably lowers the energy barrier. As it is already loosely bound, little additional energy should be necessary to transfer the NO_2-group from the N-atom. An extensive study of the numerous variations of these pathways would be required to satisfactorily determine the most favorable ones.

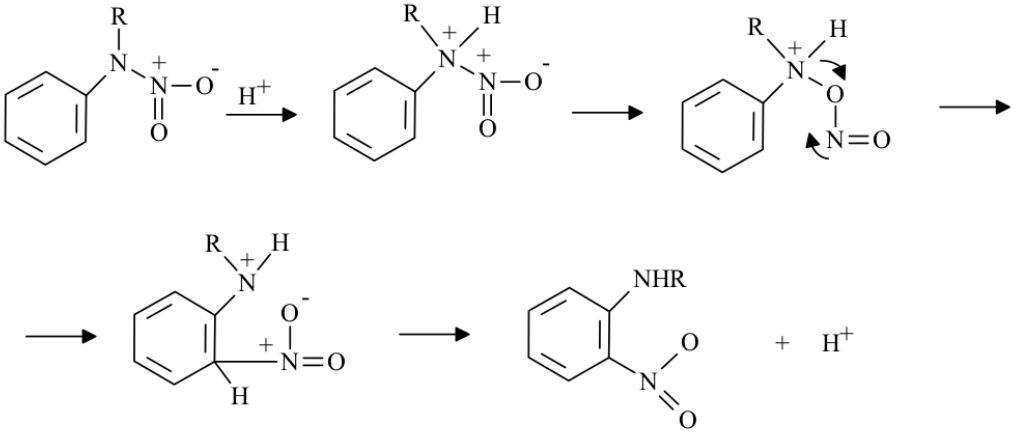

Figure 23: Proposed mechanism of a rearrangement of NNO_2-DPA to $2NO_2$-DPA from literature[69].

5.3 Other reactions and products

Attempts to extract the stabilizer with a suitable solvent at different stages of the decomposition process have demonstrated that, accounting for all compounds, i.e. DPA and its nitroso and nitro derivatives as discussed in the previous section, typically only about 55-65% of the stabilizer could be recovered. Some possible side reactions to attribute for the missing 35-45% to are suggested[71].

5.3.1 Carbazoles

At elevated temperatures carbazole (CAR) (Figure 24) is known to form from DPA, particularly at elevated temperatures in the presence of oxygen.

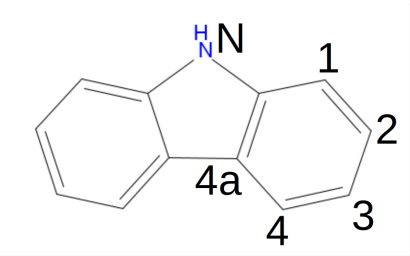

Figure 24: Structure of carbazole and numbering of positions.

The formation of CAR is known to proceed both photochemically[72] and thermally; in the latter case it can be carried out by heating DPA to around 350°C for 2 hours in the presence of a catalytic amount of iodine[73]. The high reaction temperature is a consequence of the large activation energy: The reaction is claimed to involve an intermediate as shown in Figure 25, the formation of which requires the breaking of the aromaticity of both phenyl groups. The iodine reacts with the intermediate to form CAR and HI, and is then reoxidized and recovered by atmospheric oxygen. The formation of the intermediate was computed to have a $\Delta_r G^\circ = 320.0$ kJ mol^{-1} in NC simulate relative to DPA at 90°C, with the transition state even higher. The temperature required for this reaction is higher than the autoignition temperature of NC, so that this direct mechanism is not available to DPA in propellants.
Instead, there are other pathways by which CAR could be formed from DPA. One example is given in Figure 26. In section 5.2.2 the abstraction of hydro-

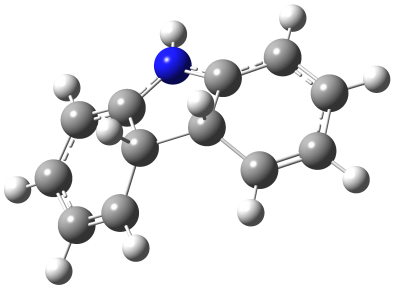

Figure 25: Structure of intermediate of the thermal reaction of diphenylamine to carbazole.

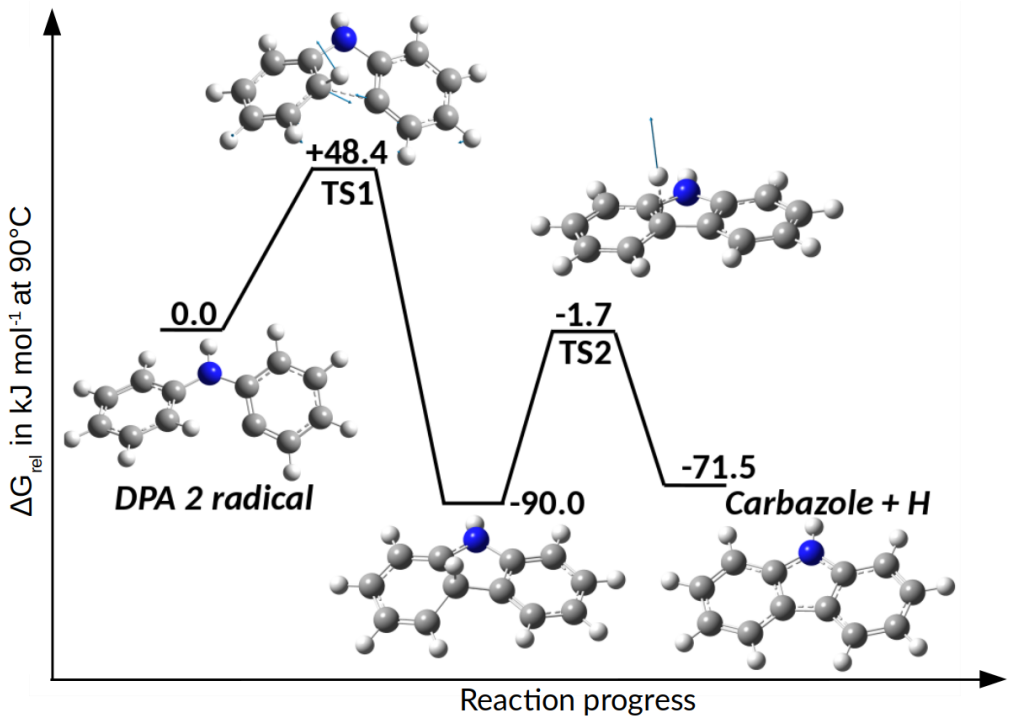

Figure 26: Gibbs free energy along reaction coordinate for the reaction of DPA-2· radical (missing H on 2-position of an aromatic ring) to carbazole with optimized geometries and tranisition states (imaginary vibration mode arrows in blue).

gen atoms from DPA by radicals has been discussed. The Gibbs free energy for the DPA-2· radical (missing H on 2-position of an aromatic ring) from DPA and NO_2 has was computed to have a $\Delta_r G^\circ$ = 127.7 kJ mol^{-1}. The resulting radical is highly unstable due to the lack of stabilization of unpaired electron in the sp^2 hybrid orbital and can forms a new C-C bond between the C with the unpaired electron and a C-atom in the 2-position of the other ring. The creation of this new bond was calculated involve a TS with a much lower barrier of $\Delta_r G^\ddagger$ = 48.4 kJ mol^{-1}. The resulting intermediate retains one aromatic ring and is thus more favorable than the intermediate in Figure 25. The excess H-atom has a very low bond dissociation enthalpy of 55.7 kJ mol^{-1} and can easily be abstracted by *P* or oxygen. If any DPA-2· radicals are produced from DPA and *P*, they should transform to CAR via this unimolecular bond-forming reaction almost instantaneously. The formation of CAR from the DPA-2· radical is favored so much, that even the reaction to CAR and a monoatomic hydrogen would be exergonic with $\Delta_r G^\circ$ = -71.5 kJ mol^{-1}. As discussed previously, the postulation of such a mechanism with radicals like DPA-2· has a few issues. The presence of the much more weakly bound aminic H, which would be removed preferentially, means that in total only a small, maybe even undedectably small amount of CAR would be formed in this manner. Furthermore, if the DPA-2· radical were to be formed, nothing should prevent a DPA-3· from being occuring. This radical would further react to e.g. experimentally unobserved 3NO_2-DPA. This also suggests that this mechanism very rare, if it occurs at all.

There are numerous other potential mechanisms, however. For instance, DPA has been reported to quantitatively transform into the cation of intermediate from Figure 25 in certain Faujasite type zeolites at temperatures much lower than in the direct thermal reaction over the course of a few hours[74]. The reaction has been associated with Brønsted/Lewis acid/base sites in the host material, all of which can be found in the decomposing NC. An intermediate is the formation of a DPA-cation.

The heterocycle carbazole is has also been investigated as an stabilizer for NC, where it generally shows analogous reactions to DPA (Figure 27). The initial products are NNO-CAR (9-Nitroso-CAR) in analogy to NNO-DPA, 1NO_2-CAR and 3NO_2-CAR. Compared to DPA, a much smaller fraction of CAR is converted to NNO-CAR. The concentration of NNO-CAR also peaks at a time when more than half of the original CAR is still present. This may point to a lower relative stability of NNO-CAR due to the constraint placed on the molecule's geometry by the additional bond. In CAR 3NO_2-CAR is

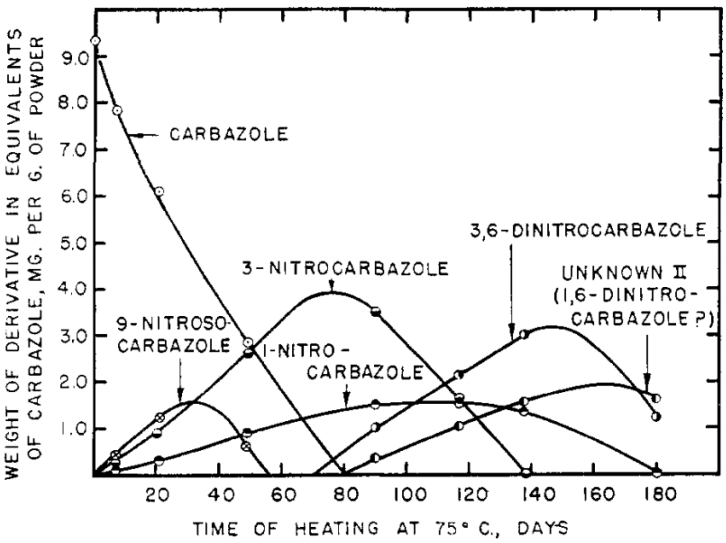

Figure 27: Concentrations of carbazole and its nitroso- and nitro-products in carbazole-stabilized C-390 propellant at 75°C[75].

preferentially formed over $1NO_2$-CAR, compared to DPA where these $2NO_2$ -DPA and $4NO_2$-DPA are formed in comparable quantities. The fact that DPA has twice as many equivalent ortho-positions to the amine group may contribute to this. Dinitro-CAR's have also been found in analogy to dinitro-DPA's in the carbazol-stabilized propellant sample.

5.3.2 Reactions with aldehydes

Nitrogen compounds are not the only products of the degradation of NC. Reactive aldehydes that are produced in the degradation process can also react with DPA. The reaction of DPA with formaldehyde is of particular interest. Depending on the relative amounts and concentrations of the reagents, the reaction of DPA with formaldehyde can form different structures ranging from oligomers to networklike aminoplast resins[76]. The reaction is poorly studied in the context of DPA-stabilized propellants and could account for at least a portion of the missing DPA. The first step of the reaction, the condensation of two molecules of DPA to N,N,N',N'-tetraphenyldiaminomethane (Figure 28) was computed to be exothermic with $\Delta_r H^\circ = -67.1 \text{kJ mol}^{-1}$ and slightly exergonic with $\Delta_r G^\circ = -5.6 \text{kJ mol}^{-1}$ at 90°C with ωB97X-D/6-31++G(d,p).

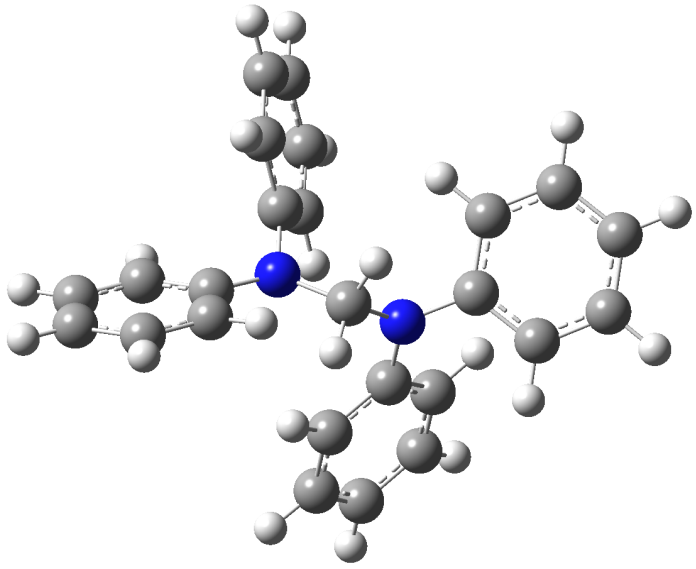

Figure 28: N,N,N',N'-tetraphenyldiaminomethane, one of the initial products of the reaction between DPA and formaldehyde.

5.4 DPA acceleration

Stabilizers are added to propellants to slow down degradation processes. While more reactive stabilizers are more efficient at destroying P and free radicals, there are known cases of stabilizers being incompatible with specific energetic materials. The introduction of an incompatible stabilizer may reduce the shelf life of a propellant and increase its sensitivity to heat. One study found that some aniline-based stabilizers like N-(2-acetoxymethyl)-p-nitroaniline (ANA) show an incompatibility with NC, while DPA was deemed to be compatible with NC[77]. Some other studies, on the contrary, have claimed the opposite.U nstabilized NC has been reported to remain virtually unaffected by exposure to a temperature of 80°C for over four weeks[78]. This unexpected stability of unstabilized NC compared to propellants stabilized in particular with DPA has lead to the introduction of the term "DPA acceleration", refering to the accelerated degradation of NC in the presence of DPA. One of the proposed mechanism for this involves a nucleophilic attack by the basic free electron pair of the amine group of DPA on a nitrate ester of NC, leading to the formation of NNO_2-DPA in a process similar to a

reesterification[69]. Based on ESR measurements, a different mechanism has been proposed: Nitrate esters, including NC, are known form charge transfer complexes with aromatic amines as electron donors[79]. The formation of such a electron donor-acceptor complex between DPA and the nitrate ester groups of NC has been proposed to exist in propellant mixtures[80]. The transfer of electron density to the nitrate ester groups has been associated with accelerated decomposition of NC and thereby been declared a potential mechanism of DPA acceleration[78]. This trend was confirmed with DFT computations. ESR measurements (Figure 29) shows the intensity of the ESR signal, which is proportional to the number of free radicals in a substance, over time in a decomposing DPA-stabilized propellant sample.

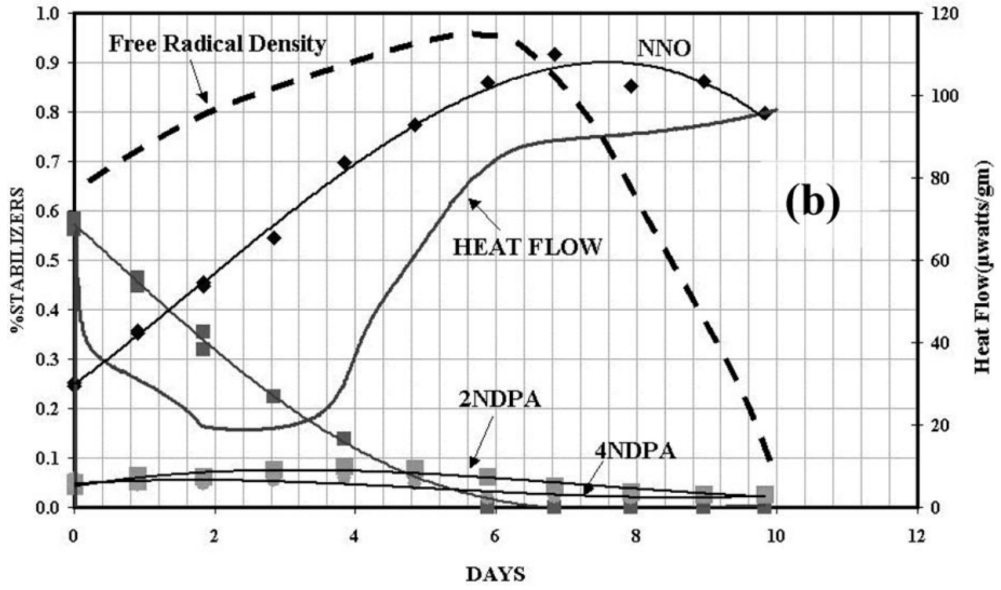

Figure 29: Heat flow curve, stabilizer mass-% and electron spin resonance signal curves for DPA-stabilized WC867 double-base propellant sample at 80°C[78]

The number of free radicals was found to gradually increase as DPA is consumed, reaching its peak close to the maximum of the heat flow curve and the peak of the NNO-DPA concentration. This curve shows that reactions and mechanisms involving radicals are undeniably proceeding at least while DPA is present. The formation of the DPA-NC charge transfer complex has been claimed to be one of the main reactions that contribute to this curve.

The formation of the persistent DPA-N-oxide $(Ph)_2NO\cdot$ radical has been proposed to form from DPA and NO_2 in a two-step process: The first step is the abstraction of the losely bound aminic H from DPA by NO_2. The second step is the oxidation of the DPA-N$\cdot$ radical by another molecule of NO_2[80]. The chemical equation for this is:

$$(Ph)_2N\cdot + NO_2 \longrightarrow (Ph)_2NO\cdot + NO \text{ with } \Delta_r H^\circ = -22.4 \text{ kJ mol}^{-1}$$

This reaction is slightly exergonic at 90°C with $\Delta_r G^\circ$=-15.8 kJ mol^{-1}.

5.5 Secondary nitration

Although they are less reactive than DPA due to the electron wihdrawing properties of the nitro group, $2NO_2$-DPA and $4NO_2$-DPA can be nitrated further. Over time up to 6 nitrations per DPA molecule are possible. Every additional nitration decreases the electron density of the aromatic rings making them gradually less likely to participate in an electrophilic aromatic substitution. As a side effect the basicity of the aminic nitrogen decreases with the number of nitro substituents. In mono-nitro DPA's the reduction of electron density is more pronounced on the already nitrated ring, so that the second nitration occurs on the other side. Enthalpies of nitration are calculated for the second nitration step, leading to 2,2'NO_2-DPA, 2,4'NO_2-DPA or 4,4'NO_2-DPA. Starting from $2NO_2$-DPA either 2,2'NO_2-DPA or 2,4'NO_2-DPA can form, while $4NO_2$-DPA can react to 2,4'NO_2-DPA or 4,4'NO_2-DPA. For nitrations with HNO_3 the reaction enthalpies are:

$$2NO_2\text{-DPA}+HNO_3 \longrightarrow 2,2'NO_2\text{-DPA}+H_2O \text{ with } \Delta_r H^\circ = -108.9 \text{ kJ mol}^{-1}$$

$$2NO_2\text{-DPA}+HNO_3 \longrightarrow 2,4'NO_2\text{-DPA}+H_2O \text{ with } \Delta_r H^\circ = -124.2 \text{ kJ mol}^{-1}$$

$$4NO_2\text{-DPA}+HNO_3 \longrightarrow 2,4'NO_2\text{-DPA}+H_2O \text{ with } \Delta_r H^\circ = -114.4 \text{ kJ mol}^{-1}$$

$$4NO_2\text{-DPA}+HNO_3 \longrightarrow 4,4'NO_2\text{-DPA}+H_2O \text{ with } \Delta_r H^\circ = -135.4 \text{ kJ mol}^{-1}$$

The nitration of the 4 position is more exothermic by 15-20 kJ mol^{-1}. A comparison to the nitration enthalpies of DPA shows a trend: The formation of 2,2'NO_2-DPA releases the least heat, more than 15 kJ mol^{-1} less than the nitration of the 2 position of unsubstituted DPA. For the formation of 2,4'NO_2-DPA from $4NO_2$-DPA only about 10 kJ mol^{-1} less are relesaed.

In the case of the formation of 4,4'NO_2-DPA no reduction in heat formation is found. This difference illustrates the spacial reach of the electron withdrawing infulence of the nitro substituents. The spacial proximity of the nitro groups in 2,2'NO_2-DPA leads to the highest destabilization, while the opposite is true for 4,4'NO_2-DPA. The liberated heat continues to drop for additional substitutions. For instance, a third nitration leading to the formation of 2,4,4'NO_2-DPA has $\Delta_r H^\circ$ = -99.8 kJ mol^{-1}:

$$2,4'\text{NO}_2\text{-DPA} + \text{HNO}_3 \longrightarrow 2,4,4'\text{NO}_2\text{-DPA} + \text{H}_2\text{O}$$

The maximum amount of heat which can be generated per mol DPA in this manner is given trough by the following net reaction with sixfold nitration:

$$\text{DPA} + 6\text{HNO}_3 \longrightarrow \text{hexanitro-DPA} + 6\text{H}_2\text{O} \text{ with } \Delta_r H^\circ = -509.7 \text{ kJ mol}^{-1}$$

The average reaction enthalpy per nitro group then is -84.9 kJ mol^{-1}.

Another set of intermediary products of the nitration of DPA are mixed nitro-nitroso compounds. NNO-2NO_2-DPA and NNO-4NO_2-DPA are known to occur around the time when the concentrations of 2NO_2-DPA and 4NO_2-DPA are around their peak. Assuming the reaction leading to these compounds is akin to that of DPA to NNO-DPA the chemical equations can be written as:

$$2\text{NO}_2\text{-DPA} + \text{NO}_2 + \text{NO} \longrightarrow \text{NNO-}2\text{NO}_2\text{-DPA} + \text{HNO}_2$$

$$4\text{NO}_2\text{-DPA} + \text{NO}_2 + \text{NO} \longrightarrow \text{NNO-}4\text{NO}_2\text{-DPA} + \text{HNO}_2$$

The reactions are less exothermic than the analogous reaction with DPA. The reaction to NNO-4NO_2-DPA has $\Delta_r H^\circ$ = -73.1 kJ mol^{-1} at 90°C and that giving NNO-2NO_2-DPA is computed as $\Delta_r H^\circ = -55.5$kJ mol^{-1} at 90°C. The amounts of these two compounds are expected to be highly variable with temperature due to a small Gibbs free energy. For the reaction to NNO-4NO_2-DPA it is still negative with $\Delta_r G^\circ$ = -15.7 kJ mol^{-1} at 90°C, while the reaction yielding NNO-2NO_2-DPA is slightly endergonic with $\Delta_r G^\circ$ = +2.9 kJ mol^{-1}.

6 Akardite II

6.1 Characterization

Akardite (Ak) is the trivial name given to a class of asymmetric diphenylurea derivatives. Unsubstituted N,N-diphenylurea is commonly known as akardite I. Akardite II (N,N-diphenyl-N'-methylurea) and akardite III (N,N-diphenyl-N'-mthylurea) are modified structures of this parent molecule. Their structures are shown in figure 30. The samples studied in this work contain Ak II. Like DPA, Ak II chemically binds *P* and thus suppresses NC degradation. Akardites find widespread use in gun propellants, especially double-base propallants[81].

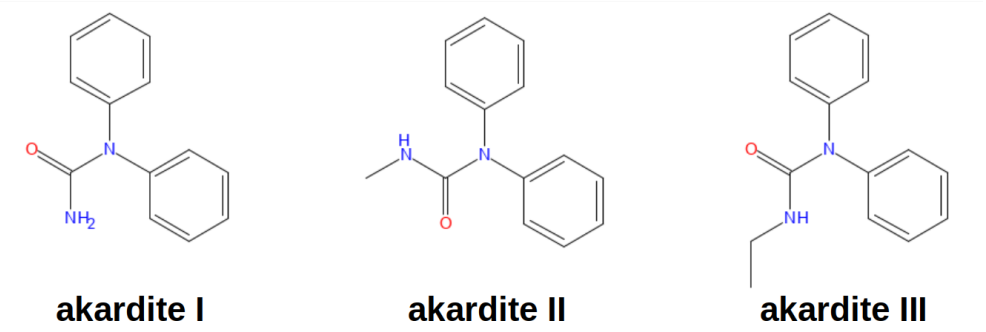

Figure 30: Structures of akardite I (left), akardite II (center) and akardite III (right).

One study using scanning electron microscopy (SEM) and energy-dispersive X-ray spectrometry (EDX) to map out microstructures on the surface of three propellant mixtures stabilized with three different compounds (DPA, Ak II and ethylcentralite) along with their elemental distribution has concluded that the sample stabilized with Ak II possesses the most compact structure. The scanned surfaces of interest (Figure 31) belong to a DPA-stabililized sample (NC-37: NC 96.70 m-% with 13.10 m-% N, DPA 1.50 m-%, graphite 0.10 m-%, K_2SO_4 0.35 m-%, residual moisture 1.35 m-%) and an Ak II-stabilized sample (EM2, NC 87.00 with 12.08 m-% N, NG 11.20 m-%, Ak II 1.22 m-%, K_2SO_4 0.17 m-%, residual moisture 0.41 m-%)[82].
The surface of NC-37 shows frizzy NC-filaments of varying diameter with

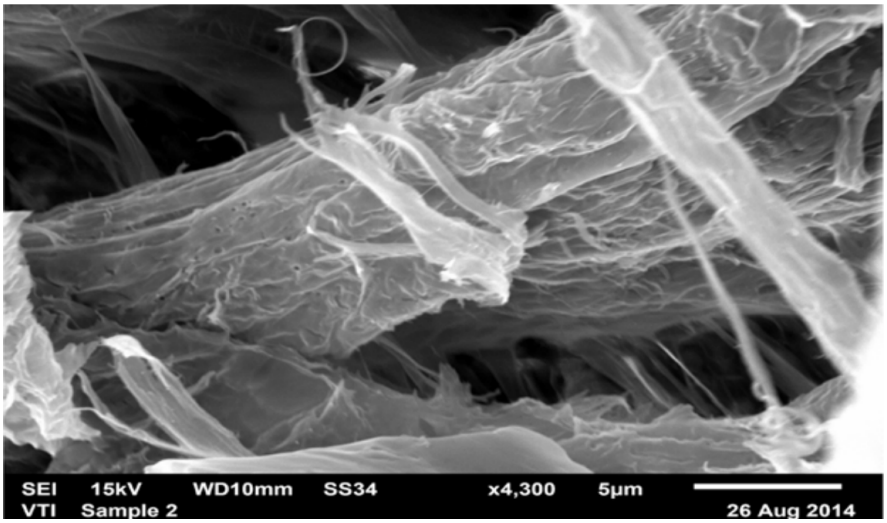

(a) Single-base propellant with DPA, 4300 magnification.

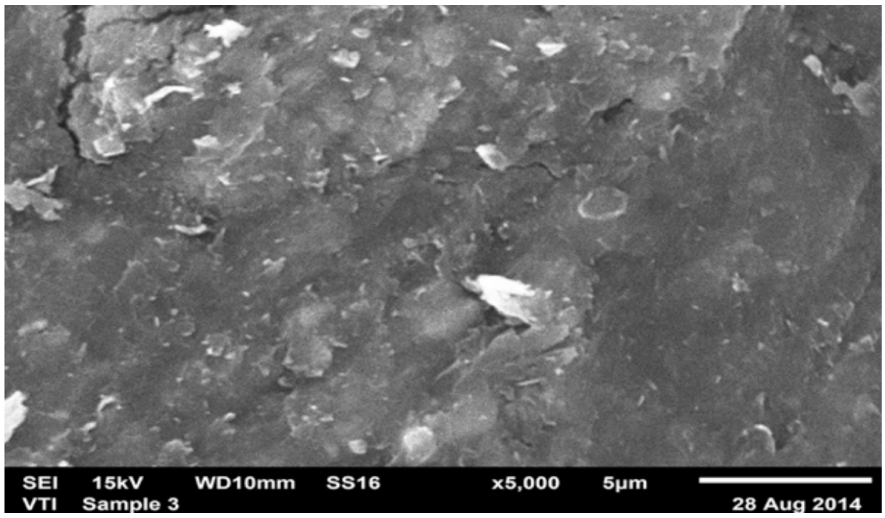

(b) Double-base propellant with Ak II, 5000 magnification.

Figure 31: SEM recordings of propellant mixtures NC-37 (top) with DPA and EM2 (bottom) with Ak II[82].

gaps in between. EM2 on the other hand shows a much more compact microstructure. Different substances called gelatinizing agents are added to propellants to favorably modify this parameter. Examples include nitroglycerin and phthalate esters. Different levels of gelatinization have the implication that NC-37 is more accessible to air and oxygen down to its bulk.

Outgassing of P, water and CO_x is also facilitated by the microstructure. Elemental mapping indicates that the stabilizer distribution is largely inhomogenious in NC-37 (with DPA found almost exclusively on the surface of NC) while Ak II is more evenly distributed in EM2. The authors of the study suggest that the observed differences between the samples are caused by Ak II "piercing into the matrix, which shows its is soluble in NC"[82]. While this conclusion disregards the effects the presence of nitroglycerin in the double-base propellant might have on its physical properties and stabilizer solubilities, thus potentially misattributing the difference in solubilities of the two stabilizers, it is clear that the distribution and availability of stabilizer as well as permeability to gases vary between the samples. The mutual solubility of stabilizer and NC is commonly referred to as gelatinization and has in fact also been documented in the absence of NG for AK II. Other stabilizers like Ak III and centralites I and II have also been found to act as gelatinizers for NC, while DPA and Ak I were concluded not to have this property[83]. Finally, the characteristics of such NC-stabilizer-gelatinizing agent mixtures further depend on the sample's temperature, in particular around the melting point of the stabilizers, and represent an active field of current research.

6.2 Stabilizer reactions

DPA and Ak II share many similarities in their reactions with P and their substitution patterns, particularly on the aromatic rings. Hence, the general conclusions drawn from section 5.2 continue to be valid for Ak II. The distinguishing factor is the availability of a weakly bonded aminic hydrogen. Table 11 contains the bond dissociacion enthalpies for the 2 and 4 positions of the aromatic rings and the N-H bond at 90°C. Note that for Ak II the N of the N-H bond refers to the methyl-substituted nitrogen atom.

Table 11: Computed N-H and C-H bond dissociation enthalpies at 90°C for DPA and Ak II. For Ak II the N-H bond is the $(H_3C)N-H$ bond.

Position	N	2	4
DPA: $\Delta_{bond}H$	357.6	471.3	471.2
Ak II: $\Delta_{bond}H$	428.0	470.3	469.9

The C-H bond enthalpies are unaffected by the carbamide group, within the

computational accuracy. The weak aminic N-H bond in DPA on the other hand is replaced by an amide N-H bond which is 70 kJ mol^{-1} stronger. The overall stronger bonds render Ak II less reactive then DPA. Ak II, consequently, is also less aggressive towards NC and nitrate ester groups as well, thus mitigating the risk of unwanted interactions akin to the previously mentioned DPA acceleration.

fThe products of the reaction of Ak II with *P* include $2NO_2$-Ak II, $4NO_2$-Ak II, NNO-DPA and nitro derivatives of DPA. A thin-layer chromatography assay of these products in a propellant sample at 90°C has found that singly substituted DPA derivatives appear on the first day of the experiment and dinitro-DPA's become detectable on the second day. $2NO_2$-Ak II and $4NO_2$-Ak II only appear on the third, after the doubly substituted DPA's[84]. This reflects the higher reactivity of DPA towards *P*.

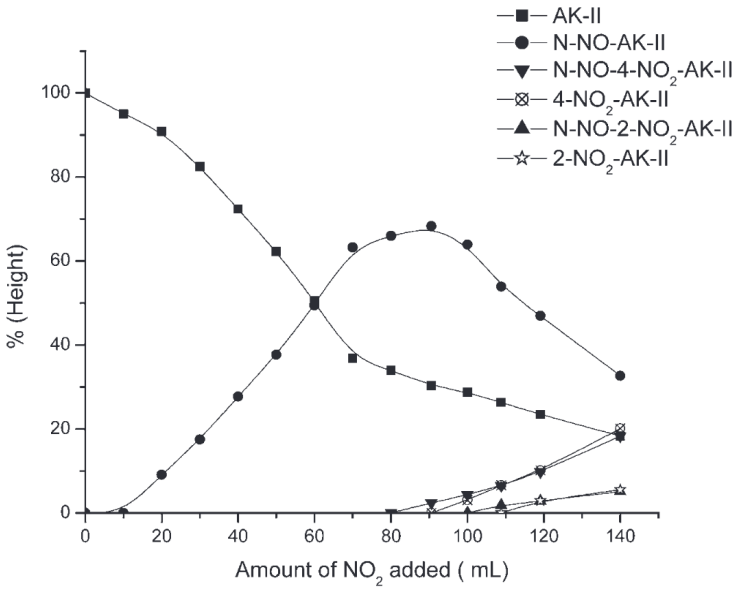

Figure 32: Relative HPLC signal strength of derivatives of Ak II over the course of its reaction with gaseous NO_2 at room temperature[85].

Another study has focused on the interaction of Ak II with gaseous NO_2 at room temperature. Nitrogen dioxide was gradually added and the Ak II sample was analyzed using HPLC after every addition. The relative HPLC signal heights (signal peak, not integrated signal) of the Ak II consecutive products (Figure 32) show a somewhat different picture. Initially, the main

product in NNO-Ak II, which has not been found in the propellant sample at 90°C. With the addition of more NO_2, nitro-Ak II derivatives as well as NNO-$2NO_2$-Ak II and NNO-$4NO_2$-Ak II are encountered. Reactions involving N-Nitroso and N-nitro derivatives of Ak II are discussed in section 6.4. The

DPA derivatives found in Ak II-stabilized propellants are formed from Ak II and its nitro derivatives by hydrolysis. Unstable N-methyl carbamic acid forms as an intermediate, and further decomposes to CO_2 and methylamine:

$$\text{Ak II} + H_2O \longrightarrow HN(CH_3)COOH + \text{DPA with } \Delta_r H^\circ = -17.7 \text{ kJ mol}^{-1}$$

$$HN(CH_3)COOH \longrightarrow CO_2 + H_2NCH_3 \text{ with } \Delta_r H^\circ = +31.4 \text{ kJ mol}^{-1}$$

This reaction is further discussed in section 6.5.

6.3 Reactions of the phenyl groups

The bond dissociation energy for the C-H bonds of the phenyl rings are also practically unchanged compared to DPA. As no nearby amine is available to make the molecule susceptible to attacks by radicals, the types of radical substitution considered for DPA is not available to Ak II. Therefore radical reactions are fairly unlikely to occur on the phenyl rings of Ak II due to the lack of stabilization of the resulting radicals.

For electrophilic aromatic substitution, the reactivity of the phenyl rings in Ak II is reduced with respect to DPA. The carbonyl group in the vicinity of the amine nitrogen acts as an electron withdrawing group, thus reducing the electron donor on the aromatic rings and making them less susceptible to aromatic electrophilic substutution. This is reflected in a side by side comparison of the natural bond orbital (NBO) charges of DPA and Ak II (Fig. 33), as derived from a natural population analysis. Atomic charges like NBO charges help to quantify the local electron density on single atoms or groups[86]. While the exact numbers depend on the level of theory and basis set used and are thus unreliable, they can effectively reflect overall trends. The NBO charges of the carbon atoms on the aromatic rings, except for the two in ipso position to the amine, are negatively charged in both Ak II and DPA. One trend shared by DPA and Ak II is that the 3 position has a lower electron density than the 2 and 4 positions. This difference manifests in the ortho-para substitution pattern on the aromatic rings. Comparing the 2 and 4 carbons of Ak II with the corresponding positions of DPA indicates that

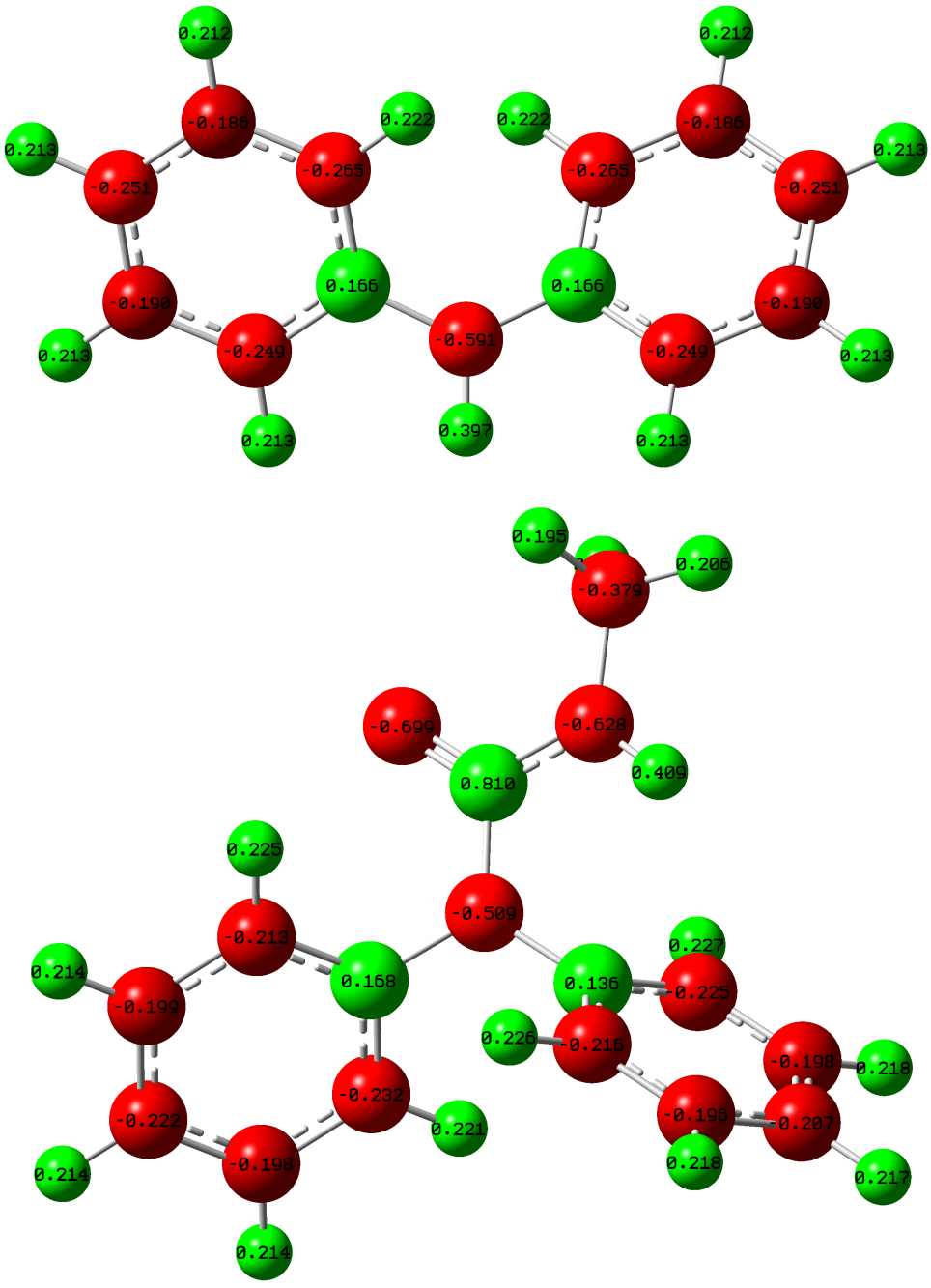

Figure 33: Natural bond orbital NBO charges of optimized structures of DPA (top) and Ak II (bottom) in NC simulate; red for atoms with overall negative, green for net positive charge.

a lower electron density is found for Ak II resulting in the observed lower reactivity of Ak II. At the same time, the trends for the overall reaction enthalpies for the nitration of Ak II remain in line with the values for DPA. The absolute values of enthalpies are all lower by about 15 kJ mol^{-1}. This difference can be again attributed to the lower electron density of the aromatic rings. The rising nitration enthalpies must be offset by lower (more exothermic) hydrolysis reacions. Through a combination of increased susceptibility to hydrolysis and decreased reactivity in comparison to DPA, no dinitro-Ak II derivatives are found in decomposing propellants. The chemical reactions for the nitration are given as:

$$\text{Ak II} + HNO_3 \longrightarrow 2NO_2\text{-Ak II} + H_2O \text{ with } \Delta_r H^\circ = -108.8 \text{ kJ mol}^{-1}$$

$$\text{Ak II} + HNO_3 \longrightarrow 4NO_2\text{-Ak II} + H_2O \text{ with } \Delta_r H^\circ = -119.8 \text{ kJ mol}^{-1}$$

$$\text{Ak II} + N_2O_5 \longrightarrow 2NO_2\text{-Ak II} + HNO_3 \text{ with } \Delta_r H^\circ = -169.1 \text{ kJ mol}^{-1}$$

$$\text{Ak II} + N_2O_5 \longrightarrow 4NO_2\text{-Ak II} + HNO_3 \text{ with } \Delta_r H^\circ = -180.0 \text{ kJ mol}^{-1}$$

6.4 Reactions of the methylurea group

The arguably most interesting part of Ak II is the methylurea group. Many reaction centered around the secondary amide N can take place. As illustrated in Figure 32, the reaction of NO_x at room temperature first produces N-methyl-N-nitroso-N',N'-diphenyl-urea (NNO-Ak II). Given below is a possible pathway to NNO-Ak II. For this reaction $\Delta_r H^\circ = -67.2$ kJ mol^{-1} and $\Delta_r G^\circ = -0.1$ kJ mol^{-1} at 90°C in NC simulate.

$$\text{Ak II} + NO_2 + NO \longrightarrow \text{NNO-Ak II} + HNO_2$$

With $\Delta_r G^\circ$ close to 0, this reaction has a $K_p \approx 1$ at 90°C. When the amount of P present is small, the equilibrium for this reaction lies on the side of Ak II. Given a lower temperature, the reaction can be favorable, however. The entropy change for this reaction is $\Delta_r S^\circ$=-184.8 J mol^{-1} K^{-1}. Extrapolating this to 298 K using the Gibbs-Helmholtz equation indicates that $\Delta_r G^\circ = -12.1$ kJ mol^{-1} and a $K_p \approx 134$. Such an proposition can explain why no or little NNO-Ak II is found at elevated temperatures while being the main initial product in experiments at room temperature.
NNO-Ak II is a generally undesirable intermediate product. It is a reactive nitrosamide which, like most other members of this class, is a carcinogen and

poses a serious health hazard[87]. NNO-Ak II can rearrange through a four-membered transition state to produce a diazo ester (Figure 34). The barrier for this reaction lies at $\Delta G^{\ddagger}$=128.1 kJ mol^{-1}. Other pathways involving proton shifts are also possible. The diazo ester can release methyldiazohydroxide upon decomposition, which in turn dissociates to diazomethane or methanediazonium. The latter two are potent methylating agents and have the potential to methylate e.g. DNA bases[88]. The overall reaction is slightly endothermic with $\Delta_r H°$=7.4 kJ mol^{-1}.

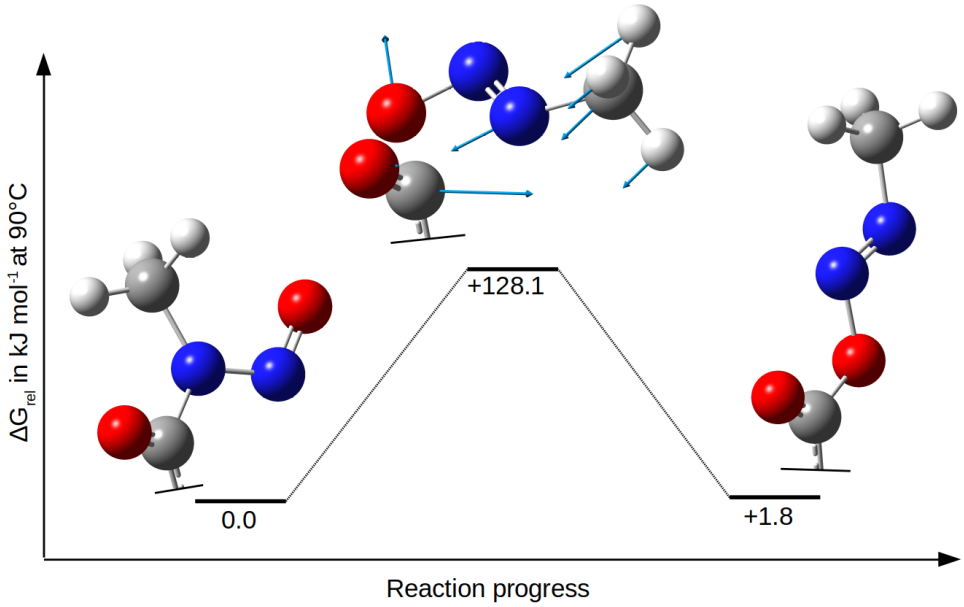

Figure 34: Gibbs free energy along reaction coordinate for the transformation of NNO-Ak II to a diazo ester and optimized structures of relevant part of the educt, tranisition state (with imaginary vibration mode arrows in blue) and product.

Starting from NNO-Ak II again, another possible course of reaction is the cleavage of the N-N bond, releasing NO. In section 6.2 the N-H bond was found to be much stronger than in DPA. The reason for this is that the resulting radical is poorly stabilized. The sp^2 valence orbital holding the lone electron is orthogonal to the π-electron system of the urea group. This circumstance is also revealed by the high bond dissociation enthalpy of $\Delta_{\text{bond}}H°$ = 172.0 kJ mol^{-1} for the N-N bond in Ak II-NNO versus $\Delta_{\text{bond}}H°$ = 121.6

kJ mol^{-1} for the N-N bond in DPA-NNO. The bond also possesses partial double bond character as is evident from its optimized bond length of 1.33 Å, which is comparable to the 1.32 Å resonance bonds found in peptides[89]. The reaction with HNO_3 could also yield a nitrate salt [HAkII][NO_3]. The basicity of Ak II is lower than that of DPA. Like in urea, the free electron pair on N are delocalized and therefore not basic; instead protonation would first occur on O. In the presence of N_2O_5 or potentially also HNO_3, the nitramide N-methyl-N-nitro-N',N'-diphenyl-urea (NNO_2-Ak II) could be formed:

$$\text{Ak II} + HNO_3 \longrightarrow \text{NNO}_2\text{-Ak II} + H_2O \text{ with } \Delta_r H^\circ = -25.5 \text{ kJ mol}^{-1}$$

$$\text{Ak II} + N_2O_5 \longrightarrow \text{NNO}_2\text{-Ak II} + HNO_3 \text{ with } \Delta_r H^\circ = -85.8 \text{ kJ mol}^{-1}$$

The Gibbs free energies are both exergonic, $\Delta_{\text{bond}}G^\circ$ = -72.3 kJ mol^{-1} for the nitration with N_2O_5 and just $\Delta_{\text{bond}}G^\circ$ = -13.4 kJ mol^{-1} for HNO_3. Similar to the NO_2 migrations in section 5.2.4, NNO_2-Ak II could intramolecularly nitrate itself. The urea group is surprisingly flexible, leading to many new possibilities. A realxed scan of $2NO_2$-Ak II around the bond between carbonyl-C and the N bonded to the phenyl rings in ωB97X-D/6-31+G*(figure 35) shows that the rotation barrier is around 50 kJ mol^{-1} at the most. With the additional steric hindrance of the nitro group and the partial double bond character of the amide bond, the rotation around the C-N bond is energetically low enough to be possible at elevated temperatures. In unsubstituted Ak II the barrier should be even lower, better represented by the 20 kJ mol^{-1} of the smaller barrier. Rotations around this bond can bring the NO_2 group in NNO_2-Ak II close to position 2 of the aromatic rings.

One such representative pathway leading to $2NO_2$-Ak II as shown in figure 36 has been studied. Beginning with NNO_2-Ak II, the NO_2-group is transferred to the closest 2-position of one of the aromatic rings. This step has a fairly high $\Delta G^\ddagger$=245.5 kJ mol^{-1}. A proton transfer from the aromatic ring back to the nitrogen atom that previously held the NO_2-group leads to $2NO_2$-Ak II. The overall reaction enthalpy is $\Delta_r H^\circ$ =-83.3 kJ mol^{-1}.

Additionally a second option exists for the decay of the intermediate following the NO_2-transfer, namely a decomposition to $2NO_2$-DPA. In the intermediate the bond between the carbonylic C and the N bonded to the phenyl rings is weakened and elongated to 1.56 Å. A transition state with a very low $\Delta G^\ddagger$= 4.0 kJ mol^{-1} leads to the cleavage of this bond. The overall process can then be expressed as:

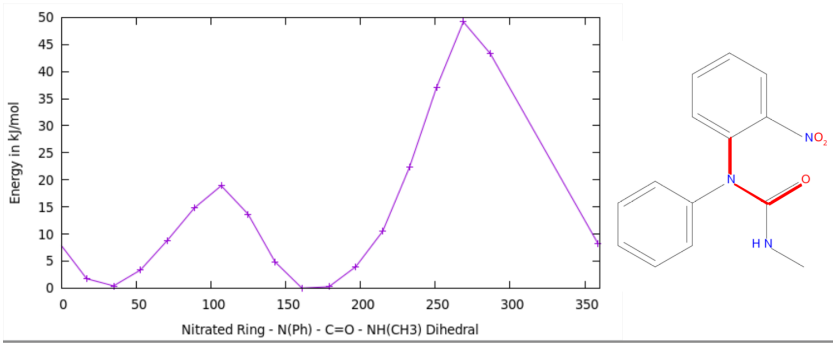

Figure 35: Scan of relative electronic energy following a relaxed scan of the dihedral angle with interpolation; the energetic global minimum can be found around 180°; scanned dihedral angle highlighted in $2NO_2$-Ak II on the right.

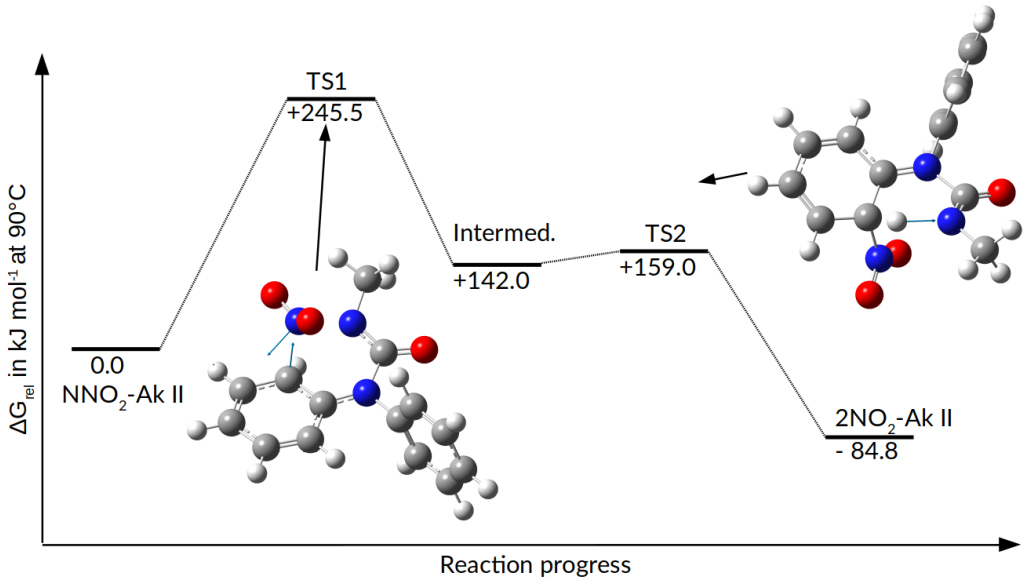

Figure 36: Gibbs free energy along reaction coordinate for the reaction of NNO_2-Ak II to $2NO_2$-Ak II with geometries of tranisition states and imaginary vibration mode.

The products of this reaction are reactive methyl isocyanate and the isomer of $2NO_2$-DPA in that was proposed to exist as an intermediate in the radical reaction mechanism of DPA with NO_2 in section 5.2.2. The overall reaction

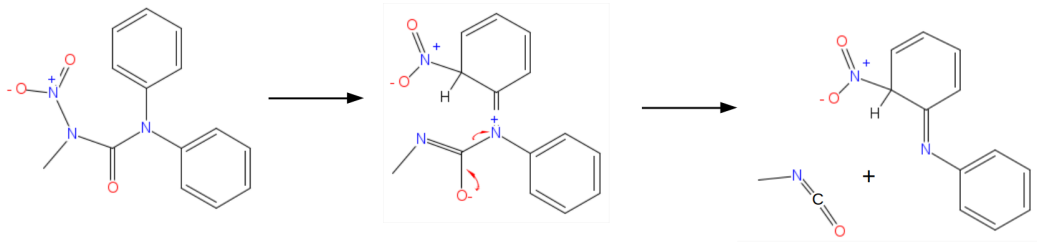

starting from NNO_2-Ak II can be written as:

$$NNO_2\text{-Ak II} \longrightarrow 2NO_2\text{-DPA} + H_3CNCO \text{ with } \Delta_r H^\circ = -25.1 \text{ kJ mol}^{-1}$$

This means that the inner-molecular NO_2-transfer is not only a possile reaction yielding $2NO_2$-Ak II, but could also be involved in turning Ak II into DPA if not enough water is available for hydrolysis. The formation of N-methyl-N-nitrito-N',N'-diphenyl-urea, i.e. an isomer of NNO_2-Ak II with NO_2 bonded as N-O-N=O, on the other hand is endergonic. The nitro isomer is lower by 78.6 kJ mol^{-1} in terms of Gibbs free energy and by 80.6 kJ mol^{-1} of enthalpy at 90°C in NC simulate. The formation of an amide N-oxide is not considered, as no known instances of such compounds are known. Calculations show, that their formation is unfavorable due to the loss of the approx. 75 kJ mol^{-1} amide resonance energy upon oxidation[90].

6.5 Hydrolysis

In the presence of water the amide bonds in Ak II can be hydrolyzed. In the first step a tetrahedral intermediate forms upon a nucleophilic attack by the water molecule on the carbonyl C. From here, the hydrolysis could in principle go two ways: Yielding methylamine and diphenylcarbamic acid, or DPA and methylcarbamic acid. Both carbamic acids are highly unstable even at cryogenic temperatures and will quickly decarboxylate[91]. Thus in both cases the final products are DPA, methylamine and carbon dioxide. For this overall reaction the Δ_rH° = 13.7 kJ mol^{-1} and Δ_rG° = -44.0 kJ mol^{-1} For a hydrolysis with neutral water and no preceeding proton shifts, the tranisition state found to have the lower activation energy is the one leading to DPA and methylcarbamic acid (Figure 37). Without catalysis by an acid or base, the activation energy is quite high. To get a more accurate lower value, such interactions should be considered in a more detailed theoretical study.

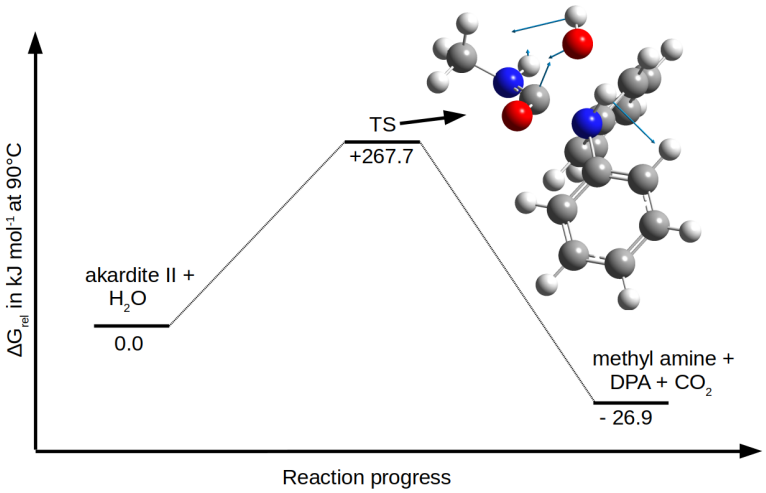

Figure 37: Gibbs free energy along reaction coordinate for the hydrolysis of Ak II to DPA and methylamine with geometry of the tranisition state (imaginary vibration mode arrows in blue).

As DPA is formed from Ak II, it in turn undergoes further reactions with the decomposition products of NC. Since DPA is more reactive than Ak II, DPA quickly binds any NO_2 in its proximity. The small amount of DPA produced acts as a potent radical scavanger thus helping to maintain a low concentration of *P*. In DPA-stabilized propellants at 90° DPA is completely depleted within a few days, after which its subsequent nitrations take place. Since the reactivity of these compounds decreases with higher degrees of nitration, DPA and its mono nitro derivatives are mostly used up before double and triple nitration is observed. In Ak II-stabilized propellants on the other hand, fresh DPA is constantly supplied through hydrolysis as long as Ak II is present. The DPA generated in small amounts it is quickly nitrated instead of the less reactive Ak II. Consequently, nitrated DPA's have been detected before nitrated Ak II's in Ak II-stabilized propellants[84]. In this way the high reactivity of DPA more evenly spread out over a longer period of time.

7 Kinetic modelling

7.1 Unstabilized NC: 1st order autocatalysis

First the decomposition of pure, unstabilized NC is considered. For this a simple model of only two reactions is employed:

(I) $O-NO_2$ groups decompose in a first order reaction, liberating P.
(II) P catalyzes the decomposition of $O-NO_2$ groups.

The autocatalytic decomposition of NC is assumed to be first order in the concentration of both nitrate ester groups and P. Since the heat output of the samples is measured in µW g^{-1} the concentration of all substances involved in the reaction will be expressed in µmol/g for easy interconversion. The rate laws for the two reactions in this scheme are as follows:

$$\frac{d[\mathrm{ONO_2}]}{dt} = -k_{NC} \cdot [\mathrm{ONO_2}] - k_{auto} \cdot [\mathrm{ONO_2}] \cdot [P] \tag{4}$$

$$\frac{d[P]}{dt} = k_{NC} \cdot [\mathrm{ONO_2}] + k_{auto} \cdot [\mathrm{ONO_2}] \cdot [P] \tag{5}$$

This model for autocatalytic degradation is commonly used to model different energetic materials[92]. From these rate laws it follows that k_{NC} must have dimensions of time^{-1} and k_{auto} dimensions of $(\mathrm{time} \cdot \mathrm{molality})^{-1}$. This set of differential equations is analytically solvable. The method used for this and the explicit solution are described in detail in the appendix to this work. With $[\mathrm{ONO_2}](t)$ known the heat generation rate with the sign convention as used in HFMC (liberated heat positive) is calculated from this using equations (6) and (7). The enthalpies $\Delta_r H_{NC}$ and $\Delta_r H_{auto}$ of the intrinsic and autocatalytic reactions are assumed to be equal and are included in the form of ΔH. In equation (7) an abbreviation for $[\mathrm{ONO_2}](0) + [P](0) = \delta$ is used.

$$\frac{dQ}{dt} = \Delta H \cdot \frac{d[\mathrm{ONO_2}]}{dt} \tag{6}$$

$$\frac{d[\mathrm{ONO_2}]}{dt} = -\frac{[\mathrm{ONO_2}](0) \cdot (k_{NC} + k_{auto} \cdot \delta)^2 \cdot (k_{NC} + k_{auto} \cdot [P](0)) \cdot e^{(k_{NC} + k_{auto} \cdot \delta)t}}{\left[[\mathrm{ONO_2}](0) \cdot k_{auto} + (k_{NC} + k_{auto} \cdot [P](0)) \cdot e^{(k_{NC} + k_{auto} \cdot \delta)t}\right]^2} \tag{7}$$

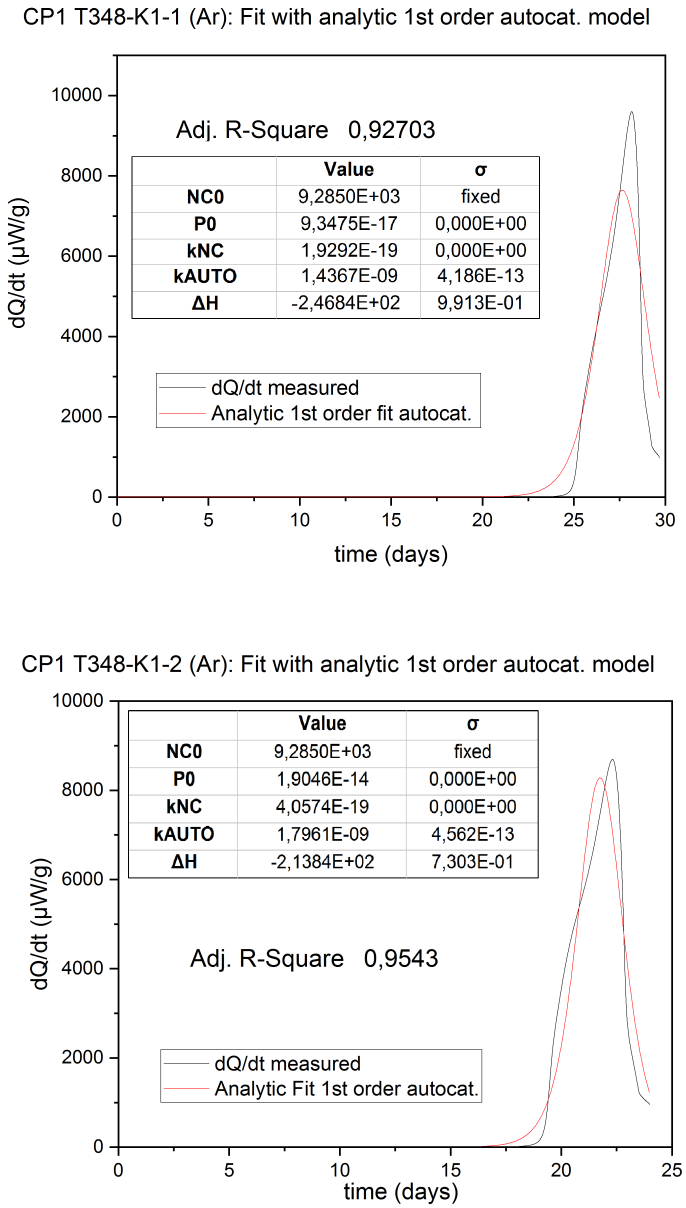

Figure 38: Kinetic modeling of unstabilized NC of type CP1, 13 mass-% N, at 70°C. Two samples under argon atmosphere. [P](0) and $[ONO_2](0) = NC0$ in µmol g^{-1}, k_{NC} in s^{-1}, k_{auto} in g µmol^{-1} s^{-1} and ΔH in kJ mol^{-1}.

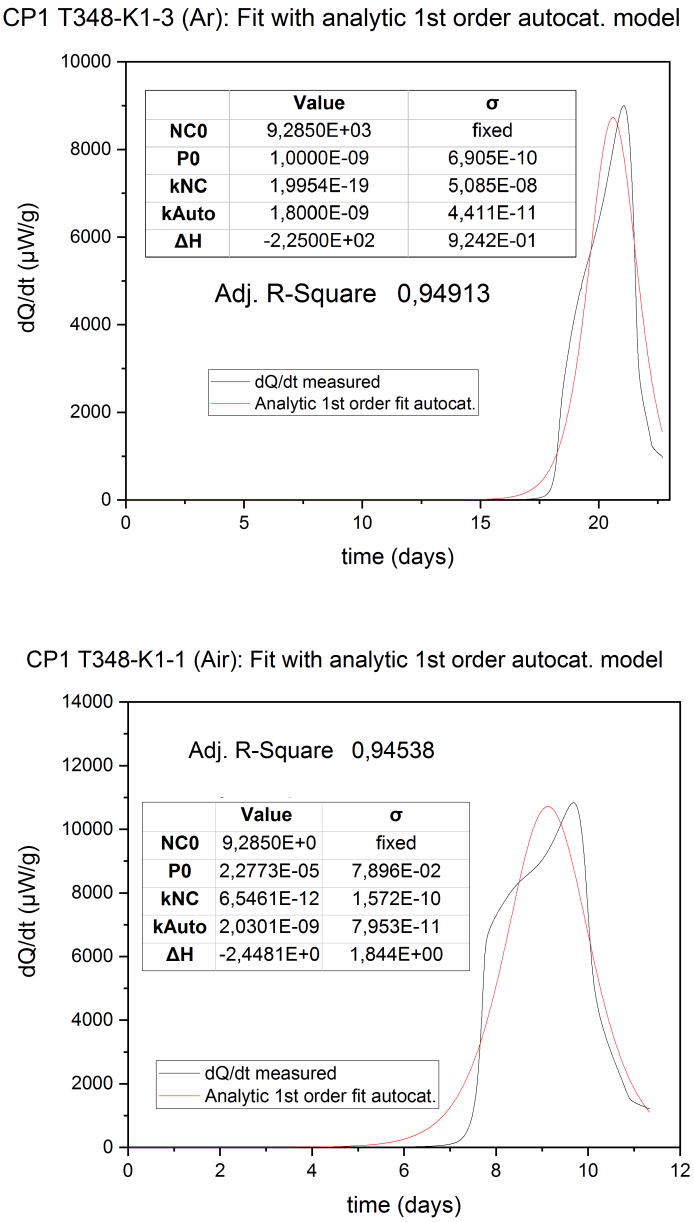

Figure 38 (continued): Kinetic modeling of unstabilized NC of type CP1, 13 mass-% N, at 70°C. Top sample under Ar, bottom sample in air. [P](0) and $[ONO_2](0)$ = NC0 in µmol g^{-1}, k_{NC} in s^{-1}, k_{auto} in g µmol^{-1} s^{-1} and ΔH in kJ mol^{-1}.

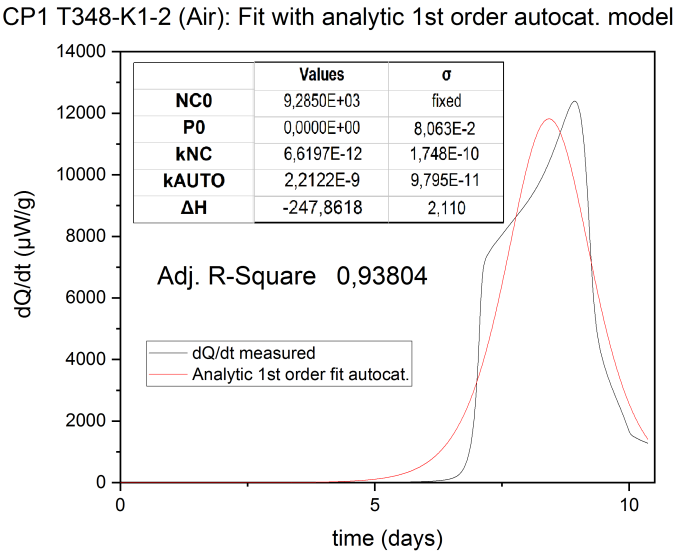

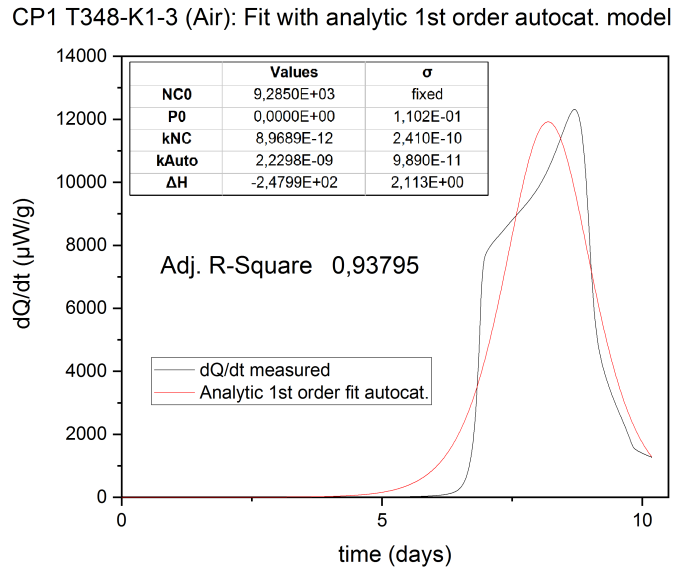

Figure 38 (continued): Kinetic modeling of unstabilized NC of type CP1, 13 mass-% N, at 70°C. Two samples in air. [P](0) and [ONO_2](0) = NC0 in µmol g^{-1}, k_{NC} in s^{-1}, k_{auto} in g µmol^{-1} s^{-1} and ΔH in kJ mol^{-1}.

Experimental heat flow curves from several samples of stabilizer-free NC at 70°C in air and argon gas have been fitted using this kinetic model. For each sample, $[ONO_2](0)$ (concentration of nitrate ester at initial conditions) is calculated from the nominal nitrogen content of NC as it is assumed that the samples' degradation prior to the experiment is negligible. The heat flow curves and fits for samples of the type CP1 (13 mass-% nitrogen content N) under Ar and air, three each, are summarized in Figure 38. Tables containing the optimized values for every parameter and their corresponding $[ONO_2](0)$ is easily calculated as 0.13 g N = 9280 µmol N are present per g sample. The curves under Ar show a steep rise in liberated heat after a somewhat variable incubation period ranging from 15 to 25 days. This variation can be accounted for a variation of k_{auto} of only a factor of 1.25. This difference can be explained by slight inhomogeneities in the NC. Adjusted R^2-values of between 0.92 and 0.96 are achieved, indicating that the heat flow curves are generally well-replicated using a first-order model. However, it is also evident, that the model is lacking, in particular it fails to capture the abrupt slope changes near the base of the peak. This signifies a very strong accelerated decomposition, which is faster than the model is able to reproduce. One of the aspects that is ignored in the model is the rise in temperature owing to very high heat generation rates. The deviation from isothermal conditions is usually be neglected but can be quite significant if the generated heat can not be drained fast enough. Reaction rates rise exponentially with temperature according to the Arrhenius equation, hence an increase in temperature leads to a feedback loop generating more and more heat. This effect would cause the real heat flow curves to be more pointed towards the top, as is experimentally observed. It does, however not account for the steep initial increase, as the heat generation rates at the beginning of the exothermal peaks are not high enough to cause a significant temperature increase. A steep increase might indicate an additional higher-order dependency of the decomposition rate on P or another reaction that is unaccounted so far. The initial concentration of P is found to be very low, $< 10^{-9}$ µmol/g and enthalpy release per mol nitrate are consistently between -214 kJ mol^{-1} and -247 kJ mol^{-1} with an average of -229 kJ mol^{-1}. Another common point between the samples under argon was the unexpectedly low k_{NC}. A possible program error has been encountered in samples T348-K1-1 and T348-K1-2 in argon that gave an unrealistic standard deviation of 0.000 for this parameter among others. This is probably an artefact of the used software. A more probable value of the standard deviation of this value is the one for T348-K1-3 in Ar,

$\sigma = 5.1 \cdot 10^{-8}$, many orders of magnitude larger than the actual value of k_{NC}. What this indicates is low relative dependency on k_{NC} of the final shape of the curve. A change of k_{NC} by a factor 2 or so has less of an effect on the quality of the fit than other parameters. Samples exposed to oxygen have a distinctly different peak shape to those under Ar. The autocatalytic peak is encountered after only 7-8 days. Again initial concentrations of P are very low. The reaction enthalpies are consistent and within 3 kJ mol^{-1} of each, averaging at -247 kJ mol^{-1}. This value only differs from the average under Ar by 18 kJ mol^{-1}, indicating that the majority of enthalpy released in the decomposition is due to the degradation of NC rather than the oxidation of the degradation products by atmospheric oxygen. The reaction enthalpies in argon and in air in particular are remarkably close to the -246.5 kJ mol^{-1} value which was calculated using DFT-data in section 4.3.2. To reach that value it was necessary to assume that NO_2 reacted with other degradation products of NC to form NO, CO and CO_2, indicating that a similar reaction might have occured in the NC samples. The consistently higher k_{auto} values are responsible for the earlier onset of the autocatalytic peaks in samples exposed to oxygen. As shown in section 4.1, the composition of P varies between samples with and without access to air. Without air the major component of P is NO_2 while with air and moisture a significant amount of HNO_3 is also present. These two species presumably have different k_{auto}. Some evidence for this can be found in the distinct forms of the exothermic peaks: Both the peaks under Ar and air have a shoulder peak on the left side indicating two separate reactions. This side peak is evidently much more expressed in samples with access to oxygen. Consequently, this side peak might be attributed to the HNO_3 content in P. The right main peak then would be an expression of the reactions with NO_2. Additional experiments are required to prove or disprove this hypothesis. Using a model of a two-component P consisting of NO_2 and HNO_3 at equilibrium with separate autocatalytic reactions to correlate O_2 exposure/ HNO_3 content with the perceptibility of the shoulder peak should grant a clearer insight into the mechanistics of NC degradation. The presence of oxygen furthermore replenished any NO_2 that is reduced to NO. This raises the autocatalytic impact of P and increases the effective k_{auto}.

What is astonishing is the exceedingly low k_{NC} predicted for every single sample. A very slow intrinsic buildup and low initial concentration of P are necessary to allow for the high k_{auto} and a steep exothermic autocatalytic peak. However, a k_{NC} around $10^{-19}\mathrm{s}^{-1}$ is about 10^{10} less than is found with

most kinetic fits of stabilized NC at the same temperature. One study using the kinetic model which is used to model DPA-stabilized NC in section 7.3 for example has reported a reaction rate of $7.92 \cdot 10^{-5}$ day^{-1} or $9.17 \cdot 10^{-5}$ s^{-1}[93]. This contradicts the premise that k_{NC} should be intrinsic and independent of factors like stabilizer concentrations. A disparity this large points towards a deeper issue. One possible approach to rationalizing this observation is by invoking the concept of DPA acceleration as introduced in section 5.4.

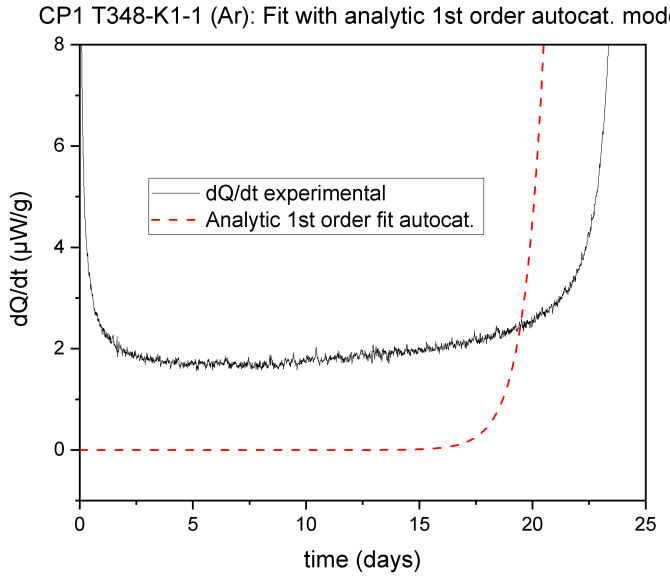

Figure 39: Kinetic modeling of unstabilized NC sample 1 of type CP1, 13 mass-% N, at 70°C. Zoom of the time frame before the exothermic peak as shown in Figure 38.

A closer look at the fit for sample 1 under Ar atmosphere (Figure 39) discredits this claim, however: Before the exothermic peak there is a long plateau of heat generation around 2 µW g^{-1}. At the same time, the fit using the model of a first order autocatalytic decay predicts that the heat flow curve should only begin to noticably rise after about 15 days. Before that, the modeled heat flow lies at a much lower baseline close to 0 µW g^{-1}. By the end of the first day, the modeled dQ/dt curve is still smaller than 10^{-7} µW g^{-1} or about 10^7 times less than the experimental value. This means that it is not the case that stabilized NC degrades this much faster but more interestingly,

that NC can degrade over a long period of time without building up an excessive concentration of P. To add, judging from the rate constants, one would expect that NC should be extraordinarily sensitive towards external sources of P. The exposure of NC to even a small amount of P would be expected to practically momentarily initiate the autocatalytic peak at, which is not observed to that extent[94]. There are multiple potential explainations this result, some of which will be evaluated in section 7.4 after taking into account the more information about stabilized NC in the following sections.

7.2 NC and Ak II

Ak II-stabilized propellants usually show heat flow curves very similar in form to those of unstabilized NC samples. The propellants studied in this section are C/S0200 (2.04 % Ak II, 13 mass-% nitrogen content N) and C/S0400 (2.14 % Ak II, 13 mass-% nitrogen content N). Kinetic data in the form of stabilizer curves for Ak II is only available for C/S0200. Measurements of heat flow curves of C/S0400 have been performed at 90°C in both an Ar atmosphere. As the two propellant mixtures are very similar in composition, it is assumed that the stabilizer curve of one can be correlated to the heat flow curve of the other. The heat flow curves from NC samples stabilized with Ak II show a fairly consistent profile: An initially high heat generation rate that quickly drops off and settles at a constant plateaued baseline of ca. 50 µW g^{-1} after about 4-5 days at 90°C. These two features, i.e. the constant baseline and the initial high heat flow, are examined seperately. Different models are used for the parts of the heat flow curve. The proposed separation in the heat flow curve of C/S0400 at 90°C is shown in Figure 40.

The high initial heat flow in the Ak II-stabilized propellant could not be modeled as a stabilizer reaction successfully, as unrealistically high values of the initial concentrations of P and the rate constants for the reaction of P and Ak II were fitted in such attempts. A different model is thus applied to this particular area of the the heat flow curve. As the reaction has an initially rate that drops over time it is probable that this reaction involves the breakdown of some reactive non-P species such as peroxides, trapped radicals, etc. called X in the model. In the unheated propellant these compounds might persist for long periods of time due to their limited mobility. Upon heating these compounds would begin moving through the propellant matrix and could then rapidly react with one another. The result would be a n-th order decay reaction, depending on the order of the reaction

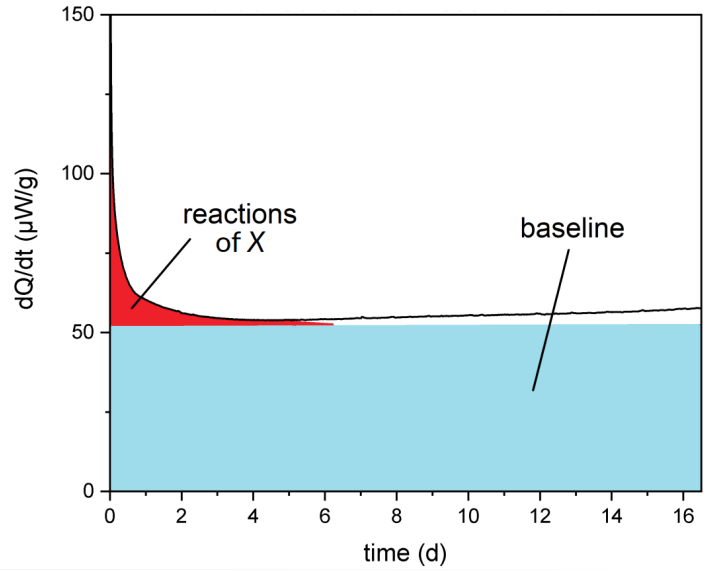

Figure 40: Heat flow curve of AK II-stabilized C/S0400 at 90°C. Two regions, the initial reactions of X and the constant baseline, are signified. Heat flow rate in µW g^{-1}.

of these compounds. The baseline of 50 µW/g is handled later and is for this fit subtracted from the curve. The remaining part of the curve is fitted using following first order ODE with a rate constant k_X:

$$\frac{d[X]}{dt} = -k_X \cdot [X]^n$$

As the order and rate constant for the reaction are unknown, both need to be fitted. The expression for the heat flow curve can derived from this expression by introducing the enthalpy for this reaction $\Delta_r H_X$:

$$\frac{dQ}{dt} = -(\Delta_r H_X \cdot k_X) \cdot [X]^n$$

The parameters $\Delta_r H_X$ and k_X in this model cannot be fitted separately. To reduce the number of superfluous variables a new parameter $H = \Delta_r H_X \cdot k_X$ is introduced. This changes the expression for the heat flow rate to:

$$\frac{dQ}{dt} = -H \cdot [X]^n$$

H is a combined parameter with units kJ mol^{-1} s^{-1} (g µmol^{-1})^n with the reaction order n. The parameters in this differential equation are fitted to the initial heat flow pattern (Figure 41). The fit has a high adj. R^2 value of 0.996. The optimized reaction order is 1.80. This suggests that the major contribution comes from a second order with respect to $[X]$, with some first order processes involved.

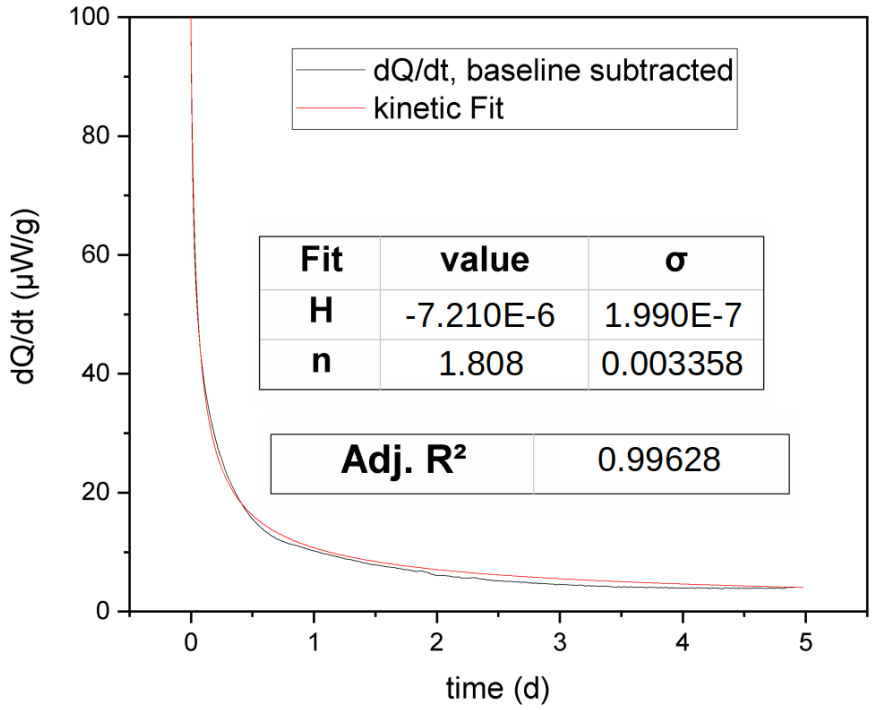

Figure 41: Kinetic fit of initial heat flow of Ak II-stabilized propellant C/S0400 at 90°C with an n-th order decay reaction; constant baseline of 50 µW g^{-1} subtracted from heat flow curve. n is a dimensionless reaction order, H is the product of the rate constant and enthalpy of the reaction in kJ mol^{-1} s^{-1} (g µmol^{-1})^n.

The initial heat flow pattern of Ak II furthermore closely resembles the behavior of unstabilized NC, so it is attempted to apply the same model to both samples. The first four days of the heat flow curve in Figure 39 are fitted using the same equation (Figure 42). This fit results in a reasonably good adj. R^2 of 0.96603. The reaction order in unstabilized NC is much closer to a

pure second order reaction with n=1.984. This result supports the hypothesis as a second order reaction points to a reaction of two equivalents of X, as may be expected from the recombination of radicals. The radicals in question may be the peroxy radicals referenced in section 4.3.1. A second order reaction between these radicals has been reported based on measurements of chemiluminescene. As the second order reaction takes place even in the absence of stabilizer, Ak II can be assumed to be nonessential in it. The first order contribution to the fitted reaction rate in the Ak II-stabilized propellant might point towards a reaction between X and Ak II, which manifests itself as a pseudo-first order reaction with respect to X. Before reaching a final conclusion on this reaction and its first and second order contributions, however, more heat flow curves need to be studied to better understand the random variations of the reaction order.
The previosly subtracted baseline of 50 µW g^{-1} represents a dynamic equilibrium. P is constantly formed from nitrate ester and destroyed by the stabilizer at the same rate. The model used to fit this baseline includes the nitrate, P and stabilizer S concentrations. The concentration of P is assumed to quickly be suppressed in this model, so that autocatalysis is not included here. The reactions that are included are as follows:

$$NC \xrightarrow{k_{NC}} P + R \quad \text{Intrinsic degradation of NC}$$

$$\mathrm{S} + P \xrightarrow{k_S} [S - P] \quad \text{Stabilization by Ak II}$$

This system of coupled ODE's can be solved analytically as discussed by Bohn[95]. With the initial condition that $[P]_0 = [S]_0$ a simplified version of the equation can be used. $[\mathrm{NC}]_0 = [\mathrm{ONO_2}]_0$ is the initial molality of nitrate ester groups. It can be calculated from the mass percentage of nitrogen as 13 % N = 0.13 g N g^{-1} sample = 9280 µmol g^{-1}. As 2 mass-% of the sample are stabilizer, the effective molality is somewhat lower, around 9160 µmol g^{-1}. The initial molality of Ak II is 2.04 mass-% Ak II = 90.2 µmol g^{-1}. The stabilizer curve for Ak II can be fitted using equation (8), where exp is the exponential function and erf is the error function:

$$[S](t) = \frac{\sqrt{\exp(-k_S \cdot k_{NC} \cdot [NC]_0 \cdot t^2)}}{\frac{1}{[S]_0} + \sqrt{\frac{\pi}{2} \cdot \frac{k_S}{k_{NC} \cdot [NC]_0}} \cdot \left[\mathrm{erf}\left(\sqrt{\frac{k_S \cdot k_{NC} \cdot [NC]_0}{2}} \cdot t\right)\right]} \tag{8}$$

The concentration of Ak II in a C/S0200 sample at 90°C is fitted using this model as shown in Figure 43. With an adj. R^2-value of 0.998, the model is in

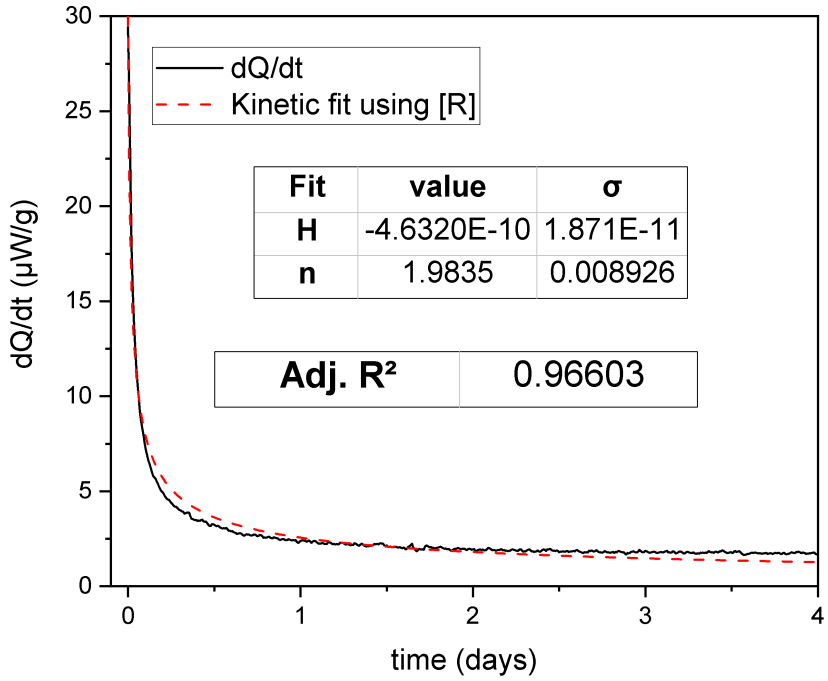

Figure 42: Kinetic fit of unstabilized NC of type CP1 (T348-K1-1) in Ar at 70°C with a n-th order decay reaction. n is a dimensionless reaction order, H is the product of the rate constant and enthalpy of the reaction in kJ mol^{-1} s^{-1} (g $\mu mol^{-1})^n$.

very good agreement with the experiment. The stabilizer is slowly depleted over a period of more than 80 days. The amount of stabilizer decreases rather slowly; compared to the unstabilized NC the stabilized propellant can be stored for far longer without entering its autocatalytic decay phase. Comparing this to the timeframe of the heat flow curve (16 days) means that only the first part of the kinetic fit is included. Over the course of the first days of the experiment the stabilizer depletion is nearly linear. Over the first 5 days 8.85 µmol g^{-1} Ak II are consumed, which is equivalent to 1.77 µmol AkII being consumed per day. How does this compare to the heat flow baseline? A reaction rate of 1.77 µmol g^{-1} day^{-1} can be converted to a rate of $2.05 \cdot 10^{-5}$ µmol g^{-1} s^{-1}. The nitration enthalpy of Ak II (to $4NO_2$-Ak II)

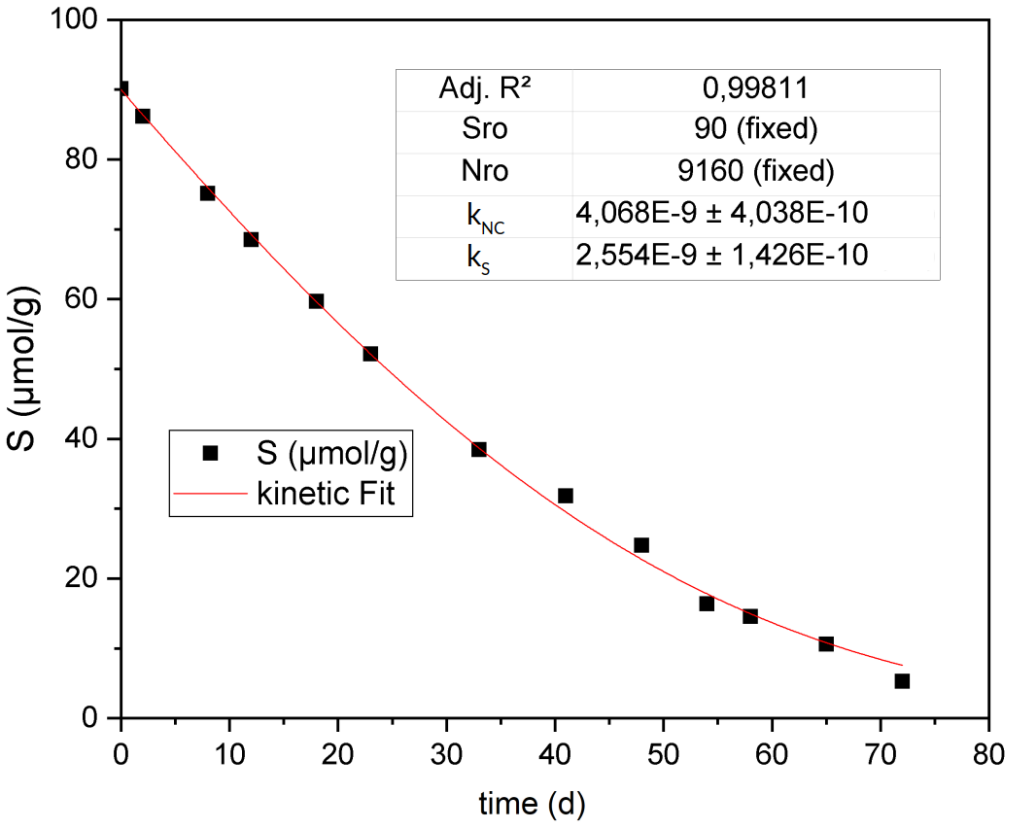

Figure 43: Kinetic fit of Ak II in C/S0200 at 90°C using analytical [S](t) function. Sro = $[S]_0$ and Nro = $[NC]_0$ in µmol g^{-1}, k_{NC} in s^{-1} and k_S in g µmol^{-1} s^{-1}.

was computed to be -119.8 kJ mol^{-1} in section 6.3. It is briefly assumed that all Ak II is transformed into 4NO_2-Ak II for the sake of simplicity. Using this enthalpy, the contribution to the heat generation rate of 50 µW g^{-1} from the nitration of Ak II amounts to about 2.5 µW g^{-1}. The binding of P by Ak II requires P to form from the degradation of nitrate esters nearly in tandem with the former. Using the intrinsic decomposition rate from Figure 43 and a high estimate for the reaction enthalpy equal to the experimental value of unstabilized NC (-229 kJ mol^{-1}), the expected heat generation rate from NC decomposition becomes $4.068 \cdot 10^{-9} \frac{1}{s} \cdot 9160 \frac{\mu mol}{g} \cdot 229 \frac{kJ}{mol} = 8.5$ µW/g. The degradation and nitration enthalpies combined can explain ca. 11 µW g^{-1} or about 22% of the observed heat flow. The nitration of Ak II by itself

accounts for only ca. 5% of the total heat flow. With the fitted degradation rates, about twice as much P is formed as Ak II is consumed, so that it is reasonable to assume that a second nitration takes occurs for every molecule of Ak II. This would still only raise the reaction enthalpy from 11 µW g^{-1} to ca. 13.5 µW g^{-1}. Even doubling the rate of NC degradation and assuming quadruple nitration for every molecule of Ak II only produces a heat flow rate of ca. 27 µW mol^{-1} or slightly of half of the observed value. To justify a heat flow rate of 50 µW g^{-1}, about 3-4 times as much degradation and stabilizer consumption would have to take place.
In conclusion, the origin of 36.5 µW g^{-1} (78% of the total heat flow) is unclear from just the fitted stabilizer consumption and degradation rates. A different, so far neglected reaction needs to be invoked. This could e.g. be a degradation of NC without the formation of P. The initial high heat flow in Ak II-stabilized and unstabilized NC can be modeled as a (near) second order reaction. The combination of a 50 µW g^{-1} constant baseline and the heat flow from the second order reaction reproduce the heat flow curve of Ak II with an adj. R^2=0.996.

7.3 NC with DPA

In DPA-stabilized gun propellants a notable reduction in heat flow is detected during the first days of heat exposure. Kinetic modeling is used in conjunction the thermodynamic data from the previous sections to try and explain this phenomenon.

7.3.1 Reaction system III

The first kinetic model, referred to as reaction system III (RSIII) has originally been proposed by Bohn[96]. It can be described as follows: The degradation of the stabilized NC is treated analogously to the the model applied to unstabilized NC previously. Nitrate ester groups decompose in a first order reaction (9) to release P and leave behind a rest R. The autocatalytic reaction (10) is also included. DPA can react with P to NNO-DPA in reaction (11), to $2NO_2$-DPA in reaction (12) and to $4NO_2$-DPA in reaction (13). NNO-DPA can either re-release P in reaction (14) or continue to bind P in reaction (15). $2NO_2$-DPA and $4NO_2$-DPA can also react with more P in reactions (16) and (17). The consecutive products of (12)-(14) are not further specified in the original RS3.

$$NC \xrightarrow{k_{NC}} P + R \tag{9}$$

$$NC + P \xrightarrow{k_{auto}} 2P + R \tag{10}$$

$$\text{DPA} + P \xrightarrow{k_{NNO}} \text{NNO-DPA} \tag{11}$$

$$\text{DPA} + P \xrightarrow{k_{2N}} 2\text{NO}_2\text{−DPA} \tag{12}$$

$$\text{DPA} + P \xrightarrow{k_{4N}} 4\text{NO}_2\text{−DPA} \tag{13}$$

$$\text{NNO-DPA} \xrightarrow{k_{DPANNO}} \text{DPA} + P \tag{14}$$

$$\text{NNO-DPA} \xrightarrow{k_{NNO-}} \text{DPA}_{NNO-} \tag{15}$$

$$2\text{NO}_2\text{−DPA} \xrightarrow{k_{2N-}} \text{DPA}_{2N-} \tag{16}$$

$$4\text{NO}_2\text{−DPA} \xrightarrow{k_{4N-}} \text{DPA}_{4N-} \tag{17}$$

The rate laws for RSIII are written as a system of six coupled differential equations for six compounds (nitrate esters, DPA, NNO-DPA, $2NO_2$-DPA, $4NO_2$-DPA, P) for which the rate constants can be fitted to experimental data:

$$\frac{d[\text{ONO}_2]}{dt} = -k_{NC}[\text{ONO}_2] - k_{auto}[\text{ONO}_2][P]$$

$$\begin{aligned}\frac{d[P]}{dt} = {} & k_{NC}[\text{ONO}_2] + k_{auto}[\text{ONO}_2][P] - (k_{NNO} + k_{2N} + k_{4N})[\text{DPA}][P] \\ & + k_{DPNNO}[\text{NNO-DPA}] - k_{NNO-}[\text{NNO-DPA}][P] \\ & - k_{2N-}[2\text{NO}_2\text{-}DPA][P] - k_{4N-}[4\text{NO}_2\text{-}DPA][P]\end{aligned}$$

$$\frac{d[\text{DPA}]}{dt} = -(k_{NNO} + k_{2N} + k_{4N})[\text{DPA}][P] + k_{DPANNO}[\text{NNO-DPA}]$$

$$\frac{d[\text{NNO-DPA}]}{dt} = k_{NNO}[\text{DPA}][P] + k_{DPANNO}[\text{NNO-DPA}] - k_{NNO}[\text{NNO-DPA}][P]$$

$$\frac{d[2NO_2\text{-DPA}]}{dt} = k_{2N-}[\text{DPA}][P] - k_{2N}[2NO_2\text{-DPA}][P]$$
$$\frac{d[4NO_2\text{-DPA}]}{dt} = k_{4N-}[\text{DPA}][P] - k_{4N}[4NO_2\text{-DPA}][P]$$

The rate constants for second order reactions have dimensions of time^{-1}· molality^{-1}, while the first order reactions are given in dimensions of time^{-1}. The sample used in this study is the gun propellant K6210. It is a classified as a ball powder, a double-base propellant commonly used in small firearms. Its primary components are 74 mass-% NC (13.1 % N) amd 18.4 mass-% nitroglycerin. This translates to 6924 µmol/g nitrate groups in the form of NC and 2431 µmol/g nitrate groups as nitroglycerin, adding to a total concentration of nitrate esters of 9355 µmol per g sample. All nitrate esters are collectively treated as one species in RSIII. The propellant additionally contains 4.5 mass-% dibutyl phthalate as a gelatinization agent and plasticizer, 0.5 mass-% KNO_3 and 0.2 mass-% graphite. These compounds are not considered in the kinetic model. 0.5 mass-% DPA, 0.55 mass-% NNO-DPA, 0.033 mass-% $4NO_2$-DPA and 0.031 mass-% $4NO_2$-DPA were found as the initial concentrations of stabilizer derivatives. The amounts of these compounds as well as NNO-$4NO_2$-DPA and NNO-$2NO_2$-DPA were followed over the course of 10 days at 80°C. MFMC curves were also measured with this propellant type at the same temperature so that direct correlations between kinetic data and heat flow can be examined. For the experimental concentration data set a kinetic fit was performed using *FitODE* (Figure 44). As initial molalities the following values were used: 9355 µmol g^{-1} for the nitrate ester molality, 29 µmol g^{-1} for DPA and NNO-DPA and 1 µmol g^{-1} for $2NO_2$-DPA and $4NO_2$-DPA. The fit returned a high adj. R^2= 0.983, pointing to good agreement between the model and data set. The initial concentration of P was set as an optimizable variable, totaling to 10 free parameters. Due to the high number of intricately coupled parameters a some degree of uncertainty remains for the fitted values as is reflected in the high standard deviations, which are up to 10-100 higher than the optimized parameter values. A deviation in most of the fitted kinetic parameters has little influence on the overall quality of the plot and can be attenuated by the other coupled parameters.

Given that the kinetic model satisfactorily fits the experimental data, the next step is to fit the heat flow curve based on these results. The heat flow curve of K6210 (Figure 45) follows the pattern typically observed in DPA

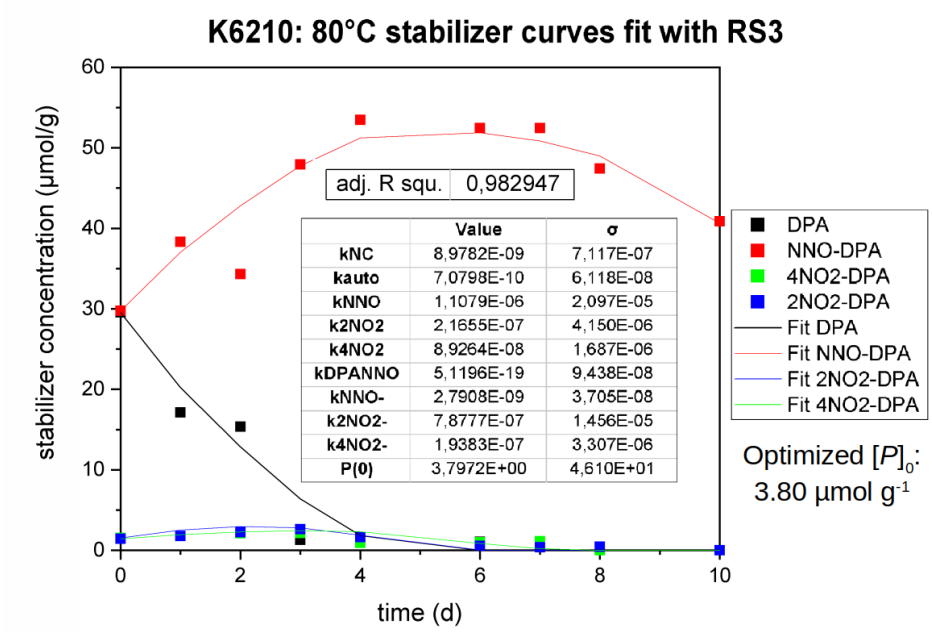

Figure 44: RS3 kinetic fit of molalities of DPA and some of its derivatives over the course of 10 days at 80°C and optimized results of the fit with their standard deviations. Rate constants for first order reaction are given in s^{-1} (k_{NC}, k_{DPANNO}), those for second order reactions in g μmol^{-1} s^{-1} (all other rate constants).

stabilized NC. This curve and in particular the time frame of days 0 to 6 will be used as the experimental data for the fits. The second included curve shows the cululated heat output Q(t) that is generated by the sample over time. This curve corresponds to the integrated heat flow rate over time and can be computed from the dQ/dt curve and vice versa.

For modeling the heat flow rate must first be expressed in terms of fittable parameters and the concentrations of the involved compounds. The measured heat flow rate dQ/dt can be thought of the net energy generated by all the chemical reactions in sample. The heat generation rate from one of these reaction can be expressed as the product of the enthalpy change per reacted mol and the reaction rate of said reaction, as was done for NC and AkII before. The convention labeling heat generation as a positive heat flow is used again. There are 9 reactions that need to be accounted for, namely the ones expressed in (9)-(17). This leads to the introduction of 9 reaction enthalpies

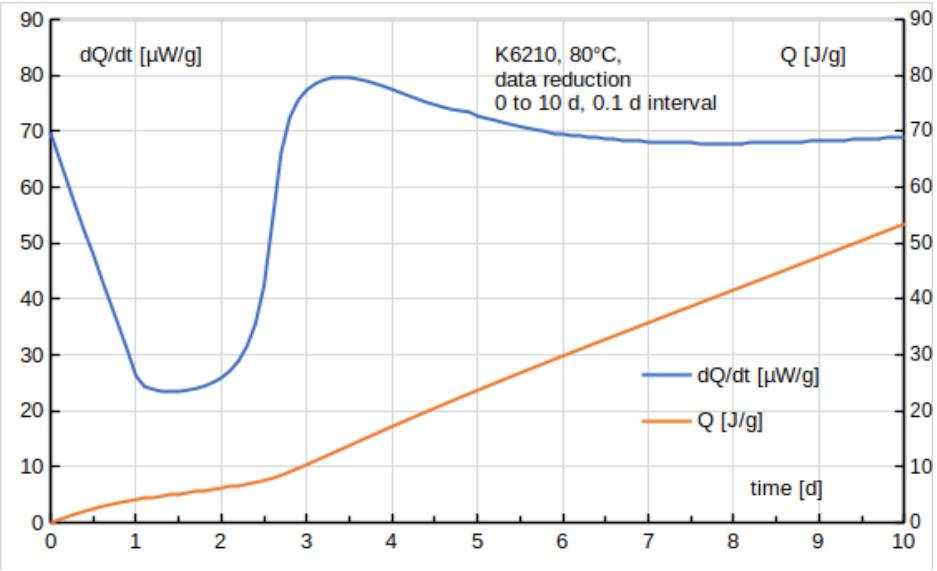

Figure 45: dQ/dt and cumulative Q(t) curves of K6210 sample at 80°C.

as additional parameters for the heat flow curve. These are $\Delta_r H_{NC}$, $\Delta_r H_{auto}$, $\Delta_r H_{NNO}$, $\Delta_r H_{DPANNO}$, $\Delta_r H_{4N}$, $\Delta_r H_{2N}$, $\Delta_r H_{4N\text{-}}$, $\Delta_r H_{NNO\text{-}}$ and $\Delta_r H_{2N\text{-}}$. The naming convention used for the reaction rate constants applies here. The total heat flow can be written as the sum over all i reactions with enthalpies $\Delta_r H_i$ and reaction rates ν_i:

$$\frac{dQ}{dt} = -\sum_i \Delta_r H_i \cdot \frac{d\nu_i}{dt}$$

Written out explicitly this becomes:

$$\begin{aligned}\frac{dQ}{dt} = &-k_{NC}\cdot[ONO_2]\cdot\Delta_r H_{NC} - k_{auto}\cdot[ONO_2]\cdot[P]\cdot\Delta_r H_{auto} - k_{NNO}\cdot[DPA]\cdot[P] \\ &\cdot\Delta_r H_{NNO} - k_{2N}\cdot[DPA]\cdot[P]\cdot\Delta_r H_{2N} - k_{4N}\cdot[DPA]\cdot[P]\cdot\Delta_r H_{4N} - k_{DPANNO} \\ &\cdot[NNO\text{-}DPA]\cdot\Delta_r H_{DPANNO} - k_{NNO-}\cdot[NNO\text{-}DPA]\cdot[P]\cdot\Delta_r H_{NNO\text{-}} \\ &- k_{2N-}\cdot[2NO_2\text{-}DPA]\cdot[P]\cdot\Delta_r H_{2N\text{-}} - k_{4N-}\cdot[4NO_2\text{-}DPA]\cdot[P]\cdot\Delta_r H_{4N\text{-}}\end{aligned}$$

The concentrations of 6 substances and the heat flow curve are modeled, resulting in a total of 7 equations with 18 parameters and 7 initial conditions. At this point a problem with the current version of the *FitODE* application used for the kinetic fits is encountered: The program can fit up to 9 coupled ordinary differential equations, which all must be given in an explicit form

with the derivative of the fitted function on one side of the equation. This means to fit a function f(x) to a data set, one needs to enter an explicit expression for the derivative of the function f'(x). In the case of heat flow, this has the consequence that the expression for dQ/dt can only be used to fit a Q(t) curve, the cumulative heat generated by a sample over time. Mixed fits of differential equations and normal equations are not possible with the current version of *FitODE* (as of February 2020). This issue has been brought to the attention of the Origin™ service team and might be resolved at some point in the future. For the time being, another approach has been developed to fit dQ/dt curves with the current *FitODE* version: To fit a function, one needs it's derivative. Accordingly, to fit dQ/dt one needs an expression for it's derivative, d^2Q/dt^2. The numerical integration of this function returns back its antiderivative, dQ/dt:

$$\int \frac{\mathrm{d}^2\mathrm{Q}}{\mathrm{dt}^2} dt = \frac{\mathrm{dQ}}{\mathrm{dt}} + c \quad \text{or} \quad \int_{t_0}^{t_1} \frac{\mathrm{d}^2\mathrm{Q}}{\mathrm{dt}^2} dt = \frac{\mathrm{dQ}(t_1)}{\mathrm{dt}} - \frac{\mathrm{dQ}(t_0)}{\mathrm{dt}}$$

The integration introduces a new integration constant c. While there is no way to directly choose the value of this constant, it can be controlled indirectly through the initial value of dQ/dt in the program. What remains is to derive an expression for d^2Q/dt^2 from dQ/dt. This is done analytically using the linearity of the differential operator and the product rule for derivatives:

$$\frac{\mathrm{d}}{\mathrm{dx}}(f(x) \cdot g(x)) = f'(x) \cdot g(x) + f(x) \cdot g'(x)$$

The time derivative of dQ/dt can therefore be analytically written as:

$$
\begin{aligned}
\frac{\mathrm{d}^2\mathrm{Q}}{\mathrm{dt}^2} = &-\left(k_{NC}\cdot\frac{\mathrm{d}[\mathrm{ONO_2}]}{\mathrm{dt}}\right)\cdot\Delta_r\mathrm{H_{NC}}\\
&-\left(k_{auto}\cdot\frac{\mathrm{d}[\mathrm{ONO_2}]}{\mathrm{dt}}\cdot[P]+k_{auto}\cdot[\mathrm{ONO_2}]\cdot\frac{\mathrm{d}[P]}{\mathrm{dt}}\right)\\
&\cdot\Delta_r\mathrm{H_{auto}}-\left(k_{NNO}\cdot\frac{\mathrm{d}[\mathrm{DPA}]}{\mathrm{dt}}\cdot[P]+k_{NNO}\cdot[\mathrm{DPA}]\cdot\frac{\mathrm{d}[P]}{\mathrm{dt}}\right)\\
&\cdot\Delta_r\mathrm{H_{NNO}}-\left(k_{2N}\cdot\frac{\mathrm{d}[\mathrm{DPA}]}{\mathrm{dt}}\cdot[P]+k_{2N}\cdot[\mathrm{DPA}]\cdot\frac{\mathrm{d}[P]}{\mathrm{dt}}\right)\\
&\cdot\Delta_r\mathrm{H_{2N}}-\left(k_{4N}\cdot\frac{\mathrm{d}[\mathrm{DPA}]}{\mathrm{dt}}\cdot[P]+k_{4N}\cdot[\mathrm{DPA}]\cdot\frac{\mathrm{d}[P]}{\mathrm{dt}}\right)\\
&\cdot\Delta_r\mathrm{H_{4N}}-\left(k_{DPANNO}\cdot\frac{\mathrm{d}[\mathrm{NNO\text{-}DPA}]}{\mathrm{dt}}\right)\cdot\Delta_r\mathrm{H_{DPANNO}}\\
&-\left(k_{NNO-}\cdot\frac{\mathrm{d}[\mathrm{NNO\text{-}DPA}]}{\mathrm{dt}}\cdot[P]+k_{NNO-}\cdot[\mathrm{NNO\text{-}DPA}]\cdot\frac{\mathrm{d}[P]}{\mathrm{dt}}\right)\\
&\cdot\Delta_r\mathrm{H_{NNO\text{-}}}-\left(k_{2N-}\cdot[2\mathrm{NO_2}\cdot\text{-}DPA]\cdot\frac{\mathrm{d}[P]}{\mathrm{dt}}\right)\\
&\cdot\Delta_r\mathrm{H_{2N\text{-}}}-\left(k_{4N}\cdot[4\mathrm{NO_2}\text{-}DPA]\cdot\frac{\mathrm{d}[P]}{\mathrm{dt}}\right)\cdot\Delta_r\mathrm{H_{4N\text{-}}}
\end{aligned}
$$

This formula now contains a number of mixed products of concentrations and their derivatives. At this point the expressions for these derivatives can be explicitly substituted in since they are known from the rate laws for the kinetic system. This leads to a long and somewhat convoluted formula for $\mathrm{d}^2\mathrm{Q}/\mathrm{dt}^2$ which can be used to find dQ/dt. The outlined method can be used for any kinetic model and heat flow curve so long as the derivatives can be written explicitly. The heat flow curve and kinetic data can either be fitted together or consecutively, i.e. finding the optimal kinetic parameters first and then optimizing the enthalpy parameters. Optimizing together gives a better result as the kinetic parameters can change to better describe the data set as a whole, while fitting separately has the advantage of being much faster. In practice *FitODE* limits the number of free parameters so that fitting the kinetic data and heat flow curves with all parameters simultaneously results in an error message. One must fix a number of either enthalpies or kinetic parameters; for this reason fits were done for only the kinetic data first and then for the heat flow curve with the preoptimized kinetic parameters fixed. Appropriate values from DFT calculations are selected as reasonable parameters to initialize the fit and as references for expected ranges of the

reaction enthalpies. For $\Delta_r H_{NNO}$ a value around -87.3 kJ mol^{-1} as given in Table 9. The reverse reaction should have the enthalpy but positive. $\Delta_r H_{4N}$ = -134.7 kJ mol^{-1} and $\Delta_r H_{2N}$=-124.9 kJ mol^{-1} are assumed. These are the values for an electrophilic aromatic substitution of DPA with HNO_3 as given in section 5.2.3. For the other reactions no specific products are available. For 2NO_2-DPA and 4NO_2-DPA, a reasonable follow-up reaction is the binding of more *P*, forming NNO-2NO_2-DPA and NNO-4NO_2-DPA respectively. As calculated in section 5.5, the enthalpies for these reactions are $\Delta_r H_{4N\text{-}}$=-73.1 kJ mol^{-1}, and $\Delta_r H_{2N\text{-}}$=–55.5 kJ mol^{-1}. The enthalpies for these reactions could, however, be as high as -135.4 kJ mol^{-1} if more electrophilic aromatic substitutions take place instead. For $\Delta_r H_{NNO\text{-}}$ one could assume the same products, i.e. NNO-2NO_2-DPA and NNO-4NO_2-DPA. The enthalpy of nitration for a 1:1 product mixture is $\Delta_r H_{NNO\text{-}}$=-106.8 mol^{-1}. The enthalpy of decomposition of NC is more complicated as no single reaction can be referenced here. In the previous section values of up to -250 mol^{-1} were fitted for the complete degradation of NC. The initial stages are likely lower in enthalpy. Values between -69.4 kJ mol^{-1} and -93.7 kJ mol^{-1} have beeon computed for the elimination of HONO in section 4.2. A value in this range seems reasonable as it would describe the formation of NO_2 and the subsequent abstraction of a hydrogen atom from the NC chain by it. As a high (endothermic) estimate one could also imagine a reaction in which only the O$-NO_2$ bond in NC is broken and nothing else happens. This would place the highest resonable enthalpy at +161.5 kJ mol^{-1} for both $\Delta_r H_{NC}$ and $\Delta_r H_{auto}$. For the initial fitting a value of -80 kJ mol^{-1} is used as a middle position between the extremes. These values are summarized in Table 12.

Fitting a combination of kinetic parameters and enthalpies also introduces an additional issue: The weighting of the data sets depends on their respective number of data points. Heat flow curves are measured at a much higher frequency than the stabilizer concentrations so that using an unmodified data set would lead to the heat flow measurements being overemphasized in their effect on R^2. A modified data set with the same number of points for each of the curves has been created to counteract this. The stabilizer data has been interpolated to 10 data points per day and the heat flow measurements were reduced to the same point density. This data set is used and kinetically fitted in the next section. For the following fits in this section, the kinetic parameters from Figure 44 are used and the enthalpies are fitted

Table 12: Suggested DFT-backed enthalpies for enthalpies in RS3 in NC simulate at 90°C. Enthalpies in kJ mol^{-1}.

Enthalpy	Expected DFT value
$\Delta_r H_{NC}$	-80.0
$\Delta_r H_{auto}$	-80.0
$\Delta_r H_{NNO}$	-87.3
$\Delta_r H_{DPANNO}$	+87.3
$\Delta_r H_{4N}$	-134.7
$\Delta_r H_{2N}$	-124.9
$\Delta_r H_{4N\text{-}}$	-73.1
$\Delta_r H_{NNO\text{-}}$	-106.8
$\Delta_r H_{2N\text{-}}$	-55.5

separately so that this data weighting question does not arise.

As a reference, a heat flow curve with the enthalpies backed up by DFT calculations and kinetic data from Figure 44 is simulated. No fitting is done, the ODE system is simply solved with a set of fixed parameters. The initial heat flow, i.e. dQ/dt at t=0, is set to match the experimental value as well. This simulated curve (Figure 46) does not show much resemblance with the experimental heat flow curve. There are some problems with the resulting curve. First of all, it has a low adj. R^2=0.0099. This value is used to gauge the quality of the raw simulated curve. The curve barely follows the experimental curve. A small decrease in generated heat is observed for the first five days, which is in fact in line with the DPA heat dip. An intuitive conclusion that could be made from the kinetic data is that the reaction rate of DPA to NNO-DPA is higher than that of DPA to the other products, mostly NNO-DPA is produced in this time frame. As more and more of the DPA is converted into nitro-DPA's in a process that has a higher reaction enthalpy, the heat flow rate increases.. This interpretation is in a sence correct, as the kinetic data does predict this heat flow decrease; however, this decrease is only on the order of 5-10 µW g^{-1} and much smaller than is experimentally observed.

Furthermore, after about 6 days the expected heat flow rate becomes much larger than the experimental value. This increase is the start of an exothermic autocatalytic peak. As the kinetic model only includes the concentrations of DPA, NNO-DPA and the mononitro-DPA's this type of behav-

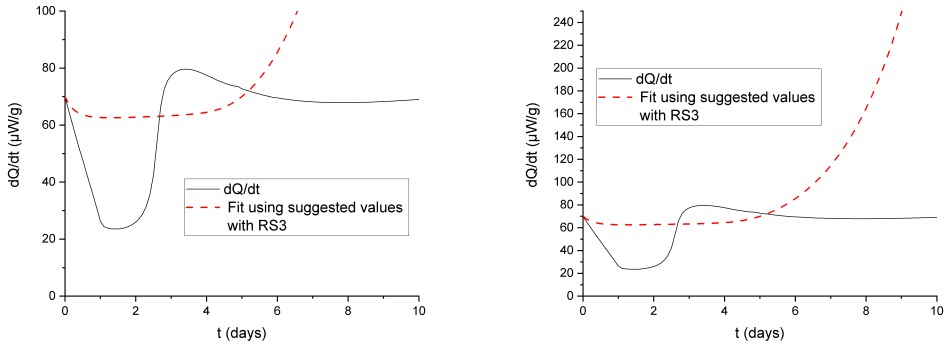

Figure 46: Kinetic simulation of K6210 double base propellant with stabilizer DPA at 80°C with RS3. Same curves with different scaling. Rate constants from Figure 44 and presumed DFT-based give an adj. R^2=0.0099.

ior is to be expected to some degree as soon as most of these stabilizer species are removed from the system. It is, however, around the time when most of the stabilizer is present in the form of NNO-DPA and smaller amounts of mononitro-DPA that this increase begins. These compounds still have one more reaction step included even in RS3, which makes such an early run-away reaction unforeseen. Reducing the data set to a time frame of only 6 days helps to improve the same fit. Figure 47 shows a fitted heat flow curve for using the same fixed enthalpies and rate constants as before, with the exception that the initial heat flow rate was used as a free fitting parameter to allow for baseline adjustments and that only the first 6 days were fitted. With these improvements, the optimized fit still has been found to have only an adj. R^2=0.206.

Fitting the system without these restraints on the enthalpies in place can give an estimate of what the values of the reaction enthalpies would have to be for the given kinetic model to produce the observed heat flow. Out of the necessity to limit the number of free parameters the enthalpies of the formation of $2NO_2$-DPA and $4NO_2$-DPA were fixed at -200 kJ mol^{-1}. This value corresponds to the most exothermic expected enthalpy value for a nitration by N_2O_5. Making this parameter more exothermic has consistently improved the fit quality in previous runs. The initial heat flow rate was again set fitted as a free parameter. This unrestricted fit (Figure 48) gives a much

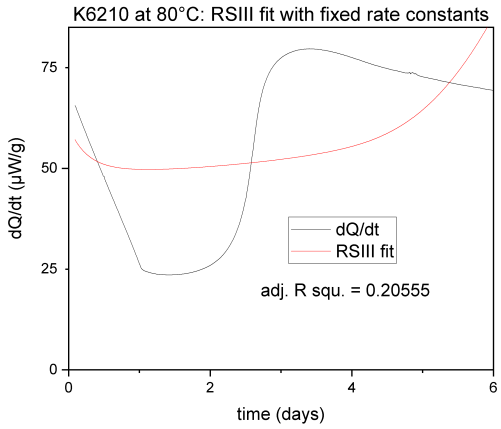

Figure 47: HMFC curve of K6210 sample at 80°C and fitted curve with fixed kinetic data as given in figure 44 and suggested DFT-based enthalpies.

better fit with an adj. R^2=0.843. The initial reduction of the heat generation rate is steeper than the observed curve and the flow is restored more slowly, but the overall trends of the DPA heat flow curve are captured rather well.

While the form of the resulting curve is acceptable, the values of the optimized enthalpies are far from it. Not only do impossibly high values in the range of MJ/mol and GJ/mol appear, but the standard deviations are also significantly smaller than e.g. what was encountered in Figure 44. A lower standard deviation suggests that deviations from the optimized values lead to more of a decrease in the quality of the fit or, in other words, only values close to the faulty results can adequately account for the experimental observation. The sheer size of the necessary enthalpies points to a deeper problem with the kinetic model, which can also be discovered by considering the Q(t) curve included in Figure 45. Using the 5th day as an example, one can try to account for the heat generated up to that point. Over the course of 5 days approximately 25 J of heat are generated per g of sample. At the same time the majority of stabilizer is found in the form of NNO-DPA, i.e. for the most part only one nitration has taken place at this point. Using the reaction enthalpy for the formation NNO-DPA from DPA Δ_rH = -87.3 kJ mol^{-1} according to chemical reaction (Ib) as given in table 8 as an reference, the estimated heat generated by 30 µmol DPA reacting to NNO-DPA would be on the order of 30 µmol · 87.3 mJ µmol^{-1} = 2.62 J. The heat

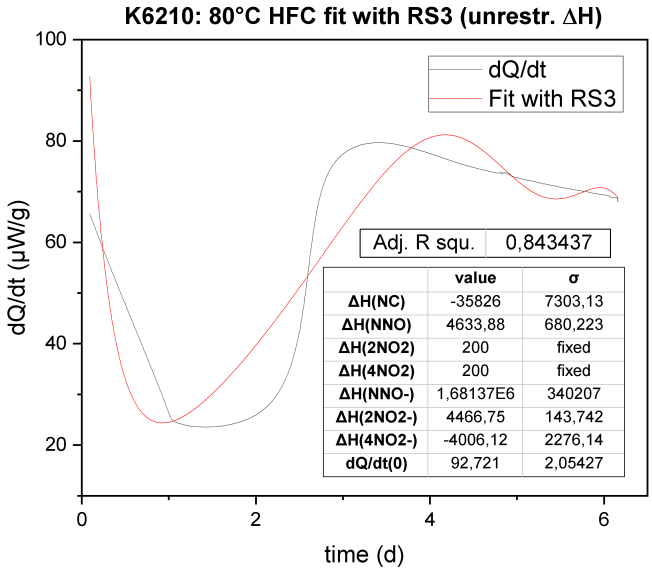

Figure 48: HMFC curve of K6210 sample at 80°C and fitted curve with fixed kinetic data as given in Figure 44 without restraints on $\Delta_r H_i$ along with results of fit. Initial dQ/dt in µW g^{-1}, enthalpies in kJ mol^{-1}.

generated by DPA reacting to NNO-DPA accounts for only about 10% of the total generated heat. Taking nitrations to $2NO_2$-DPA and $4NO_2$-DPA slightly increases this estimate to 3.1 J or 13% at the most. Turning this around implies that 87-90% of the observed heat flow cannot realistically be attributed to reactions with stabilizer but must rather be due to the decomposition of NC and subsequent reactions between the products of this decomposition. With this observation the high reaction enthalpies from the enthalpy fit become more intuitive: To compensate for the missing bulk of reaction enthalpy, reactions contributing only a fraction to the total heat must be exaggerated by multiple orders of magnitude. Reexamining the arguments made to rationalize the high baseline in AkII in fact does not help for DPA. For AkII the claim was made that by assuming around 4 nearly instantaneous nitrations of the phenyl rings and the generation of P with the high estimate of $\Delta_r H_{NC}$ =-227 kJ mol^{-1} one could explain the 50 µW/g baseline. For DPA the heat generation rate shifts from about 25 µW/g at the least and about 75 µW/g at the most. The modest heat generation

through stabilizer reactions cannot possibly explain a drop of this magnitude by itself. In the next section an modified extended RSIII that better matches the kinetic data is examined. From it one more hint concerning the possible origin of this contradiction is discussed.

7.3.2 Extended reaction system III

Reaction system III only includes the stabilizer concentrations up to the first nitration step. To improve it two additional concentration curves are fitted: The concentrations of NNO-2NO_2-DPA and NNO-4NO_2-DPA become relevant particularly around the time when the concentrations of 2NO_2-DPA, 4NO_2-DPA and NNO-DPA are at their peak. As the concentrations of the NNO-2NO_2-DPA and NNO-4NO_2-DPA increase, those of NNO-DPA and the mononitro-DPA's begin to fall. For this reason it is suggested that there may be two pathways for the formation of each of these products. These two pathways are either the nitration of NNO-DPA or the nitrosation of mononitro-DPA:

$$\text{2NO}_2\text{-DPA} + \text{NO}_2 + \text{NO} \longrightarrow \text{NNO-2NO}_2\text{-DPA} + \text{HNO}_2$$
$$\text{NNO-DPA} + \text{HNO}_3 \longrightarrow \text{NNO-2NO}_2\text{-DPA} + \text{H}_2\text{O}$$
$$\text{4NO}_2\text{-DPA} + \text{NO}_2 + \text{NO} \longrightarrow \text{NNO-4NO}_2\text{-DPA} + \text{HNO}_2$$
$$\text{NNO-DPA} + \text{HNO}_3 \longrightarrow \text{NNO-4NO}_2\text{-DPA} + \text{H}_2\text{O}$$

The enthalpies for these reactions have been given in Table 12 as $\Delta_r H_{\text{4N-}}$, $\Delta_r H_{\text{NNO-}}$ and $\Delta_r H_{\text{2N-}}$. As there are two different products for the reaction of NNO-DPA in this model, k_{NNO-} needs to be replaced with two rate constants. k_{NNO4N-} is used for the reaction yielding NNO-4NO_2-DPA and k_{NNO2N-} refers to the reaction to NNO-2NO_2-DPA.The rate laws for the additional two compounds are:

$$\frac{d[\text{NNO-2NO}_2\text{-DPA}]}{dt} = k_{NNO2N-}[\text{NNO-DPA}][P] + k_{2N-}[\text{2NO}_2\text{-DPA}][P]$$

$$\frac{d[\text{NNO-4NO}_2\text{-DPA}]}{dt} = k_{NNO4N-}[\text{NNO-DPA}][P] + k_{4N-}[\text{4NO}_2\text{-DPA}][P]$$

With this there are eight ODE's for a total of eight substances. This changes two of the rate laws in RS3 to:

$$\frac{d[P]}{dt} = k_{NC}[\mathrm{ONO_2}] + k_{auto}[\mathrm{ONO_2}][P] - (k_{NNO} + k_{2N} + k_{4N})[\mathrm{DPA}][P] + k_{DPNNO}[\mathrm{NNO\text{-}DPA}] - k_{NNO4N-}[\mathrm{NNO\text{-}DPA}][P] - k_{NNO2N-}[\mathrm{NNO\text{-}DPA}][P] - k_{2N-}[2\mathrm{NO_2}\text{-}DPA][P] - k_{4N-}[4\mathrm{NO_2}\text{-}DPA][P]$$

$$\frac{d[\mathrm{NNO\text{-}DPA}]}{dt} = k_{NNO}[\mathrm{DPA}][P] - k_{DPANNO}[\mathrm{NNO\text{-}DPA}] - k_{NNO4N-}[\mathrm{NNO\text{-}DPA}][P] - k_{NNO2N-}[\mathrm{NNO\text{-}DPA}][P]$$

The expressions for the heat flow dQ/dt and dQ^2/dt^2 are assumed to remain practically unchanged as $\Delta_r H_{\mathrm{NNO\text{-}}}$ already uses the average the reactions to NNO-$2NO_2$-DPA and NNO-$4NO_2$-DPA. For the next fits a modified stabilizer concentration data set derived from the one used in section 7.3.1. Only nine data points have been measured per stabilizer species. These data point have been interpolated and smoothed out to generate a data set with concentration values in 0.1 day-intervals by using the data interpolation tool in Origin 2019b™.

Using the same initial conditions as previously and 0 µmol g^{-1} for NNO-$2NO_2$-DPA and NNO-$4NO_2$-DPA three fits with the interpolated data set have been performed. For one fit, the initial concentration of P is set to 0 µmol g^{-1}. This fit has been found to be in very good agreement with the interpolated with adj. R^2=0.99855. For another fit the initial concentration of P was set to 5 µmol g^{-1}. For this fit a similarly good adj. R^2=0.99889 was found. Finally, one fit was performed with $[P]_0$=10 µmol g^{-1}. This fit resulted in an adj. R^2=0.99891. As the data has been modified and smoothed the adj. R^2-metrics are higher for the same original data set.

What has not yet been mentioned for RS3 is how the simulated concentration of P evolves over time. To answer this question, the calculated concentration of P over time is addition to the concentrations of the stabilizers and their fitted curvesfor the curve with an initial value of $[P]_0 = 0$ µmol g^{-1}.

For a short initial period, the $[P]$ slightly decreases. Following this, the curve clearly shows the beginning of a runaway increase of $[P]$ as early as the first or second day. After two days $[P]$ is higher than the concentration of DPA and around the fourth to fifth day it becomes higher than the total concentration of all stabilizer species combined. The rising heat flow rate as shown in Figure 46 matches and closely follows the increasing $[P]$.

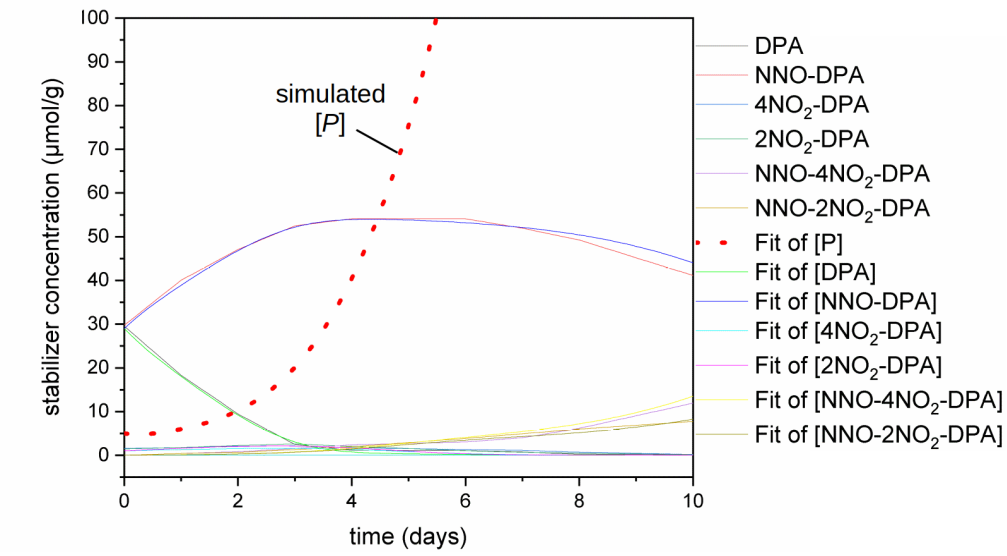

Figure 49: Kinetic modeling of K6210 DPA-stabilized double-base propellant at 80°C. [P](0)=5 µmol g^{-1} fixed. Fit corresponding to Figure 51. Adj. R^2=0.99855. Focus on simulated concentration of P over time.

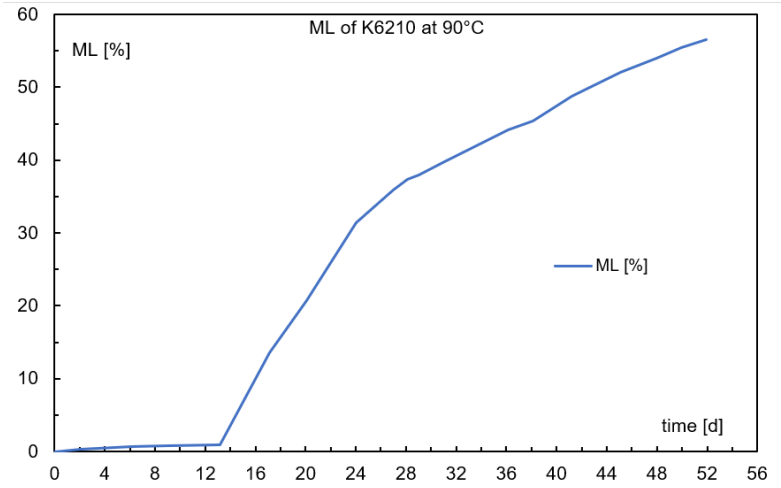

Figure 50: Experimentally detected mass loss of K6210 DPA-stabilized double-base propellant at 90°C over time.

This increase follows the pattern that was observed for the runaway autocatalytic degradation and indicates that the high heat flow rate can mostly be attributed to the autocatalytic degradation reaction. Other initial concentrations of P show a similarly early and steep rise. The inclusion of di- and trinitro-DPA's does not account for such an early rise since practically no such products are found until much later. Even when reaction rates are even higher at 90°C, appreciable amounts of dinitro-DPA's are only found on the seventh day, as can be seen in Figure 17. A reaction that produces these compounds from the mononitro-DPA's or NNO-mononitro-DPA's cannot account for a runaway autocatalytic increase that occurs days before these compounds appear. In an experiment measuring the mass loss of a sample of K6210 at 90°C (Figure 50) it was estabilished that a runaway autocatalytic reaction does not occur until after 13 days, much later than the two to four days pre[97]. At a lower temperature the stabilization period should be much longer, by about a factor 3 for a temperature of 80°C. The early autocatalytic peak is therefore not in accordance with experimental data. It is an inadequate prediction made by RS3.

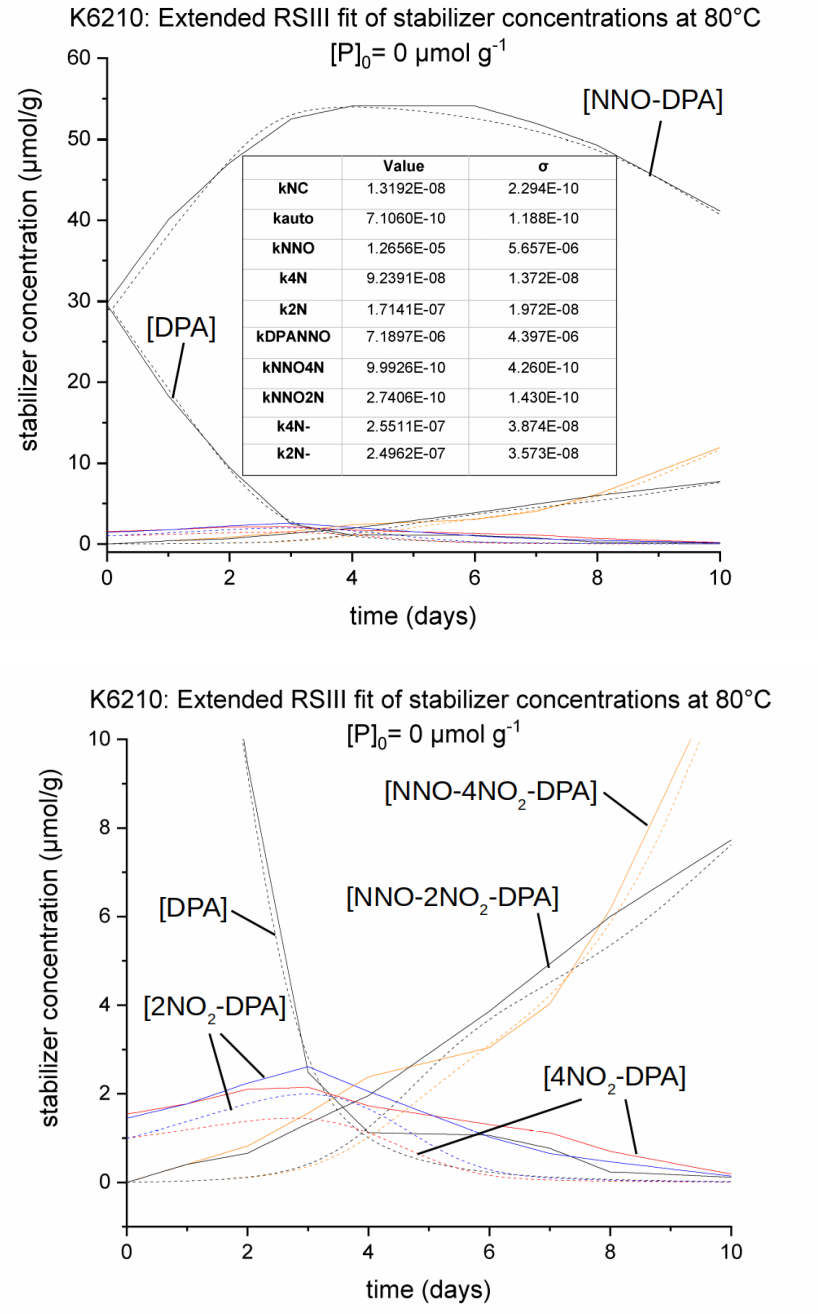

Figure 51: Kinetic modeling of K6210 DPA-stabilized double-base propellant at 80°C. [P](0)=0 µmol g^{-1} fixed. k_{NC} and k_{DPANNO} in s^{-1}, all other rate constants in g µmol^{-1} s^{-1}. Zoomed-in graph below. Adj. R^2=0.99855. Interpolated data in solid lines, fitted data dotted.

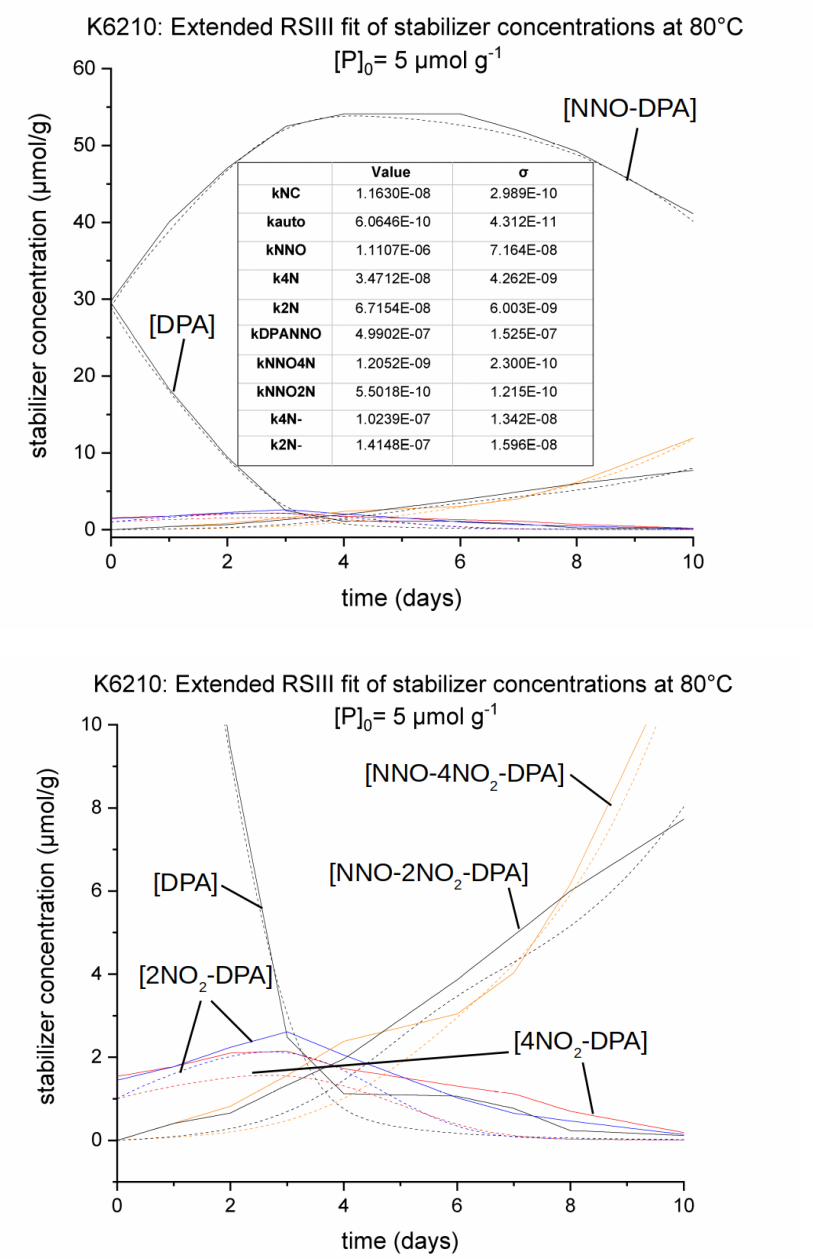

Figure 38 (continued): Kinetic modeling of K6210 DPA-stabilized double-base propellant at 80°C. [P](0)=5 µmol g^{-1} fixed. k_{NC} and k_{DPANNO} in s^{-1}, all other rate constants in g µmol^{-1} s^{-1}. Zoomed-in graph below. Adj. R^2=0.99889. Interpolated data in solid lines, fitted data dotted.

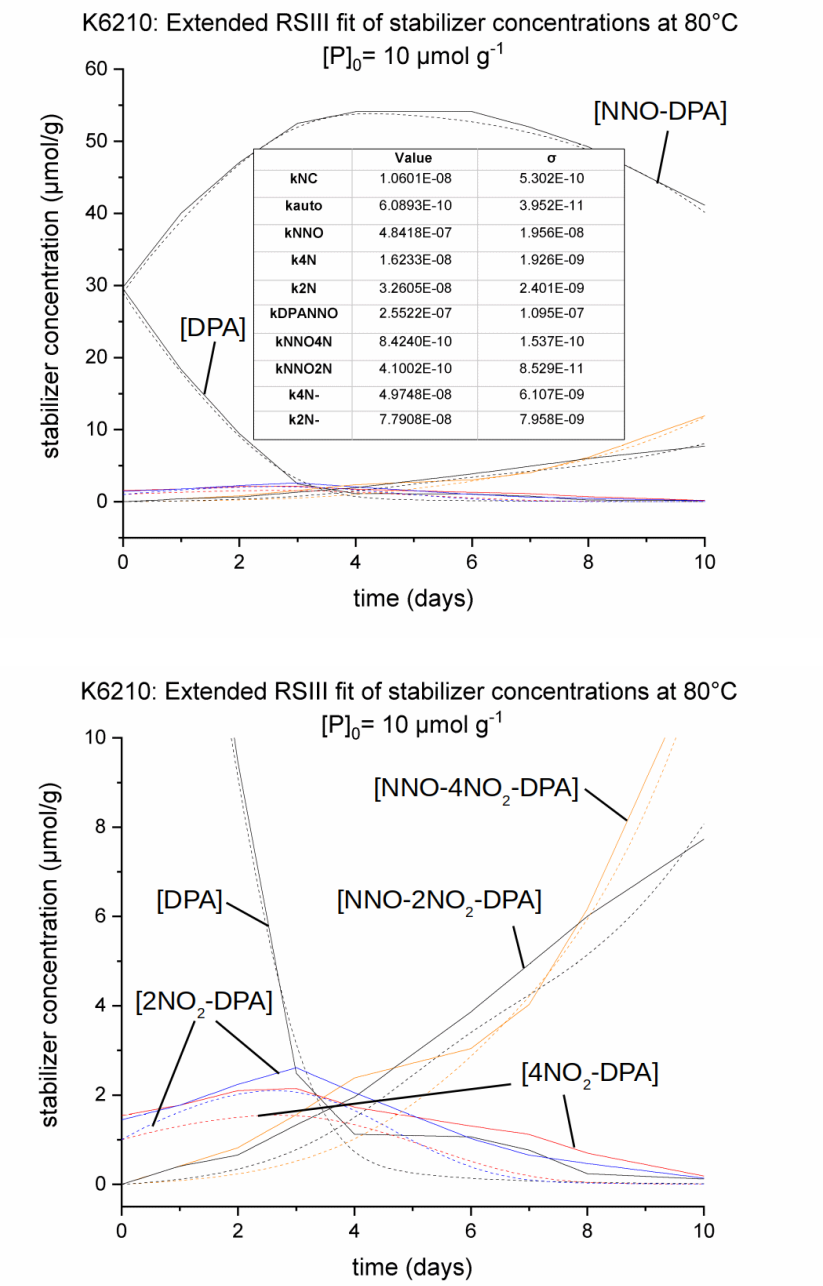

Figure 38 (continued): Kinetic modeling of K6210 DPA-stabilized double-base propellant at 80°C. [P](0)=10 µmol g^{-1} fixed. k_{NC} and k_{DPANNO} in s^{-1}, all other rate constants in g µmol^{-1} s^{-1}. Zoomed-in graph below. Adj. R^2=0.99891. Interpolated data in solid lines, fitted data dotted.

7.4 Potential solution: nitrocellulose autostabilization

7.4.1 Recapitulation

In section 7.1 it was found that to account for the time a NC sample can be exposed to high temperatures before reaching its autocatalytic peak, it must have a high k_{auto}-value and a very low k_{NC}-value for intrinsic degradation. This combination would inaccurately predict that NC-samples would practically immediately enter their autocatalytic peak following an exposure to tiny amounts of P. At the same time, the predicted heat flows preceeding the autocatalytic exothermic peak are up to 10,000,000 times lower than the experimental values.

A similar conclusion was reached in section 7.2. The Ak II-stabilized sample shows a higher-than-predicted heat flow baseline. Assuming a one-to-one reaction between a stabilizer and P for each reaction step, about four instantaneous nitrations per stabilizer molecue would need to be assumed to account for this high baseline, which is in contradiction with experimental stabilizer curves. It was also established that the initial heat decrease count be modeled using a second order reaction of one or two compounds. The same model was also successfully used for a NC sample from section 7.1, showing that a similar reaction takes place in pure NC and that no stabilizer is necessary to explain this reaction.

It was established in section 7.3.1 that the initial drop in heat generation is too large to be accounted for by reactions of DPA with P, meaning the dip would have to be attributed to reactions of NC and its decomposition products instead. At the same time this reaction would in some way need to depend on P, as otherwise the same heat flow pattern would be observed in NC and Ak II.

In section 7.3.2 it was found, that in the extended RS3 the concentration of P cannot be suppressed longer than two to four days. This is excessively short and not in line with the experimental heat flow curves. However, an initially rising $[P]$ is necessary to achieve a fit which is in good agreement with the (interpolated) experimental data. The low standard deviation indicates that the unreasonably high k_{auto} is in fact required to achive a good fit with RS3.

7.4.2 Effect of diffusion

Up to this point it was assumed that reactions with stabilizers are the only force suppressing a P-buildup. In that view, the entirety of P is also actively involved in autocatalytic reactions and is fully available to react with the stabilizer. What is neglected is that P is a gas and can diffuse out into the gas phase making it unavailable for both autocatalytic processes and unavailable to stabilizers. This would mean that a significant amount of P may be constantly forming without manifesting itself in the kinetic data. While the diffusion of gases into and out of the NC matrix is fairly complicated, one can estimate that with $\Delta_r H_{NC}$ =-227 kJ mol^{-1} about 1.5-2 times as much P needs to gas out than is bound by stabilizer to account for the remaining 22 J from the previous calculation for DPA. This effect could also lead to the type of heat dip as is seen in DPA. During the first two days most of P would have to diffuse out of the NC matrix and the partial pressure of gaseous P would have to gradually build up without much interference by the stabilizer. Upon reaching a certain threshold pressure, the infusion rate back into the NC might start to reach an equilibrium with the outgassing; at this point the a majority of the generated P begins to build up inside the NC matrix, increasing the binding and autocatlytic decomposition rates and thus increasing the heat flow. While this certainly is a possible explaination, it falls somewhat short in some respects: For one, as has been referenced in Figure 32, AkII as well as DPA and ethyl centralite can bind gaseous NO_2, even at room temperature. This means that if P was released into the gas phase it would not be completely unavailable for the stabilizer. Due to the higher temperature the reaction between stabilizer and P would be much faster than at room temperature and most of the gaseous P would in the end be bound by stabilizer. Additionally, if diffusion predominantly controlled the heat flow curve during the first days, why would an Ak II-stabilized sample not show the same behavior? It is true that the outgassing properties and exposedness to air are different for DPA-stabilized samples and AkII-stabilized samples as was pointed out with Figure 31. The microstructure of DPA-stabilized NC was, however, found to closely resemble that of unstabilized NC as DPA does not gelatinize NC. If diffusion was the main reason for the difference of the heat flow curves, one would expect that the heat flow curves of unstabilized NC and DPA-stabilized NC should resemble each other, while the curve of the gelatinized Ak II-stabilized sample should look distinctly different. In reality, the Ak II-stabilized sample and unstabilized NC are remarkably

similar. This comparison is nevertheless not ideal, as the unstabilized NC sampled is a loose material, while the stabilized samples are compressed into denser propellant grains. Another consequence would also be that the choice of gelatinization agents and plasticizers should have a much stronger effect on the heat flow curves of propellants than the choice of the stabilizer, which is not the case[50]. The shape of the heat flow curve of a propellant is characteristic to the stabilizer, so the stabilizer must play an important role in controlling the reaction rates leading to the observed heat flow curves without itself being able to contribute much of the generated heat.

7.4.3 NC autostabilization

Another potential resolution to this brainteaser is contained in RS3 itself, namely equations (9) and (10): It is the thus far overlooked R. During the course of the decomposition of NC a number of products are generated besides P. These range from organic radicals, aldehydes to the final degradation products like CO_2 and CO. In section 4.1 the reduction of different species of P by formaldehyde was discussed. Formaldedhyde has been detected as one of the products of the degradation of NC. It has also been mentioned that formaldehyde reacts with NO_2, one of the main components of P to form NO, CO and CO_2. Supporting DFT calculation showed that CH_2O can act as a reducing agent strong enough to exergonically and exothermally reduce any species of P down to NO. NO has been found to be the primary species of P detected in the gas phase around decomposing NC rather then the initially formed NO_2. This would suggest that substances like formaldehyde, glyoxal and aldehyde groups bound to the degrading NC backbone might themselves react with autocatalytically active NO_2/HNO_3 and reduce them to a less potent form. This proposed concept will be called "autostabilization", in a sense the reverse of autocatalysis. Autostabilization means that products of the degradation of NC remove P and slow down the degradation process. As more P forms from the degradation of NC, so does R, which, in turn, decreases the overall degradation rate. Oxygen and stabilizers can influence this process: Oxygen can reoxidize the harmless NO to autocatalytically active NO_2. This process is similar to the catalytic cycle mentioned in Figure 9. This increases the concentration of autocatalytically active P, which would increase the degradation rate. Autostabilization would explain many of the issue that were encountered with the first order autocatalytic system for NC and the stabilized propellant models. It would allow for a higher long term

concentration of P, without an immediate risk of entering the exothermic degradation peak. NC could gradually decompose at a stable, near constant rate, as is manifested in the long plateaued heat flow curve. The heat flow rate in stabilized samples could be much higher than is can be accounted for with only stabilizer and P-producing reactions.

7.4.4 Simple kinetic model

A kinetic model based on the premise of NC autostabilization is presented and tested. The simplest possible reaction system involves the concentration of nitrate esters, P, the concentration of a stabilizer S and, as a new feature, the concentration of the stabilizing by-product of NC degradation R. None of the stabilizing products of the reaction of P and S are included in this model. The chemical equations describing this system are:

$$\mathrm{NC} \xrightarrow{k_{NC}} P + R \qquad \text{intrinsic decomposition}$$

$$\mathrm{NC} + P \xrightarrow{k_{auto}} 2P + R \qquad \text{autocatalysis}$$

$$P + R \xrightarrow{k_R} \mathrm{CO} + \mathrm{CO_2} + \mathrm{NO} + ... \qquad \text{autostabilization}$$

$$S + P \xrightarrow{k_S} [S - P] \qquad \text{normal stabilization}$$

The rate laws describing this system of reactions can be written as:

$$\frac{d[\mathrm{ONO_2}]}{dt} = -k_{NC}[\mathrm{ONO_2}] - k_{auto}[\mathrm{ONO_2}][P]$$

$$\frac{d[P]}{dt} = k_{NC}[\mathrm{ONO_2}] + k_{auto}[\mathrm{ONO_2}][P] - k_S[\mathrm{S}][P] - k_R[R][P]$$

$$\frac{d[R]}{dt} = k_{NC}[\mathrm{ONO_2}] + k_{auto}[\mathrm{ONO_2}][P] - k_R[R][P]$$

$$\frac{d[\mathrm{S}]}{dt} = -k_S[S][P]$$

While this model is limited in its ability to capture the whole range of stabilizer-P-interactions, it can be used to understand what NC autostabilization would mean for a NC sample. This reaction system has three

reaction enthalpies: $\Delta_r H_{NC}$ for the degradation of NC, $\Delta_r H_S$ for the reaction between stabilizer and P and $\Delta_r H_R$ for the reaction between P and R. For $\Delta_r H_{NC}$=-80 kJ mol^{-1} the same value is used as before. $\Delta_r H_S$ = -87.4 kJ mol^{-1} in the case of the DPA-stabilized sample for the reaction of DPA to NNO-DPA and $\Delta_r H_S$ = -119.8 kJ mol^{-1} could be used for the nitration of AK II to 4NO_2-Ak II. Under the assumption that the autostabilizing species is CH_2O, enthalpy $\Delta_r H_R$ for the following reaction will be used:

$$CH_2O + NO_2 \longrightarrow CO + H_2O + NO \text{ with } \Delta_r H_R = -156.2 \text{ kJ mol}^{-1}$$

Starting with the DPA-stabilized K6210 sample from section 7.3, the new model system is fitted to the heat flow curve and the concentration of DPA = $[S]$. The initial concentrations of nitrate ester was set to 9355 µmol g^{-1} and that of DPA was set to 29 µmol g^{-1}. The initial values of $[P]$ and $[S]$ were fitted as free parameters.

The result of the fit is shown in Figure 52. Even this simple model successfully captures the inital dip of the heat generation rate. Features like the heat output maximum after the dip are not recreated and the modeled heat flow curve is generally less steep than the measured curve around that time. The fit has an adj. R^2=0.94511. The rate constant for the intrinsic degradation of NC has been optimized to 0 as the autocatalytic process degradation process is much more significant for the shape of the heat flow curve. Figure 53 shows how the calculated concentrations of R and P evolve over time in this fit. Initially, the concentration of P is around 14 µmol g^{-1} and much higher than that of R. DPA is the only stabilizer that is present. The concentration of P rises to around 20 µmol g^{-1}, while the amount of R rapidly increases. It reaches a practically constant the formation and autostabilization reactions reach an effective equilibrium. This process automatically prevents the concentration of P from becoming too high.

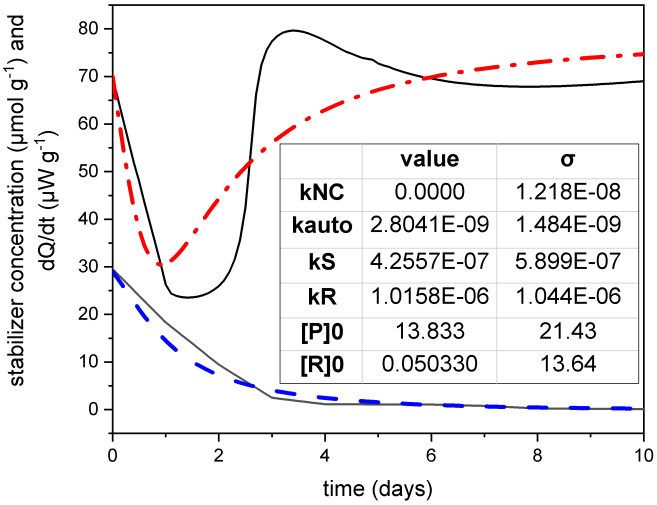

Figure 52: HMFC curve of K6210 sample at 80°C and fitted curve with autostabilization model and fitted parameters. k_{NC} in s^{-1}, all other rate constants in g µmol^{-1} s^{-1}. $[P]_0$ and $[R]_0$ in µmol g^{-1}. Adj. R^2=0.94511.

7.4.5 AK II and unstabilized NC

Given different initial conentrations of P and R as well as a different k_S, completely different shapes of heat flow curves are possible. A high initial $[R]$ gives a heat flow curve that has a smaller initial dip or none at all. This could be the case for Ak II-stabilized propellant and in particular unstabilzed NC, which could be modeled with $k_S = 0$. In these samples the presence of oxygen can significantly distort the shape of the heat flow curves, as NO_2 can constantly be recovered. The result is a higher heat flow baseline and a faster degradation, as is e.g. manifested in the unstabilized NC samples.

What remains unclear, is why the initial concentration of R in DPA stabilized propellants and those with Ak II or no stabilizer should be so different. It should be expected that similar amounts of R should build up in NC over time, no matter the stabilizer. Possibly, the reactivity of DPA can justify this. DPA is more reactive than Ak II and can remove free radical and related species more effectively than Ak II. This is true for P, and may also apply to R. As was discussed in section 5.3, DPA is also known to react with aldehydes (formaldehyde) to form oligomers and polymers. Such a reaction would not only explain why so little R is initially found in DPA-stabilized

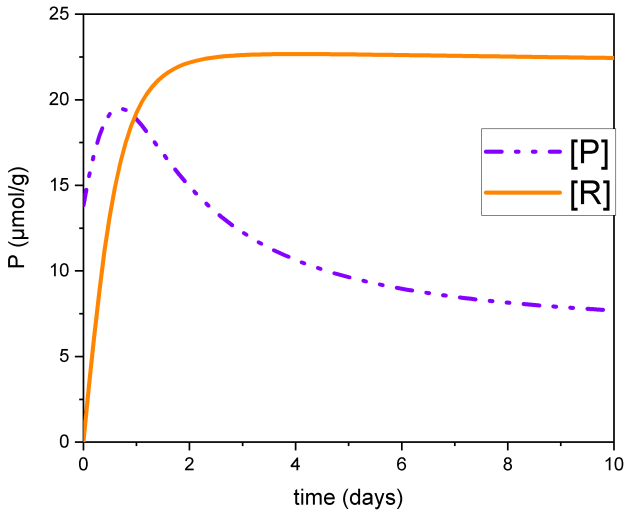

Figure 53: Simulated concentrations of R and P over time in fit in Figure 52.

NC, but also resolve the mystery of the disappearing DPA. Even the concept of DPA acceleration would have to be revisited. The unexpectedly high stability of some NC samples compared to DPA stabilized samples may not be due to detrimental interactions between DPA and NC but rather due to the fact that even otherwise unstabilized NC has its internal autostabilizer. Furthermore, rather than exclusively focusing on the interaction of DPA with nitrate esters, if DPA undergoes e.g. a condensation reaction with R it would similarly remove both stabilizers and accererate the degradation. In general the interactions between P, NC, DPA and R are in general quite complex and further experiments are necessary to conculsively clear up these questions.

7.4.6 Future outlook and improvements

A simple model system based on the idea of NC autostabilization has been introduced in this work to account for different inconsistencies between experimental data and the first order autocatalytic NC degradation model and RS3. The new model could successfully model the form of the heat flow curve of a DPA-stabilized propellant. There are many improvements that can be

made to this model in the future to create a more accurate model.

Species other than the primary stabilizer (DPA) need to be added to better capture the heat flow curve's details. A kinetic system similar to RS3 but with autostabilization is the logical extension. The rate law for the new reactand R is:

$$\frac{\mathrm{d[R]}}{\mathrm{dt}} = k_{NC}[\mathrm{ONO_2}] + k_{auto}[\mathrm{ONO_2}][P] - k_R[R][P]$$

This changes the rate law for P in RS3 to:

$$\begin{aligned}\frac{d[P]}{dt} = {} & k_{NC}[\mathrm{ONO_2}] + k_{auto}[\mathrm{ONO_2}][P] - (k_{NNO} + k_{2N} + k_{4N})[\mathrm{DPA}][P] \\ & + k_{DPNNO}[\mathrm{NNO\text{-}DPA}] - k_{NNO-}[\mathrm{NNO\text{-}DPA}][P] \\ & - k_{2N-}[\mathrm{2NO_2}\text{-}DPA][P] - k_{4N-}[\mathrm{4NO_2}\text{-}DPA][P] - k_R[R][P]\end{aligned}$$

The expression for the heat flow dQ/dt becomes:

$$\begin{aligned}\frac{\mathrm{dQ}}{\mathrm{dt}} = {} & -k_{NC} \cdot [\mathrm{ONO_2}] \cdot \Delta_r\mathrm{H_{NC}} - k_{auto} \cdot [\mathrm{ONO_2}] \cdot [P] \cdot \Delta_r\mathrm{H_{auto}} - k_{NNO} \\ & \cdot [\mathrm{DPA}] \cdot [P] \cdot \Delta_r\mathrm{H_{NNO}} - k_{2N} \cdot [\mathrm{DPA}] \cdot [P] \cdot \Delta_r\mathrm{H_{2N}} - k_{4N} \cdot [\mathrm{DPA}] \\ & \cdot [P] \cdot \Delta_r\mathrm{H_{4N}} - k_{DPANNO} \cdot [\mathrm{NNO\text{-}DPA}] \cdot \Delta_r\mathrm{H_{DPANNO}} - k_{NNO-} \\ & \cdot [\mathrm{NNO\text{-}DPA}] \cdot [P] \cdot \Delta_r\mathrm{H_{NNO\text{-}}} - k_{2N-} \cdot [\mathrm{2NO_2} \cdot \text{-}DPA] \cdot [P] \cdot \Delta_r\mathrm{H_{2N\text{-}}} \\ & - k_{4N-} \cdot [\mathrm{4NO_2}\text{-}DPA] \cdot [P] \cdot \Delta_r\mathrm{H_{4N\text{-}}} - k_R \cdot [R] \cdot [P] \cdot \Delta_r\mathrm{H_R}\end{aligned}$$

The expression for the derivative of the heat flow becomes:

$$\begin{aligned}\frac{\mathrm{d}^2\mathrm{Q}}{\mathrm{dt}^2} = &-\left(k_{NC}\cdot\frac{\mathrm{d}[\mathrm{ONO_2}]}{\mathrm{dt}}\right)\cdot\Delta_r\mathrm{H_{NC}}\\ &-\left(k_{auto}\cdot\frac{\mathrm{d}[\mathrm{ONO_2}]}{\mathrm{dt}}\cdot[P]+k_{auto}\cdot[\mathrm{ONO_2}]\cdot\frac{\mathrm{d}[P]}{\mathrm{dt}}\right)\\ &\cdot\Delta_r\mathrm{H_{auto}}-\left(k_{NNO}\cdot\frac{\mathrm{d}[\mathrm{DPA}]}{\mathrm{dt}}\cdot[P]+k_{NNO}\cdot[\mathrm{DPA}]\cdot\frac{\mathrm{d}[P]}{\mathrm{dt}}\right)\\ &\cdot\Delta_r\mathrm{H_{NNO}}-\left(k_{2N}\cdot\frac{\mathrm{d}[\mathrm{DPA}]}{\mathrm{dt}}\cdot[P]+k_{2N}\cdot[\mathrm{DPA}]\cdot\frac{\mathrm{d}[P]}{\mathrm{dt}}\right)\\ &\cdot\Delta_r\mathrm{H_{2N}}-\left(k_{4N}\cdot\frac{\mathrm{d}[\mathrm{DPA}]}{\mathrm{dt}}\cdot[P]+k_{4N}\cdot[\mathrm{DPA}]\cdot\frac{\mathrm{d}[P]}{\mathrm{dt}}\right)\\ &\cdot\Delta_r\mathrm{H_{4N}}-\left(k_{DPANNO}\cdot\frac{\mathrm{d}[\text{NNO-DPA}]}{\mathrm{dt}}\right)\cdot\Delta_r\mathrm{H_{DPANNO}}\\ &-\left(k_{NNO-}\cdot\frac{\mathrm{d}[\text{NNO-DPA}]}{\mathrm{dt}}\cdot[P]+k_{NNO-}\cdot[\text{NNO-DPA}]\cdot\frac{\mathrm{d}[P]}{\mathrm{dt}}\right)\cdot\Delta_r\mathrm{H_{NNO\text{-}}}\\ &-\left(k_{2N-}\cdot[2\mathrm{NO_2}\text{-}DPA]\cdot\frac{\mathrm{d}[P]}{\mathrm{dt}}\right)\cdot\Delta_r\mathrm{H_{2N\text{-}}}-\left(k_{4N}\cdot[4\mathrm{NO_2}\text{-}DPA]\cdot\frac{\mathrm{d}[P]}{\mathrm{dt}}\right)\\ &\cdot\Delta_r\mathrm{H_{4N\text{-}}}-\left(k_R\cdot\frac{\mathrm{d}[R]}{\mathrm{dt}}\cdot[P]+k_R\cdot[R]\cdot\frac{\mathrm{d}[P]}{\mathrm{dt}}\right)\cdot\Delta_r\mathrm{H_R}\end{aligned}$$

The other equations from RS3 remain unchanged. This autostabilized RS3 could be fitted using the same methods as were used for the unstabilized RS3 and simultaneously with the heat flow curve.

The introduced model has an additional weak point: As R and P are constantly being produced in a one-to-one ratio, the autostabilizer R would never run out. This would mean that at no point the concentration of P would autocatalytically rise and create exothermic peaks, even in NC withoout additional stabilizers. To counteract this the stoichiometry of the degradation reactions could be modified:

$$\mathrm{NC}\xrightarrow{k_{NC}}P+\alpha R \qquad \text{intrinsic decomposition}$$

$$\mathrm{NC}+P\xrightarrow{k_{auto}}2P+\alpha R \qquad \text{autocatalysis}$$

The newly introduced coefficient α would control in what ratio R and P form. If $\alpha \geq 1$ than no autocatalytic peak would occur in unstabilized NC. If $\alpha \leq 1$ on the other hand, than over the long term autocatalysis would

prevail and more P would form than R, leading to an autocatalytic peak. The addition of a stabilizer can change this dynamic and extend the time before the autocatalytic breakdown.

Alternatively a set maximum amount of R may be set as available to a sample. While the degree of nitration between different samples varies, the underlying sugar chain does not. It might thus be better to assume that any NC sample can produce the same amount of R per anhydroglucose ring, regardless of the degree of nitration. Once the available R has been consumed, autostabilization ends and the runaway autocatalytic stage is reached. Similarly, α could be set as a function of the degree of nitration (the higher the degree of nitration, the higher α becomes). It would be interesting to apply this idea to different NC samples and examine if the threshold degree of nitration at which NC becomes susceptible no runaway autocatalysis can be correlated with the point at which α changes from less than 1 to more than 1. Further research into the effect of different organic species on the NC degradation process can additionally help to ascertain the importance of the proposed autostabilizer.

8 Summary

Isothermal heat flow microcalorimetry represents a precise and convenient method for following the degradation of nitrocellulose-based gun propellants. The addition of stabilizers which are used to prolong the shelf life of propellants, has an influence on the form of the heat flow curves. The stabilizer diphenylamine creates an initial dip in the heat flow curves, while the stabilizer akardite II does not have such an effect. Using DFT computations with the ωB97X-D functional and an aug-cc-pvtz basis set with an iefPCM solvation model to replicate the propellant matrix, reaction enthalpies and Gibbs free energies were computed for reaction pathways involving NC, DPA and Ak II.

Different initial steps for the degradation of NC have been compared. Transition states for the irreversible elimination of HONO from nitrate ester groups have been presented as a competing reaction to the reversible homolytic CO$-$NO$_2$ bond cleavage. The products of this step accelerate the degradation of NC and can lead to a runaway exothermic reaction. Their concentrations can be suppressed with stabilizers.

It is found that in an equilibrium involving a variety of nitrogen oxides, nitrogen oxoacids, water and oxygen, NO_2 and HNO_3 account for the bulk of autocatalytically active nitrogen species in NC at 90°C. In the presence of an excess of water and oxygen, the formation of HNO_3 is strongly favored, while in the absence of oxygen or in dry conditions NO_2 is much more abundant. Alternatively, organic side products of the degradation like formaldehyde of glyoxal can act as reducing agents. Is was concluded that formaldehyde could exergonically reduce any of the considered nitrogen species to NO. An additional reduction to HNO was found to represent an endergonic bottleneck for the formation of N_2O.

Several reaction mechanisms and products were computed for the subsequent degradation of NC, resulting in a wide range of reaction enthalpies between +60.1 kJ mol^{-1} and -246.5 kJ mol^{-1}. Using an autocatalytic reaction model the experimental enthalpy was found to be close to the estimated value of -246.5 kJ mol^{-1}. To achieve such a high reaction enthalpy reactions between NO_2 and the afforementioned organic side products had to be included.

The reactivity of DPA towards the autocatalytic species was examined closer. Based on computations, DPA was deemed to either react with NO_2 in a two-step radical mechanism or participate in a nitration with HNO_3

or N_2O_5. Reactions leading to carbazoles were examined as a potential side reaction for DPA. The condensation of DPA with formaldehyde was found to be exergonic even at 90°C. In this reaction, which has been widely overlooked, DPA can be polymerized into aminoplast resins.

The microscopic structure of DPA-stabilized and Ak II-stabilized propellants have been compared. It was found that DPA poorly dissolves into the propellant matrix, while Ak II has a good solubility allowing for molecular dispersion. Ak II was concluded to be overall less reactive than DPA due to the lack of the reactive aminic H and due to decreased electron density on the aromatic rings. A reaction mechanism for the intramolecular nitration has been proposed as an alternative to a direct nitration of Ak II.

Kinetic models in conjunction with reaction enthalpies from DFT computations were used to model the heat flow curves of unstabilized NC, an Ak II-stabilized propellant and a DPA-stabilized propellant. It was established that current kinetic models that only include the concentrations of nitrate ester, the autocatalytically active species and the stabilizers show three major shortcomings. (I) The simulated heat flow of the unstabilized NC sample was 10,000,000 times lower than the experimental value for parts of the experiment. (II) The heat flow rate in the Ak II-stabilized sample was higher than could be accounted for by the model. (III) Reaction enthalpies on the order of MJ mol^{-1} to GJ mol^{-1} were needed to reproduce the heat flow curve of the DPA-stabilized sample. It was concluded that a different, previously neglected reaction must be crucial for the proper description of the heat flow curves. It was proposed that the organic side products of NC degradation should be included in the kinetic model system. These species should by themselves be able to reduce autocatalytically active compounds and inhibit the autocatalytic degradation. This process was named "autostabilization", in antithesis to autocatalysis. A simple kinetic model based on this premise was found to reproduce the heat flow curve of a DPA-stabilized sample with an adjusted R^2 of 0.945. The existence of an autostabilization process would have a profound impact on the understanding of propellant shelf lives and propellant-stabilizer interactions.

The initial heat flow signatures in pure NC and the Ak II-stabilized sample were successfully fitted using a near second order reaction. It was suggested that the recombination of radicals upon heating may cause this effect.

9 Appendix: *Bernoulli* differential equations

In this section the analytic solution of the set of coupled differential equations encountered in modelling the decomposition of pure NC is covered.
The rate laws describing the system are of this form:

$$y_1{}' = -a \cdot y_1 - b \cdot y_1 \cdot y_2$$
$$y_2{}' = a \cdot y_1 + b \cdot y_1 \cdot y_2$$

Dividing $y_1{}'$ by $y_2{}'$ leaves a separable differential equation which can be directly integrated:

$$\frac{dy_1}{dy_2} = -1 \Longrightarrow y_2(x) = -y_1(x) + \Delta$$

where $\Delta =: y_1(0) + y_2(0)$. Plugging in $y_2(0)$ into the expression for $y_1(0)$ and rearranging yields:

$$y_1{}' + (a + b \cdot \Delta) \cdot y_1 = -b \cdot y_1^2$$

This ODE takes the form of a *Bernoulli* differential equation, which has the general form:

$$y_1{}' + P(x) \cdot y_1 = Q(x) \cdot y_1^n$$

with $P(x) = a + b \cdot \Delta$ and $Q(x) = -b$. The general solution to this type of ODE can be written as[98]:

$$y_1^{1-n} = \frac{1}{I(x)} \left[\int (1-n) \cdot I(x) \cdot Q(x) dx + c \right] \text{ with } I(x) = e^{\int (1-n) \cdot P(x) dx}$$

The constant of integration is set so that the boundary condition for $y_1(0)$ is fulfilled. The solution in this special case then simplifies to:

$$I(x) = e^{b \cdot x} and\ y_1(x) = \frac{y_1(0) \cdot (a + b \cdot \Delta)}{y_1(0) \cdot b + (a + b \cdot y_2(0)) \cdot e^{(a+b \cdot \Delta)x}}$$

The derivative of this expression can be written as:

$$y_1'(x) = -\frac{y_1(0) \cdot (a + b \cdot \Delta)^2 \cdot (a + b \cdot y_2(0)) \cdot e^{(a+b \cdot \Delta)x}}{\left[y_1(0) \cdot b + (a + b \cdot y_2(0)) \cdot e^{(a+b \cdot \Delta)x} \right]^2}$$

References

[1] Stephen R. Bown. *A most damnable invention: dynamite, nitrates and the making of the modern world*. Penguin Books, 2007.

[2] C. W. Saunders and L. T. Taylor. A review of the synthesis, chemistry and analysis of nitrocellulose. *Journal of Energetic Materials*, 8(3):149–203, 1990.

[3] Dschanz. Aug 2007. https://upload.wikimedia.org/wikipedia/commons/4/49/Cellulose˙nitrate.svg, usage under CC BY 2.0.

[4] R. Meyer. *Explosives*. Wiley-VCH, 2015.

[5] Michael A Hiskey, Kay R Brower, and Jimmie C Oxley. Thermal decomposition of nitrate esters. *The Journal of Physical Chemistry*, 95(10):3955–3960, 1991.

[6] B Zhao. Facts and lessons related to the explosion accident in Tianjin Port, China. *Natural Hazards*, 84(1):707–713, 2016.

[7] LS Lussier, H Gagnon, and MA Bohn. On the chemical reactions of diphenylamine and its derivatives with nitrogen dioxide at normal storage temperature conditions. *Propellants, Explosives, Pyrotechnics*, 25(3):117–125, 2000.

[8] Moritz Heil. Unpublished HFMC measurements of CP1-type unstabilized nitrocellulose at Fraunhofer Institute for Chemical Technology ICT, Pfinztal, Germany, 2019.

[9] Laurence Jeunieau, Michel H Lefebvre, and Pierre Guillaume. Ballistic stability of a spherical propellant: comparison with a flattened spherical propellant. *Central European Journal of Energetic Materials*, 4(1-2):31–44, 2007.

[10] NATO STANAG. 4582. Explosives: Nitrocellulose-Based Propellants, Stability Test Procedure and Requirements Using Heat Flow Calorimetry. *Edition, December*, 9, 2004.

[11] Douglas R Hartree. The wave mechanics of an atom with a non-Coulomb central field. Part I. Theory and methods. In *Mathematical Proceedings*

of the Cambridge Philosophical Society, volume 24, pages 89–110. Cambridge University Press, 1928.

[12] Vladimir Fock. Näherungsmethode zur Lösung des quantenmechanischen Mehrkörperproblems. *Zeitschrift für Physik*, 61(1-2):126–148, 1930.

[13] Rodney J Bartlett and John F Stanton. Applications of Post-Hartree—Fock Methods: A Tutorial. *Reviews in computational chemistry*, pages 65–169, 1994.

[14] Walter Kohn and Lu Jeu Sham. Self-consistent equations including exchange and correlation effects. *Physical review*, 140(4A):A1133, 1965.

[15] John P. Perdew and Karla Schmidt. Jacob's ladder of density functional approximations for the exchange-correlation energy. In *American Institute of Physics Conference Series*, volume 577 of *American Institute of Physics Conference Series*, pages 1–20, Jul 2001.

[16] José Gomes, José Luis Fajín, Cátia Teixeira, Paula Gomes, Renjith S. Pillai, Gerard Novell-Leruth, Jordi Toda, and Miguel Jorge. *Density functional treatment of interactions and chemical reactions at surfaces*, page Density functional treatment of interactions and chemical reactions at surfaces. 03 2013.

[17] Jeng-Da Chai and Martin Head-Gordon. Long-range corrected hybrid density functionals with damped atom–atom dispersion corrections. *Physical Chemistry Chemical Physics*, 10(44):6615–6620, 2008.

[18] Stefan Grimme. Semiempirical GGA-type density functional constructed with a long-range dispersion correction. *Journal of computational chemistry*, 27(15):1787–1799, 2006.

[19] Andre Laestadius and Michael Benedicks. Nonexistence of a Hohenberg-Kohn variational principle in total current-density-functional theory. *Physical Review A*, 91(3):032508, 2015.

[20] Rajesh K. Raju, Ashfaq A. Bengali, and Edward N. Brothers. A unified set of experimental organometallic data used to evaluate modern theoretical methods. *Dalton Trans.*, 45:13766–13778, 2016.

[21] LA Burns and Aé Mayagoitia. Density-functional approaches to noncovalent interactions: A comparison of dispersion corrections (DFT-D), exchange-hole dipole moment (XDM) theory, and specialized functionals. *J. Chem. Phys*, 134(8):084107, 2011.

[22] Sateesh Bandaru, Niall J English, Andrew D Phillips, and JM MacElroy. Exploring promising catalysts for chemical hydrogen storage in ammonia borane: a density functional theory study. *Catalysts*, 7(5):140, 2017.

[23] Ekaterina I Izgorodina, David RB Brittain, Jennifer L Hodgson, Elizabeth H Krenske, Ching Yeh Lin, Mansoor Namazian, and Michelle L Coote. Should contemporary density functional theory methods be used to study the thermodynamics of radical reactions? *The Journal of Physical Chemistry A*, 111(42):10754–10768, 2007.

[24] Stefan Dapprich, István Komáromi, K.Suzie Byun, Keiji Morokuma, and Michael J Frisch. A new oniom implementation in gaussian98. part i. the calculation of energies, gradients, vibrational frequencies and electric field derivatives1dedicated to professor keiji morokuma in celebration of his 65th birthday.1. *Journal of Molecular Structure: THEOCHEM*, 461-462:1 – 21, 1999.

[25] Aleksandr V. Marenich, Christopher J. Cramer, and Donald G. Truhlar. Universal solvation model based on solute electron density and on a continuum model of the solvent defined by the bulk dielectric constant and atomic surface tensions. *The Journal of Physical Chemistry B*, 113(18):6378–6396, 2009. PMID: 19366259.

[26] A Klamt, C Moya, and J Palomar. A comprehensive comparison of the IEFPCM and SS (V) PE continuum solvation methods with the COSMO approach. *Journal of chemical theory and computation*, 11(9):4220–4225, 2015.

[27] Herbert B. Callen. *Thermodynamics and an introduction to thermostatistics*. Wiley, second edition edition, 1985.

[28] Walter Greiner, Ludwig Neise, and Horst Stöcker. *Thermodynamics and statistical mechanics*. Springer Science & Business Media, 2012.

[29] Hiromi Nakai and Atsushi Ishikawa. Quantum chemical approach for condensed-phase thermochemistry: Proposal of a harmonic solvation model. *The Journal of chemical physics*, 141(17):174106, 2014.

[30] M. J. Frisch, G. W. Trucks, H. B. Schlegel, G. E. Scuseria, M. A. Robb, J. R. Cheeseman, G. Scalmani, V. Barone, G. A. Petersson, H. Nakatsuji, X. Li, M. Caricato, A. V. Marenich, J. Bloino, B. G. Janesko, R. Gomperts, B. Mennucci, H. P. Hratchian, J. V. Ortiz, A. F. Izmaylov, J. L. Sonnenberg, D. Williams-Young, F. Ding, F. Lipparini, F. Egidi, J. Goings, B. Peng, A. Petrone, T. Henderson, D. Ranasinghe, V. G. Zakrzewski, J. Gao, N. Rega, G. Zheng, W. Liang, M. Hada, M. Ehara, K. Toyota, R. Fukuda, J. Hasegawa, M. Ishida, T. Nakajima, Y. Honda, O. Kitao, H. Nakai, T. Vreven, K. Throssell, J. A. Montgomery, Jr., J. E. Peralta, F. Ogliaro, M. J. Bearpark, J. J. Heyd, E. N. Brothers, K. N. Kudin, V. N. Staroverov, T. A. Keith, R. Kobayashi, J. Normand, K. Raghavachari, A. P. Rendell, J. C. Burant, S. S. Iyengar, J. Tomasi, M. Cossi, J. M. Millam, M. Klene, C. Adamo, R. Cammi, J. W. Ochterski, R. L. Martin, K. Morokuma, O. Farkas, J. B. Foresman, and D. J. Fox. Gaussian˜16 Revision C.01, 2016. Gaussian Inc. Wallingford CT.

[31] Origin(Pro) Version 2019b. OriginLab Corporation, Northampton MA.

[32] ML Wolfrom, JH Frazer, LP Kuhn, EE Dickey, SM Olin, DO Hoffman, RS Bower, A Chaney, Eloise Carpenter, and P McWain. The Controlled Thermal Decomposition of Cellulose Nitrate. I1, 2. *Journal of the American Chemical Society*, 77(24):6573–6580, 1955.

[33] DA Wiegand. Diffusion in the Thermal Degradation of NC Base Propellants. Technical report, ARMY ARMAMENT RESEARCH DEVELOPMENT AND ENGINEERING CENTER PICATINNY ARSENAL ..., 1990.

[34] Milos Filipovic. Kinetic modelling of the chemical transformations of the stabiliser in single base gun propellants during ageing. *Scientific-Technical Review*, Vol.LIV:3–8, 01 2004.

[35] Jean Quinchon and Jean Tranchant. *Nitrocelluloses: the materials and their applications in propellants, explosives and other industries.* Ellis Horwood, 1989.

[36] Vernon Robert Grassie. *Possible Mechanisms for the Thermal Decomposition of Nitrocellulose*. PhD thesis, McGill University Libraries, 1946.

[37] Assa Lifshitz, Carmen Tamburu, Peter Frank, and Thomas Just. The reaction methyl + nitric oxide .fwdarw. hydrogen cyanide + water: experimental and modeling study. *The Journal of Physical Chemistry*, 97(16):4085–4090, 1993.

[38] BA Lurie. Chemical processes typical for nitro esters in propellants. In *10th International Symposium on Chemical Problems Connected with the Stability of Explosives, Margretetorp, Sweden*, 1995.

[39] Manfred A Bohn, Norbert Eisenreich, Manuela Doerich, and Heike Pontius. Characterization of ageing of nc based gun propellants by molar mass degradation of nitrocellulose and its modelling by random chain scission models including the description of the complete molar mass distribution functions. In *5th International Nitrocellulose Symposium*, pages 17–18, 2012.

[40] Manfred A Bohn and Norbert Eisenreich. Kinetic modelling of the change of molar mass distribution function of nitrocellulose during ageing. In *CD-Proceed. of 41st International Annual Conference of Fraunhofer ICT on 'Energetic Materials – High Performance, Insensitive Munitions, Zero Pollution', June 29 to July 2, 2010, Karlsruhe, Germany. ISSN 0722-4087. Fraunhofer-Institut für Chemische Technologie (ICT), D-76318 Pfinztal-Berghausen. Germany.*, volume Paper 86, pages pages 86–1 to 86–24.

[41] PC Mehta and JR Mody. Reaction of Dimethylol Ethylene Urea with Cotton. *Textile research journal*, 30(7):532–539, 1960.

[42] Yu-Ran Luo. *Handbook of bond dissociation energies in organic compounds*. CRC Press, 2003.

[43] Manfred Bohn. Measurements of stabilizer consumption in Ak II-stabilized C/S0200 DPA-stabilized double-base propellant at different temperatures at Fraunhofer Institute for Chemical Technology ICT, Pfinztal, Germany, 1996.

[44] RC Mowrey, M Page, GF Adams, and BH Lengsfield III. A binitio multireference configuration interaction study of CH2NNO2. HONO elimination vs NN bond fragmentation. *The Journal of chemical physics*, 93(3):1857–1864, 1990.

[45] Robert W Molt, Thomas Watson, Alexandre P Bazanté, Rodney J Bartlett, and Nigel GJ Richards. Gas phase RDX decomposition pathways using coupled cluster theory. *Physical Chemistry Chemical Physics*, 18(37):26069–26077, 2016.

[46] Tsan-Liang Su and Christos Christodoulatos. Destruction of nitrocellulose using alkaline hydrolysis. Technical report, STEVENS INST OF TECH HOBOKEN NJ CENTERFOR ENVIRONMENTAL ENGINEERING, 1996.

[47] Robert A Fifer. Chemistry of nitrate ester and nitramine propellants. In *Fundamentals of solid-propellant combustion*, volume 90, page 177. Progress in Astronautics and Aeronautics Series, 1984.

[48] VR Pai Verneker, K Kishore, and CBV Subhas. Mechanism of thermal decomposition of double base propellants. *Propellants, Explosives, Pyrotechnics*, 8(3):77–79, 1983.

[49] J Kimura. Chemiluminescence study on thermal decomposition of nitrate esters (PETN and NC). *Propellants, explosives, pyrotechnics*, 14(3):89–92, 1989.

[50] Ruichao Wei, Shenshi Huang, Zhi Wang, Chengming Wang, Tiannian Zhou, Junjiang He, Richard Yuen, and Jian Wang. Effect of plasticizer dibutyl phthalate on the thermal decomposition of nitrocellulose. *Journal of Thermal Analysis and Calorimetry*, 134(2):953–969, 2018.

[51] Ueber nitroglycerin. *Justus Liebigs Annalen der Chemie*, 92(3):305–306, 1854.

[52] Sanjay Divakaran and Joseph Loscalzo. The role of nitroglycerin and other nitrogen oxides in cardiovascular therapeutics. *Journal of the American College of Cardiology*, 70(19):2393–2410, 2017.

[53] A Nobel. Improved explosive and primer for the same. dynamite. *British Patent*, 1345(7), 1867.

[54] A Nobel. Verfahren zur Darstellung von zu Schießpulver geeigneter Sprenggelatine. *German Patent*, 51471, 1889.

[55] Kallmayer H-J et al. Die Benzidinblau-Reaktion in der pharmazeutischen Analytik. *Scientia Pharmaceutica*, 70(1):1–14, 2002.

[56] Henry W Turkel and Jerome Lipman. Unreliability of Dermal Nitrate Test for Gunpower. *The Journal of Criminal Law, Criminology, and Police Science*, 46(2):281–284, 1955.

[57] Kivi Grebber and JV Karabinos. A study of the diphenylamine test for aliphatic nitrocompounds. *Journal of Research of the National Bureau of Standards*, 49(3), 1952.

[58] R Scott Williams et al. The diphenylamine spot test for cellulose nitrate in museum objects. 1994.

[59] Jennifer Patterson and Cameron Mura. Rapid colorimetric assays to qualitatively distinguish RNA and DNA in biomolecular samples. *JoVE (Journal of Visualized Experiments)*, (72):e50225, 2013.

[60] MS Karawya, SM Abdel Wahab, MM El-Olemy, and NM Farrag. Diphenylamine, an antihyperglycemic agent from onion and tea. *Journal of Natural Products*, 47(5):775–780, 1984.

[61] Oliver Drzyzga. Diphenylamine and derivatives in the environment: a review. *Chemosphere*, 53(8):809–818, 2003.

[62] J Tranchant. Internal mechanism of the chemical evaluation of nitrocellulose propellants; hypothesis and consequences. In *Symp. Chem. Probl. Connected Stab. Explosiv., 6th*, pages 1–20, 1982.

[63] Homer Rogers, W. C. Holmes, and W. L. Lindsay. The melting point of diphenylamine. *Journal of Industrial & Engineering Chemistry*, 13(4):314–316, 1921.

[64] Djalal Trache, Kamel Khimeche, Riad Benelmir, and Abdallah Dahmani. Dsc measurement and prediction of phase diagrams for binary mixtures of energetic materials' stabilizers. *Thermochimica Acta*, 565:8 – 16, 2013.

[65] NJ Curtis and PE Rogasch. Determination of derivatives of diphenylamine in australian gun propellants by high performance liquid chromatography. *Propellants, explosives, pyrotechnics*, 12(5):158–163, 1987.

[66] Zhi Sun, Yong Dong Liu, Chun Lin Lv, and Ru Gang Zhong. Theoretical investigation of the isomerization of N2O3 and the N-nitrosation of dimethylamine by asym-N2O3, sym-N2O3, and trans–cis N2O3 isomers. *Journal of Molecular Structure: THEOCHEM*, 908(1-3):107–113, 2009.

[67] Inder Pal Singh Kapoor, Manisha Kapoor, and Gurdip Singh. Thermolysis of hydrogen sulphate, nitrate and perchlorate salts of diphenylamine. Part LXVIII. *Journal of thermal analysis and calorimetry*, 102(2):723–728, 2010.

[68] BL Hollingsworth. The reaction of nitrogen dioxide with some methylnitroanilines. *Journal of the Chemical Society (Resumed)*, pages 2420–2425, 1959.

[69] Torbjörn Lindblom. *Reactions in the system Nitrocellulose/ Diphenylamine with special reference to the formation of a stabilizing product bonded to nitrocellulose*. PhD thesis, 04 2004.

[70] Saul Patai. *The Chemistry of amino, nitroso and nitro compounds and their derivatives: Supplement F: Part 1*, volume 1. Wiley, 1982.

[71] WA Schroeder, Earl W Malmberg, Laura L Fong, Kenneth N Trueblood, Janet D Landerl, and Earl Hoerger. Chromatographic investigations of smokeless powder. *Industrial & Engineering Chemistry*, 41(12):2818–2827, 1949.

[72] Karl-Heinz Grellmann, Gwendolyn M Sherman, and Henry Linschitz. Photo-conversion of diphenylamines to carbazoles, and accompanying transient species. *Journal of the American Chemical Society*, 85(12):1881–1882, 1963.

[73] A Islam, P Bhattacharyya, and DP Chakraborty. Thermal cyclisation of diphenylamine to carbazole: synthesis of the natural product glycozolidine. *Journal of the Chemical Society, Chemical Communications*, (9):537a–537a, 1972.

[74] Hermenegildo García, Vicente Martí, Isabel Casades, Vicente Fornés, and Heinz D Roth. Generation and conversions of aromatic amine radical cations in acid zeolites. *Physical Chemistry Chemical Physics*, 3(14):2955–2960, 2001.

[75] WA Schroeder, Bertram Keilin, and Richard M Lemmon. Chromatographic Investigations of Smokeless Powder. Derivatives of Acardite, Carbazole, and Triphenylamine Formed in Double-Base Powder During Accelerated Aging. *Industrial & Engineering Chemistry*, 43(4):939–946, 1951.

[76] David Craig. The reaction of formaldehyde with diphenylamine. *Journal of the American Chemical Society*, 55(9):3723–3727, 1933.

[77] Djalal Trache, Ahmed Fouzi Tarchoun, Salim Chelouche, and Kamel Khimeche. New insights on the compatibility of nitrocellulose with aniline-based compounds. *Propellants, Explosives, Pyrotechnics*, 44(8):970–979, 2019.

[78] Anton Chin, Daniel S Ellison, Sara K Poehlein, and Myong K Ahn. Investigation of the decomposition mechanism and thermal stability of nitrocellulose/nitroglycerine based propellants by electron spin resonance. *Propellants, Explosives, Pyrotechnics: An International Journal Dealing with Scientific and Technological Aspects of Energetic Materials*, 32(2):117–126, 2007.

[79] T Urbański, B Hetnarski, and W Południkiewicz. Charge-transfer complexes with nitrate esters as electron acceptors. *Canadian Journal of Chemistry*, 50(20):3340–3349, 1972.

[80] T Mrzewinski. Change of diphenylamine in single-base propellants. In *Symposium on Chemical Problems Connected with the Stability of Explosives*, volume 6, pages 317–328, 1982.

[81] Josef Köhler, Rudolf Meyer, and Axel Homburg. *Explosivstoffe*. John Wiley & Sons, 2008.

[82] Nikola Bobic, Ljubica Totovski, Ljiljana Jelisavac, Jasmina B. Nikolic, R Milica Bovsnjakov, S Slobodan Markovic, and Savsa Ž. Drmanic. The gelatinization of nitrocellulose by primary stabilizers. 2017.

[83] Josef Wilken. Gelatinization tests of nitrocellulose with different stabilizers. *Proc. 42nd International ICT-Conference (June 28 –July 1, 2011, Karlsruhe, FRG)*.

[84] F Volk. Determining the Shelflife of Solid propellants. *Propellants, Explosives, Pyrotechnics*, 1(3):59–65, 1976.

[85] Louis-Simon Lussier, Eric Bergeron, and Hélène Gagnon. Study of the Daughter Products of Akardite-II. *Propellants, Explosives, Pyrotechnics: An International Journal Dealing with Scientific and Technological Aspects of Energetic Materials*, 31(4):253–262, 2006.

[86] Alan E Reed, Robert B Weinstock, and Frank Weinhold. Natural population analysis. *The Journal of Chemical Physics*, 83(2):735–746, 1985.

[87] F. Coulston and E.J. Olajos. Toxicology of n-nitroso compounds. *Ecotoxicology and Environmental Safety*, 6(1):89 – 96, 1982.

[88] E Lukášová, E Paleček, KE Kruglyakova, GP Zhizhina, and MA Smotryaeva. Properties of DNA modified with N-methyl-N-nitrosourea. *Radiation and environmental biophysics*, 14(3):231–238, 1977.

[89] Damodaran Vasudevan, Sreekumari S, and Kannan Vaidyanathan. *Proteins: Structure and Function*, pages 36–51. 01 2017.

[90] Arthur Greenberg and Thomas D. DuBois. Amide n-oxides: an ab initio molecular orbital study. *Journal of Molecular Structure*, 567-568:303 – 317, 2001.

[91] Jean-Baptiste Bossa, Fabien Borget, Fabrice Duvernay, Patrice Theule, and Thierry Chiavassa. Formation of neutral methylcarbamic acid (ch3nhcooh) and methylammonium methylcarbamate at low temperature. *The Journal of Physical Chemistry A*, 112(23):5113–5120, 2008. PMID: 18491873.

[92] Manfred A Bohn. Kinetic Description of Mass Loss Data for the Assessment of Stability, Compatibility and Aging of Energetic Components and Formulations Exemplified with ε-CL20. *Propellants, Explosives, Pyrotechnics: An International Journal Dealing with Scientific and Technological Aspects of Energetic Materials*, 27(3):125–135, 2002.

[93] M Bohn. Kinetic modelling of the concentrations of the stabilizer DPA and some of its consecutive products as function of time and temperature. *Journal of thermal analysis and calorimetry*, 65(1):103–120, 2001.

[94] LS Lussier, E Bergeron, H Gagnon, and M Bohn. A method to characterize gun powder stabilizers. In *INTERNATIONAL ANNUAL CONFERENCE-FRAUNHOFER INSTITUT FUR CHEMISCHE TECHNOLOGIE*, volume 37, page V. Berghausen; Fraunhofer-Institut fur Chemische Technologie; 1999, 2006.

[95] Manfred A Bohn. Problems and faulty uses with the prout–tompkins description of autocatalytic reactions and the solutions. *Journal of Thermal Analysis and Calorimetry*, 116(2):1061–1072, 2014.

[96] MA Bohn. Description of consumption of stabilizers in gun propellants showing pseudo-sigmoid decrease. *Paper*, 24:24–1.

[97] Manfred Bohn. HFMC measurements of K6210 DPA-stabilized double-base propellant at Fraunhofer Institute for Chemical Technology ICT, Pfinztal, Germany, 1998.

[98] Morris Tenenbaum and Harry Strange. Pollard. *Ordinary Differential Equations, etc.* Harper & Row, 1964.